Design, Manufacture, and Test of a Hybrid Solar PV-T Thermoelectric Distillation System.

A thesis submitted to Cardiff University in the candidature for the degree of

Doctor of Philosophy

By

Ali Bahr

School of Engineering

Cardiff University

September, 2024

Abstract

This thesis investigates the development and performance of a hybrid solar photovoltaic-thermoelectric (PV-T) distillation system designed to improve freshwater production efficiency. The study addresses global water scarcity by utilizing renewable energy to drive a distillation process. The primary goal is to create a system that integrates photovoltaic panels for electricity generation and thermoelectric modules for heating and cooling, augmented by direct solar heating.

The research involves a detailed literature review of desalination technologies, thermoelectric devices, and hydrophobic surfaces, followed by experimental analysis of water and condenser temperatures on evaporation and condensation rates. A prototype hybrid PV-T distillation system was designed, built, and tested, revealing significant insights into its thermal behavior and performance under different configurations.

The system reached a steady state after 5 hours, with various components showing stable temperature profiles. When using only the thermoelectric module, water temperature increased by 5.6°C (from 18.3°C to 23.9°C). Using both the thermoelectric module and PV-T panel, the water temperature rose by 31.5°C (from 18°C to 49°C). The most effective configuration, which included a submerged black absorber, increased the water temperature by 37.9°C (from 18.8°C to 56.7°C).

In terms of water production rates, the thermoelectric-only setup produced 14.78 grams of water in 5 hours. The PV-T and thermoelectric setup produced 37.5 grams, while the combined PV-T, thermoelectric, and black absorber setup yielded 84.1 grams of water, showcasing the highest efficiency.

Introducing a fan to cool the glass cover increased water productivity by approximately 33.65%. This cooling enhanced water production from the glass by

141%, despite a 30% reduction in production by the aluminum condenser, resulting in a net positive effect.

Acknowledgements

I express my gratitude to Allah for granting me the strength, courage, and health to complete this research project.

I am indebted to my supervisor, Prof. Min, for his invaluable guidance and support throughout my PhD journey.

Special thanks to my wife, Basmah, for her unwavering patience and motivation. I am also grateful to my parents for their constant love and encouragement. Additionally, I appreciate the support of my colleagues, Hamed, Godwin, and Abdullah, as well as my friend Mustafa, who stood by me during challenging times.

Table of contents

Abstract ..... **ii**

Acknowledgements ..... **iv**

Table of contents ..... **v**

List of figures ..... **ix**

List of tables ..... **xv**

Chapter 1: Introduction **1**

1.1 Background 1

1.2 Aim and Objectives 3

1.3 Thesis structure 4

Chapter 2: Literature review **6**

2.1 Introduction 6

2.2 Thermoelectricity 6

2.2.1 Seebeck Effect 7

2.2.2 Peltier Effect 8

2.2.3 Thomson Effect 9

2.2.4 Thermoelectric power generation 9

2.2.5 Thermoelectric cooling 20

2.3 Water Desalination Technologies 25

2.3.1 Multiple-stage flash distillation (MSF) 25

2.3.2 Multiple effect desalination (MED) 26

2.3.3 Vapor compression 27

2.3.4 Reverse osmosis (RO) 28

2.3.5 Electrodialysis (ED) 29

2.3.6 Solar Distillation.....30

2.3.7 Thermoelectric Distillation 33

2.4 Superhydrophobic surface 40

2.4.1 Etching 42

2.4.2 Sol-Gel.....43

2.4.3 Electrochemical deposition 44

Chapter 3: Experimental Investigation of factors affecting evaporation and condensation processes 45

3.1 Introduction.....45

3.2 Experiment to investigate factors affecting the evaporation process. ..45

3.2.1 Experimental setup 46

3.2.2 Experimental Procedure.....48

3.2.3 Results 50

3.3 Experiment to Investigate the Effect of Water Temperature, Condenser Temperature and Angle on the Condensation Rate 54

3.3.1 Experimental Setup 55

3.3.2 Results 57

3.4 Conclusion 63

Chapter 4: Design, fabrication, and test of the hybrid PV-T thermoelectric distillation system..... 64

4.1 Introduction.....64

4.2 Solar Simulator Test (Calibration) 64

4.2.1 Spectral Match.....66

4.2.2 The non-uniformity of the irradiance.....71

4.2.3 Irradiance Temporal Instability 73

4.2.4 Overall Performance Classification of the Solar Simulator 74

4.3 Hybrid PV-T thermoelectric distillation system design.....75

4.3.1 The thermoelectric module.....77

4.3.2 Evaporation/Condensation chamber 78

4.3.3 The PV panel. 79

4.3.4 The Glass Cover 81

4.3.5 Aluminium condenser 83

4.3.6 Heat Exchanger.....85

4.3.7 Instrument and sensors. 86

4.3.8 Testing and benchmarking the system. 87

4.3.9 results and discussion.....89

4.4 Conclusion 103

Chapter 5: Improve the Productivity by Using a Fan to Cool the Glass Cover and Hydrophobic Layer on the aluminium Condenser. 105

5.1 Introduction..... 105

5.2 investigate using hydrophobic layer. 105

5.2.1 Preparing the hydrophobic layer. 106

5.2.2 Result 107

5.3 Using a Fan to Cool the Glass Cover..... 112

5.3.1 Experimental Setup 112

5.3.2 Results 113

5.4 conclusion..... 121

Chapter 6: Conclusion 122

6.1 Conclusions..... 122

6.2 Future Work 124

References..... 125

List of figures

Figure 1.1 Global water stress level [2] 1
Figure 2.1 The figure of merit of some thermoelectric material as a function of temperature [12]. 7
Figure 2.2 Seebeck Effect [13] 8
Figure 2.3 Peltier Effect [13] 9
Figure 2.4 Classification of thermoelectric power generation [14] 10
Figure 2.5 waste heat recovery system to replace the conventional radiator in cars [19] 11
Figure 2.6 car exhaust gases waste heat recovery system designed by Demir et al [20] 12
Figure 2.7 waste heat recovery system from a biomas cook stove [26]. 13
Figure 2.8 : (a) An experimental prototype of the concentration solar thermoelectric generator system done by Li et al . (b) Details of the CTG unit[28] 14
Figure 2.9 residential photo-thermo-electric cogeneration system[29].....15
Figure 2.10 Schematic diagram of the concentrated solar thermoelectric system de- signed by Miljkovic et al [30]. 16
Figure 2.11 the integrated thermoelectric generatior with heat pipe evacuated tube designed by He et al[32]. 17
Figure 2.12 Thermoelectric Thermosyphom system proposed by Singh [33] 18
Figure 2.13 Efficiency of Bismuth telluride and filled-skutterudite as a function of the temperature difference [34] 19
Figure 2.14 Schematic of solar cell driven, thermoelectric refrigerator designed by Dai et al[37] 21
Figure 2.15 Position of the TE-CCP on the test chamber designed by Lertsatitthanakorn et al [42]. 23
Figure 2.16 Photo of thermoelectric unit for small-scale space conditioning applications designed by Liben et al[43]. 24
Figure 2.17 Multiple-stage flash distillation (MSF) [16] 26

Figure 2.18 Multiple effect desalination (MED) [16] 27
Figure 2.19Vapor compression [16] 28
Figure 2.20 Reverse Osmosis (RO) [16] 29
Figure 2.21 Electrodialysis (ED) [16] 30
Figure 2.22 Schematic of the weir-type distillation unit and its components [55] 31
Figure 2.23 Schematic diagram of an integrated hybrid PV active solar still[56] 32
Figure 2.24 Cross-sectional view of a single slope passive solar still [57].....32
Figure 2.25 Cross-sectional view of a double slope passive solar still [57].....33
Figure 2.26 a) a schematic of the distillation system, b) photo of the system, c) parabolic solar collector used to heat the water [61]. 34
Figure 2.27 a) schematic of the system component, b) schematic drawing of the system,c) photo of the system [62] 35
Figure 2.28 Solar distillation systems with and without cooling channel [63]. ...36
Figure 2.29 A schematic diagram of HDH experimental [64]. 36
Figure 2.30 schematic drawing of the thermoelectric distillation system designed by Hayder[65] 37
Figure 2.31 schematic drawing of the asymmetrical solar still [67].....38
Figure 2.32 Droplet state on the surface.....41
Figure 3.1 Neslab GP-300.....46
Figure 3.2 a) RS PRO Type K Thermocouple, b) digital humidity sensor 47
Figure 3.3 Pico Log TC-08 data logger 48
Figure 3.4 (a) scematic diagrame of the evaporation rate experiment setup, (b) the Neslap GP-300 with ruler and the thermocouples attached 48
Figure 3.5 Evaporation rate change with the water temperature obtained from the experiment 50
Figure 3.6 comparison between the evaporation rate obtained from the equation and the experimental results. 52
Figure 3.7 Comparing the change of evaporation rate to the heat of vaporization with water temperature 53

Figure 3.8 The plexi glass chamber :(a) top view, (b) front view, (c)and (d) side views 55
Figure 3.9 The desinged chamber with the aluminum condenser . (a) for 45 degree angle, (b) for 65 degrees angle. 56
Figure 3.10 the condensation experiment setup 56
Figure 3.11 Condensation rate change with condenser temperature and water temperature 57
Figure 3.12 the power supplied to the TE module 58
Figure 3.13 the cross sectional area of both chamber :(a) 65 degree, (b) 45degree. 59
Figure 4.1 The solar simulator system: (a) environmental chamber from outside, (b) ARRISUN 60 light source viewed from inside the chamber, (c) ARRISUN 60 light source, (d) electronic Ballast and (e) adjustable test table. 65
Figure 4.2 (a) Blue Wave Spectrometer (UV-VIS) and (b) Dwarf Star Spectrometer (NIR) 66
Figure 4.3 Schematic diagram of light source spectral measurement. 67
Figure 4.4 The setup of the of light source spectral measurement 68
Figure 4.5 spectral match of the light source compared to the limits of class A and B according to the E927-10 standards 69
Figure 4.6 comparison between the spectrum of the sun AM 1.5G and the lights source of the solar simulator 70
Figure 4.7 the bench underneath the Lightsource and the pyranometer used to identify the non- uniformity 71
Figure 4.8 Normalized irradiance under the simulator over the whole area of the bench 72
Figure 4.9 Normalized irradiance under the simulator over an area of 60*80cm in the centre of the bench 73
Figure 4.10 The change of irrediance over the period of the Temporal Instability test 74

Figure 4.11 (a) the designed system diamention, (b) exploded view of the system and it is component.....76
Figure 4.12 projected view of the system 76
Figure 4.13 The thermoelectric module used in the design 77
Figure 4.14 the evaporation/condensation chamber 79
Figure 4.15 (a) the PV panel used for this study, (b) the setup to measure the IV curve and maximum power.....80
Figure 4.16 IV curve obtained from the PV panel described above.....81
Figure 4.17 the setup used to test and compare the transmittance of the glass to the acrylic.....82
Figure 4.18 Spectrum comparison between the light source ,what is transmitted throw the glass, and throw the Acrylic.....82
Figure 4.19 Transmittance of the glass and the acrylic.....83
Figure 4.20 the aluminum condenser used in the designed system.....84
Figure 4.21 (a) the heat exchanger used with the PV panel. (b) the heat exchanger used on the hot side of the thermoelectric.....85
Figure 4.22 the setups and a schematics of the three configuration of the system to be tests.(a) the cofiguration using Thermoelectric only.(b) using PV-T and the TE.(c) using PV-T and TE and black absorber submerged in water. 88
Figure 4.23 The temperature variation of the system components PV-T+TE and black absorber submerged in the water 89
Figure 4.24 comparing the change of water temperature of different system configurations 90
Figure 4.25 the hourly temperature increase rate of the water.....91
Figure 4.26 The change of humidity insidethe champer.....92
Figure 4.27 comparision between thechange of relative humidity aginst absolute humidity.....93
Figure 4.28 the temperature diffrence between the vapor inside the chamber and condinsing surfce on the 65-degree angle 94

Figure 4.29 the temperature diffrence between the condinsing surfce on the 30-degree angle and the vapor inside the chamber 95
Figure 4.30 Accumelated water production (g).....96
Figure 4.31 Accumelated water production (g) from the 30-degree condesing surface.....97
Figure 4.32 Accumelated water production (g) from the 65-degree condesing surface.....98
Figure 4.33 TDS EC Tester used to mesure the quality of the water. 99
Figure 4.34 Temperature of the water in the evaporation chamber as a function of heating time. The inset shows the temperature profile at the initial period and a linear relationship between the temperature and time is evident..... 101
Figure 4.35 comparison between the energy available and absorbed by the water 102
Figure 4.36 Comparing the efficiency of the three configuration of the system 103
Figure 5.1 a) The aluminium condenser before the hydrophobic layer. b) the aluminium condenser submerged in potassium hydroxide solution. c) The aluminium condenser after the hydrophobic layer 106
Figure 5.2 a) Shape of the water droplet without the hydrophobic layer .b) Shape of the water droplet with the hydrophobic layer..... 107
Figure 5.3 Comparing the hourly change of temperature of the water before and after introducing the hydrophobic layer 108
Figure 5.4 total water production from the system before and after the hydrophobic layer applied to the aluminum condenser. 109
Figure 5.5 Comparing the water production of the aluminum condenser with and without the hydrophobic layey 110
Figure 5.6 Comparing the water production of the glass cover befor and after the hydrophobic layey aapplied to the aluminum. 111
Figure 5.7 Condensation on the aluminum, a) with the hydrophopic layer, b) without the hydrophopic layer..... 112

Figure 5.8 the experiment setup 113
Figure 5.9 Comparing the hourly change of temperature of the water before and after using the fan to cool the glass cover 114
Figure 5.10 Glass cover temperature change over the time period of the experiment..... 115
Figure 5.11 The temperature difference between the vapor inside the chamber and the glass cover. 116
Figure 5.12 The accumulated productivity of the system before and after the fan 117
Figure 5.13 The accumulated productivity from the aluminum condenser before and after the fan 118
Figure 5.14 The accumulated productivity from the glass cover before and after the fan..... 118
Figure 5.15 The temperature difference between the vapor inside the chamber and the the aluminum condenser. 119
Figure 5.16 the efficiency of the system before and after the fan introduced. 120

List of tables

Table 2-1 The advantages and disadvantages of current desalination technologies.....39
Table 3-1The specifications of K- type thermocouple used in the experiments [87]. 47
Table 3-2 Comparision between the condensation rate obtained from the mathimatical model and the experiment condenser angle 65 degrees 62
Table 3-3 Comparision between the condensation rate obtained from the mathimatical model and the experiment condenser angle 45 degrees 62
Table 4-1 Classification of large area solar simulators according to their performance 66
Table 4-2 the irradiance as a percentage from the total from 400-1100nm.....68
Table 4-3 Total irradiance for each wavelength interval of ARRISUN-60 light source compared with the Sun AM 1.5G spectrum data of ASTM 70
Table 4-4 Overall Performance Classification of the Solar Simulator 75
Table 4-5 the specification of The thermoelectric module used in the design ...78

Abbreviation

AM 1.5G	Air Mass 1.5 Global (solar irradiance standard)
COP	Coefficient of Performance
CTG	Concentrated Thermoelectric Generator
ED	Electrodialysis
HDH	Humidification-Dehumidification
IV Curve	Current-Voltage Curve (for solar panels)
KOH	Potassium Hydroxide
MED	Multiple-Effect Distillation
MSF	Multi-Stage Flash Distillation
MVC	Mechanical Vapor Compression
NIR	Near Infrared (spectroscopy)
PV-T	Photovoltaic-Thermal
RO	Reverse Osmosis
TDS	Total Dissolved Minerals
TE	Thermoelectric
TVC	Thermal Vapor Compression
UV-VIS	Ultraviolet-Visible (spectroscopy)
VC	Vapor Compression
ZT	Figure of Merit (for thermoelectric materials)

Chapter 1: Introduction

1.1 Background

Water is most abundant substance on earth, it covers around 70% of the total surfaces. Despite that the amount of water regarded as a fresh water is only 2.5% of the total water available on earth. Currently 40% of the total population affected by water scarcity [1], and by 2040, 44 countries will face high or extremely high-water stress level [2]. The main reason for this is the pressure comes from the increase of the population. However, it is not the only reason. In the 20th century the water use increased 6 times as compared to 3 times of population increase which indicates excessive water use [3].

Drought is one of the main contributors to the water stress. 94% of the people affected by disaster in 2016 were affected by drought. Drought mainly is resulted from the climate change and the water stress associated to it will cost some region around 6% of the total GDP[4].

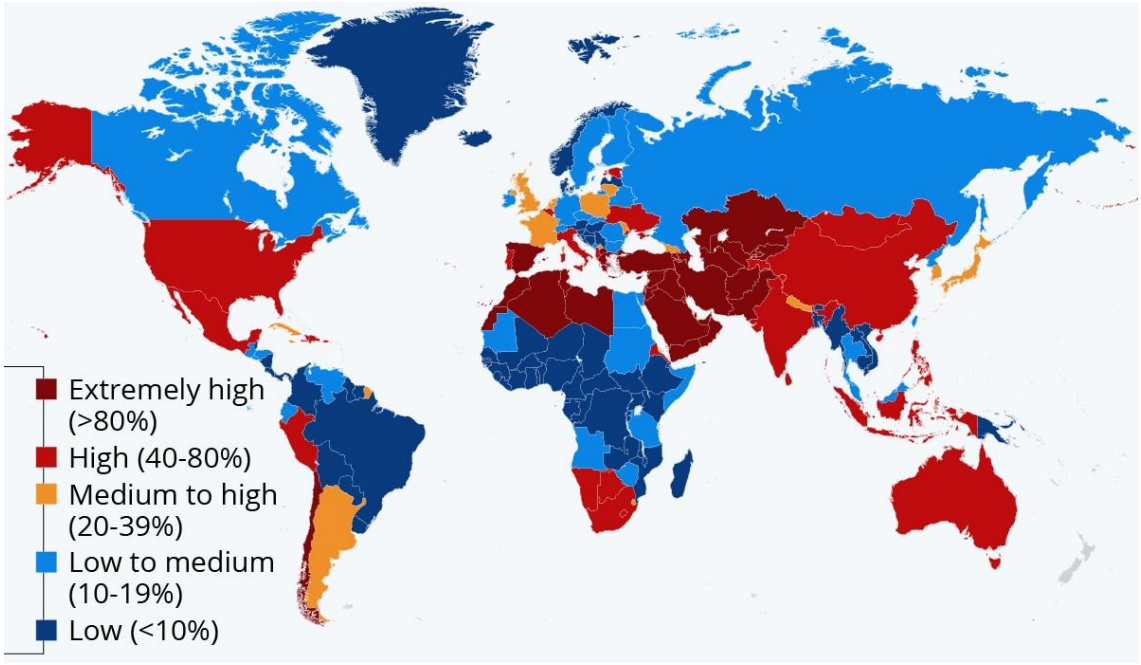

Figure 1.1 Global water stress level [2]

The first separation method ever known for human being is distillation, and still one of the most popular techniques used in variety of application nowadays. Distillation is defined as the process in which liquid mixture is separated based on the difference of the boiling point and vapor pressure of it is components. It is simply achieved by heating liquid to generate vapour, then re-condense the vapour into liquid and collect it in container. The first appearance of distillation devices was in 3500BC in what today is known as Iraq[5]. However, the first documented scientific study of distillation was found in the writings of Jabir ibn Hayyan (721–815) where he explained that by boiling wine a flammable gas is produced. After him, many other Muslim scholar studied the use of distillation in different applications, Al-Kindi (801-873) wrote a book called “book of the chemistry of perfume and distillation” where he described more than one hundred methods for Perfume-Making recipes and the equipment used for making it [5]. Crude oil distillation was first described by Muhammad al-Razi (1149- 1210) in his book “Book of secrets”, the produced product described in his book seems to resemble Kerosene [6]. The distillation of alcohol beverages believed to be started around 11th century in Italy, the process used to increase the percentage of alcohol in the spirit beverages. Later distillation of sprits become the first industrial application of the distillation process [7]. The most recently and most common application where distillation used nowadays is in petroleum refinery. Distillation is used in variety of application mainly in these industries:

- Water desalination
- Petroleum refinery
- Alcohol industry
- Pharmaceutical industry
- Perfume industry

Desalination is the term used to describe the process of separating the dissolved mineral from water. In recent year, desalination played a key role in freshwater production. The market now is led by two desalination method, Thermal distillation, and membrane method. Thermal distillation is a well-established method for freshwater production, it relies on the concept of phase change, by heating the water to produce vapor and cooling the generated vapor to produce fresh water (evaporation and condensation). The technologies used includes Multistage Flash (MSF), Mechanical Vapour Compression (MVC), Still Distillation (SD) and Multiple Effect Distillation (MED). In general, thermal distillation processes are more energy consumed and have a higher capital cost than membrane processes. However, the water produced is at higher quality[8]. Membrane processes relay on using special membrane barrier instead of boiling the water, this is called non-phase-change method and includes techniques like Electrodialysis (ED) and Reverse Osmosis (RO). This technology is not favourable for high salinity or very poor water quality, have much higher maintenance cost than thermal distillation processes [9]. Generally, water desalination technologies are expensive, highly affected by the increase in energy prices, and have a high carbon footprint .

1.2 Aim and Objectives

The aim of this project is to develop an innovative hybrid solar-thermoelectric distillation system that employs a solar panel to generate electricity for powering a thermoelectric module for water evaporation using its hot side and vapor condense using its cold side, incorporated with direct solar heating through absorption to increase the efficiency and water production. The project involves design, construct, and test the proposed hybrid PV-T TE distillation system (Hybrid photovoltaic thermal thermoelectric distillation system) and evaluate its

performance for freshwater production and efficiency. The specific tasks were as follows:

- To perform initial experiments to understand how the temperatures of the water and the condenser affect evaporation and condensation.
- To test the solar simulator to ensure it provide simulated solar irradiation that meets the criteria as specified by the ASTM E927-10 standard (ASTM E927-10 is a standard specification for solar simulators used to test photovoltaic devices indoors) [10].
- To design and construct a prototype of the proposed hybrid PV-T-TE distillation system.
- To perform systematic experiments to evaluate the performances of the prototype system and identify the factors that have significant effect on the performances of the system.
- To further improve the performances of the prototype system by implementing the promising ideas and approaches identified from the investigations of this work.

1.3 Thesis structure

The thesis consists of six chapters. A brief outline of these chapters is given below:

- Chapter one introduces the background and motivation of this work relating to the water problem facing the world, describes the aims and objectives of this research, and provides the thesis outline.
- Chapter two summaries the key outcomes of an extensive literature review on the fundamentals and recent progress on distillation and desalination technologies, thermoelectric devices, and hydrophobic layers.

- Chapter three presents two initial experiments designed to understand the effect of water and surface temperature on the condensation and evaporation processes.
- Chapter four describes the tests on the solar simulator and its assessment, explains the design and construction of the proposed prototype, and presents the outcomes of systematic investigations on the performance and characteristics of the developed prototype.
- Chapter five describes the research efforts to further improve the performances of the developed prototype via two approaches: applying a hydrophobic layer on the aluminium condenser and cooling of the glass cover.
- Chapter six summarises the key outcomes of the thesis and provides some suggestions on future work.

Chapter 2: Literature review

2.1 Introduction

The goal of this chapter is to gain the understanding necessary to establish a firm foundation of both solar distillation and thermoelectricity. The literature review starts with introduction to the thermoelectricity, reviews both thermoelectric power generation and thermoelectric cooler applications. The water desalination technologies also reviewed with concentration on the use of thermoelectric in freshwater production. Lastly a brief introduction to superhydrophobic surfaces and the techniques used to fabricate it is presented.

2.2 Thermoelectricity

A thermoelectric generation is the voltage generation results from a temperature difference across two different semiconductor materials, this phenomenon called Seebeck effect. The opposite process, which is when a voltage applied to a circuit built from two different conductors, a temperature difference will be created across the junction of the two different conductors. This is called Peltier effect. Moreover, when a single material has a current flowing though it and this material already has a temperature difference across it, heat will be absorbed or dissipated, this effect is called Thomson effect. Thermoelectric devices work based on these three effects. the performance of the thermoelectric devices can be evaluated by what is called the figure of merit (ZT). (ZT) is a dimensionless number that measures the efficiency of thermoelectric materials and devices that convert heat into electricity. the figure of merit (ZT) depends on three properties of the material that the thermoelectric is made from, these properties are the Seebeck coefficient (α), the thermal conductivity (K), and the electrical conductivity (δ). And the relationship can be written as follow:

$$ZT = \alpha 2 \sigma T / K \qquad 2\text{-}1$$

For high figure of merit, low thermal conductivity (K), and High high Seebeck coefficient (α) and electrical conductivity (δ) is required. thermoelectric material can be divided into three group based on the range of temperature where it gives the best figure of merit, Bismuth combined with antimony, tellurium, and selenium is best material to work at low temperature be- low 450 K, Lead telluride (PbTe) works in the mid-range temperature up to 850K, and Silicon germanium (SiGe) gives best performance at 1300 K [11]. The figure of merit for some commercially available thermoelectric materials as a function of temperature is shown in figure Figure 2.1.

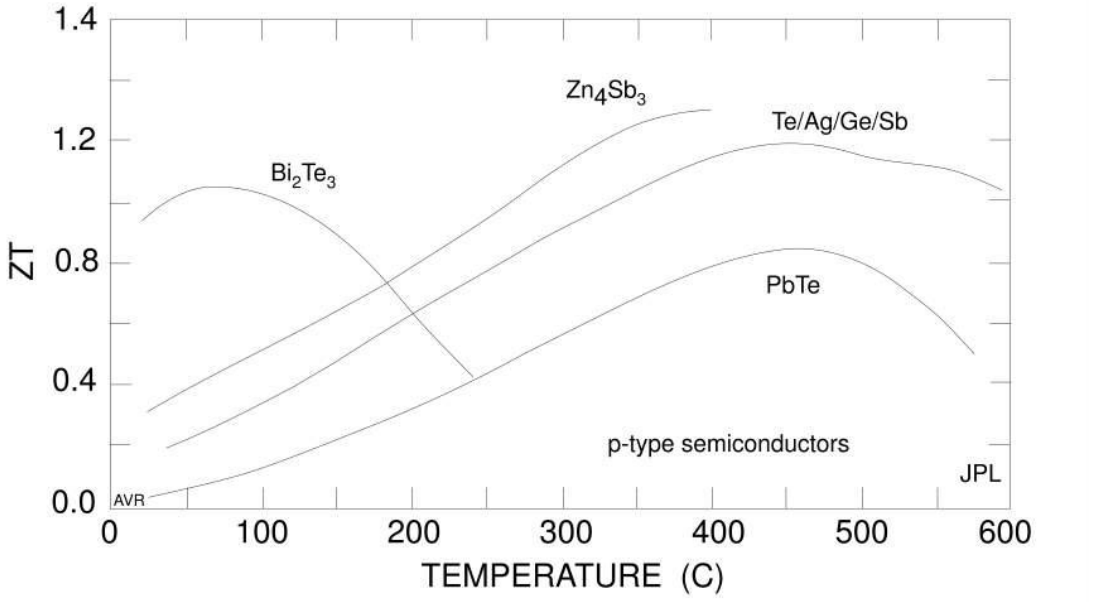

Figure 2.1 The figure of merit of some thermoelectric material as a function of temperature [12].

2.2.1 Seebeck Effect

Figure 2.2 shows a thermoelectric element work as thermoelectric generator based on Seebeck effect, the thermocouple which consist of two dissimilar semiconductor material convert the temperature difference to electrical current. When the temperature difference is imposed between the two sides of the thermoelectric element, a potential difference of voltage will flow in the system. This happens as the temperature difference causes a charge carriers to diffuse

from the hot side to the cold side of the thermoelectric. This voltage is proportional to the temperature difference by a value of α [12].

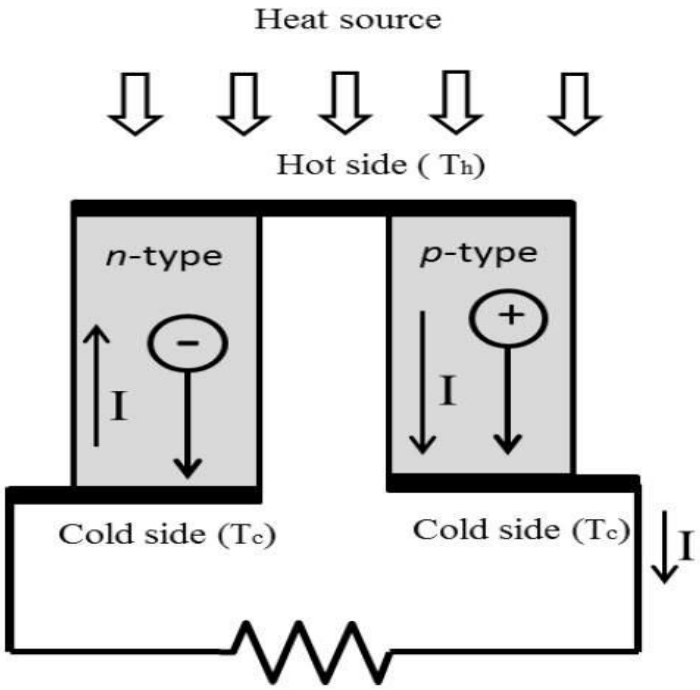

Figure 2.2 Seebeck Effect [13]

2.2.2 Peltier Effect

Figure 2.3 shows a thermoelectric element work as thermoelectric cooler based on Peltier effect, the current flows through the circuit which built from two different semiconductor materials, and this will cause a temperate difference where one end will absorb heat and the other will reject heat. The heat pumped from one end to the other due to the electrical current flow, the amount of heat removed from one end to the other end is proportional to the current flows in the circuit formed by the two dissimilar semiconductor materials [12].

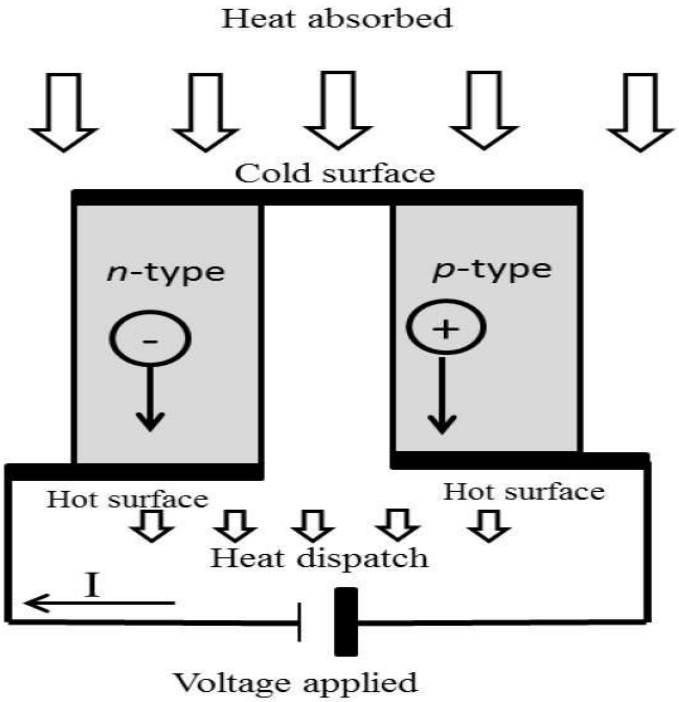

Figure 2.3 Peltier Effect [13]

2.2.3 Thomson Effect

There is more heat will be absorbed or dissipated in thermoelectric devices in both application, power generation, and refrigeration. This happens because of Thomson effect. when a current flows through a single conductor material and this material has a temperature difference across it is ends, heat will be dissipated or absorbed depending on the direction of the current flow [12]

2.2.4 Thermoelectric power generation

The use of thermoelectric for power generation can be divided into two main categories, firstly as recovery device for waste heat either from commercial

application or residential application, secondly in renewable energy [14]. Figure 2.4 shows the classification of thermoelectric generators.

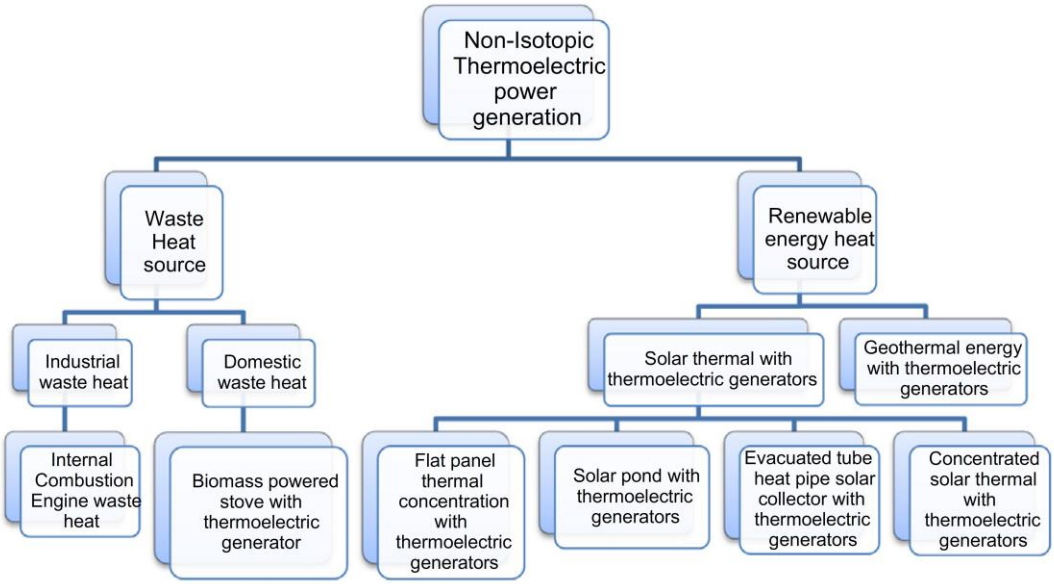

Figure 2.4 Classification of thermoelectric power generation [14]

The main factor for the limited use of thermoelectric device in power generation it is low efficiency conversion, it used in waste heat recovery and in some cooling application when the efficiency is not a problem [15]. The thermoelectric device first real application was to supply electricity to spacecraft in 1961 [14]. This was due to it is many advantages [16]:

- Endless shelf life
- the lack of moving parts and chemical reaction.
- simple structure
- silent in operation and no pollution

Thermoelectric generation has many advantages such as the high reliability, no moving parts, silent work, simple construction, and require less maintenance, the use thermoelectric generation still in certain application due to it is low conversion efficiency [15].However, it has the ability to improve further in the field of solar power generation because they live longer than Photo-Voltaic

panels and their independence from sunlight, this is what makes thermoelectric power generation attractive and can compete with the Photo-voltaic power generation [17].

Thermometric has been proposed as a waste heat recovery from industrial application as well as from automobile, the efficiency of vehicles is ranged between 20% to 45% depending on the engine type and operation condition, the remaining will be wasted as a heat from the radiator and exhaust gases [18]. Many designed to utilize the waste heat from both engine coolant and exhaust gases has been investigated.

Kim et al [19], designed a recovery system to replace the conventional radiator in cars, the system uses 128 small heat pipes to transfer the heat to 72 thermoelectric generators. The temperature difference across the thermoelectric modules was 20 C during idle and 45 C at a speed of 80 km/h, the energy produced from the system was 28W and 75W respectively.

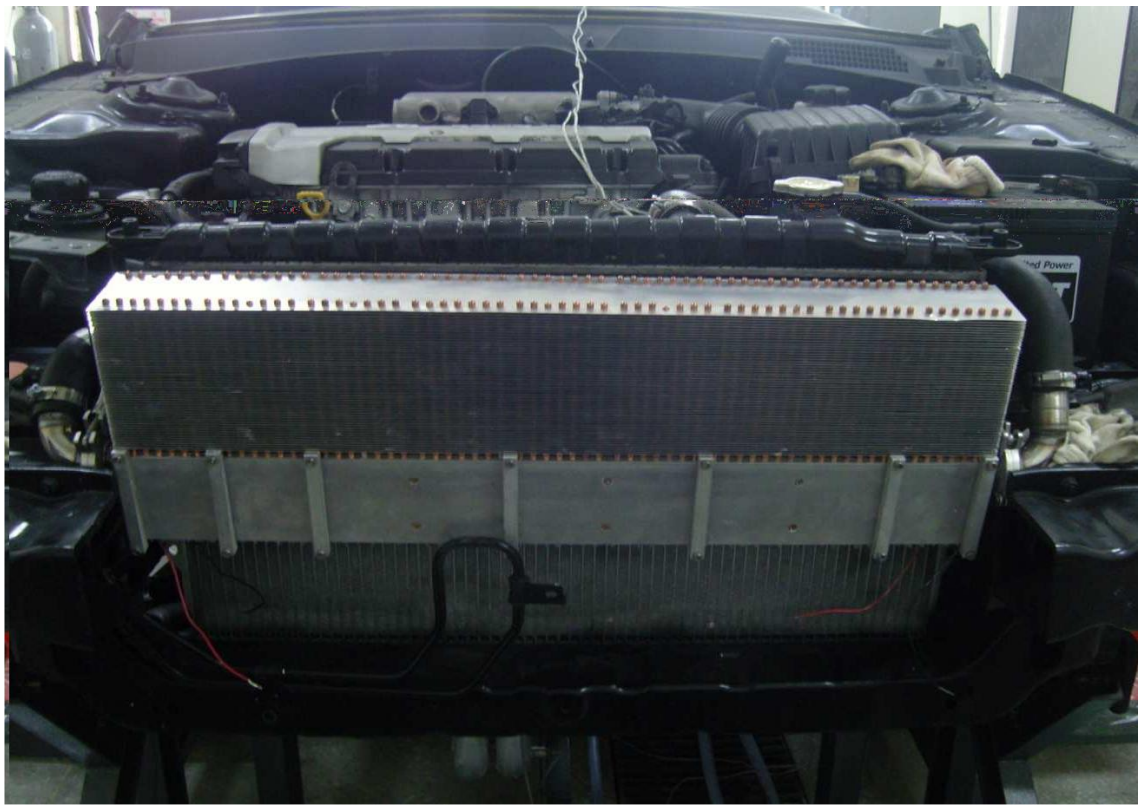

Figure 2.5 waste heat recovery system to replace the conventional radiator in cars [19]

Demir et al [20], designed a thermoelectric system utilize the wasted heat from car exhaust gases, the maximum power generated was 158W and the efficiency of the system was 0.51%.

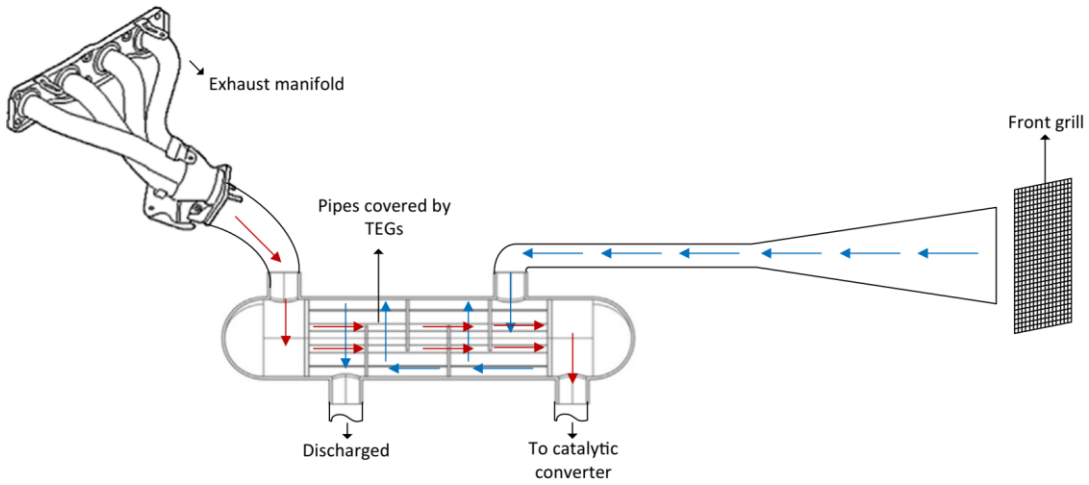

Figure 2.6 car exhaust gases waste heat recovery system designed by Demir et al [20]

Another system uses heat pipe to transfer the heat from the exhaust gases to the thermoelectric modules was designed by Kim et al [21], the system uses water to remove the heat rejected from the thermoelectric modules, the system was able to produce a 320W from 112 thermoelectric generators. similar designs using water to cool the cold side of the thermoelectric were studied by Matines et al., Goncalves et al., and Brito et al[22], [23], [24]. the only difference is instead of using traditional heat pipes, a variable conductance heat pipe is employed which unlike conventional ones can maintain a steady temperature. (The main difference between variable conductance heat pipe and a standard heat pipe is that the variable conductance heat pipe contains a non-condensable gas which allows for the ability to control the heat dissipation based on the condenser temperature and the power input) [25].

The use of thermoelectric as waste heat recovery device in domestic application has been investigated as well, Lertsatitthanakorn [26] used a commercial thermoelectric module to recover a portion of the heat wasted from a biomass cook stove. Hot side of the thermoelectric is attached to the side wall of the stove, while a heat sink is used on the cold side of the thermoelectric to maximize the temperature difference. The system was able to generate around 2.4W with maximum temperature difference of 150C and the conversion efficiency was 3.2%.

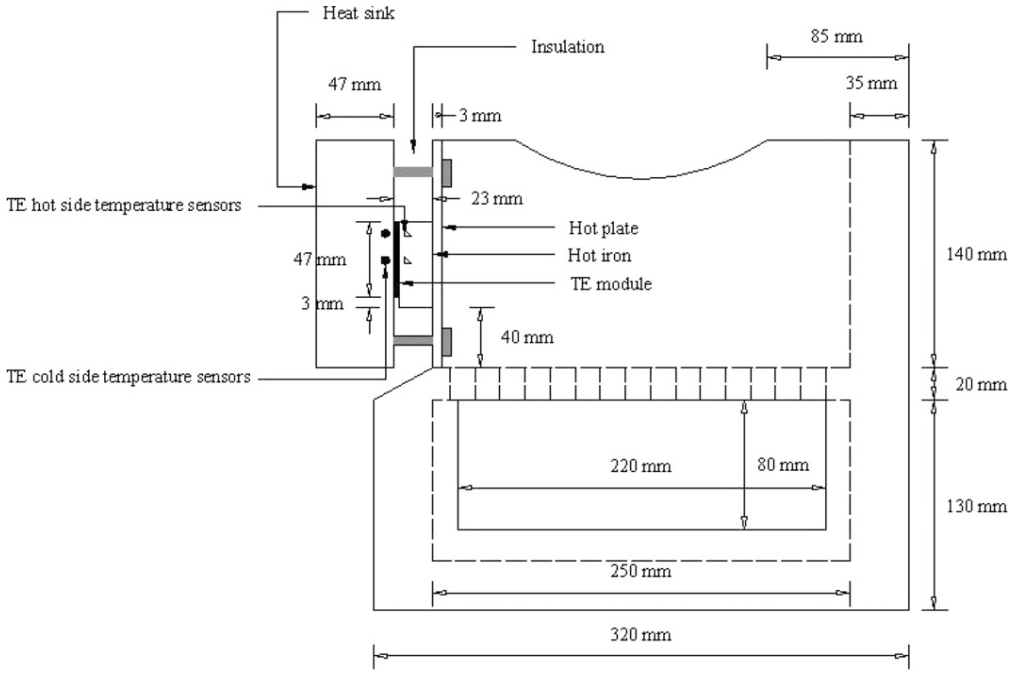

Figure 2.7 waste heat recovery system from a biomas cook stove [26]***.***

Willson et al [27], designed a system to recover heat from the chimney of a stove. It has been found that rely on natural convection only to cool the cold side is not enough to keep a sufficient temperature difference across the thermoelectric module, as a result a fan was employed to cool the cold side. The power output of the system was 3.8W used to power a high intensity light emitting diode (LED).

Thermoelectric is also used in many configurations to harvest the energy from sun. Li et al [28], has introduced the numerical model and designed the experiment for concentrated solar thermoelectric power generation, the system

comprises of a two Fresnel lens with reflector mirrors to guide the solar radiation that has been concentrated to the heat collector. Two thermoelectric devices are attached to both sides of the heat collector which is coated with a selective absorber layer to increase the absorbed radiation. An active cooling system using a fluid flow through the heat ex- changer water tank is used to maintain the temperature of the cold side as low as possible. The effect of cooling methods on the performance of three different type of thermoelectric materials has been investigated, three different ways to cool the cold side of the thermoelectric device (Forced water cooling, natural water cooling, and natural air cooling) has been analysed numerically.

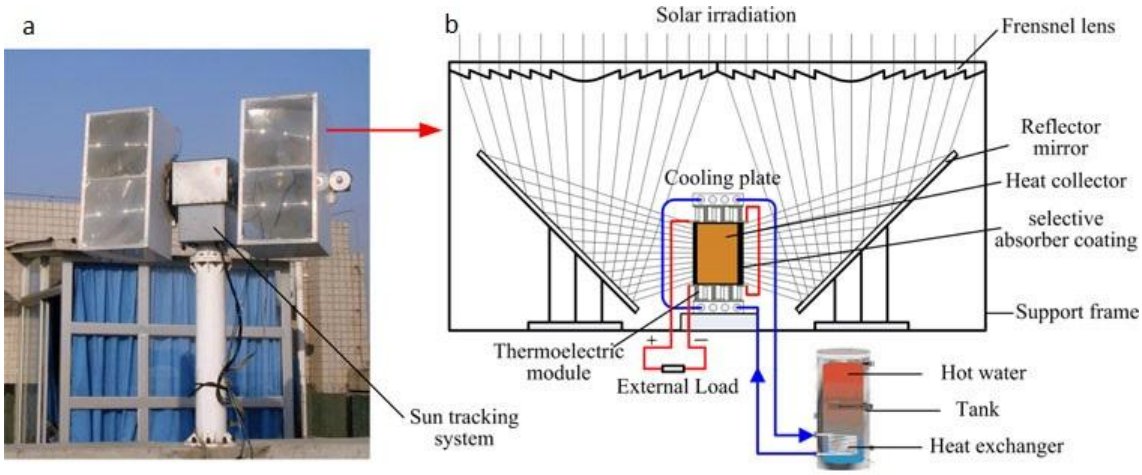

Figure 2.8 : (a) An experimental prototype of the concentration solar thermoelectric generator system done by Li et al . (b) Details of the CTG unit[28]

Yazawa et al [29], has proposed a co-generation system to produce electricity from a concentrated solar thermoelectric system and the hot water generated from the active cooling system, a theoretical model and a feasibility study has been carried out for the design. The change of the conversion efficiency of the thermoelectric system and the heat sink temperature with regard the change of the concentration ratio has been studied, it has been found that the best concentration ratio for the best conversion efficiency is 200 suns, a comparison of this system to conventional concentrated photo- voltaic system has been done.

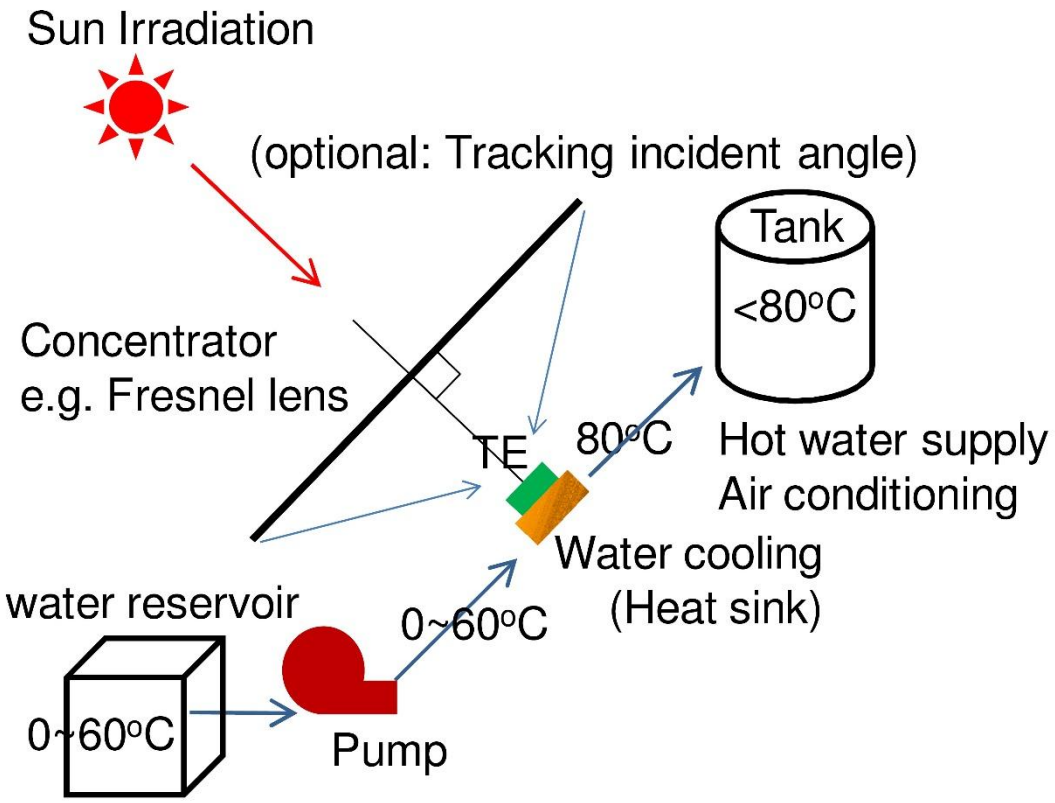

Figure 2.9 residential photo-thermo-electric cogeneration system[29]

Miljkovic has conducted a study of a concentration solar thermoelectric system using a parabolic concentrator, the thermoelectric device is inside the absorber tube, the hot side of the thermoelectric is coated with a selective absorber material, the cold side is attached to thermosyphon tube where the heat is transferred to from the thermoelectric cold side to a working fluid. The use of three thermoelectric material is investigated in the study, Bismuth telluride, lead telluride and silicon germanium, a temperature range from 300K to 1200K is investigated and a concentration ratio from 1 to 100 suns. The maximum combined efficiency achieved by the system was 52.6% at concentration ratio of 100 for silicon germanium thermoelectric material, 48.1% for lead telluride thermoelectric material, and finally 34.4% at and 50 suns for Bismuth telluride material [30].

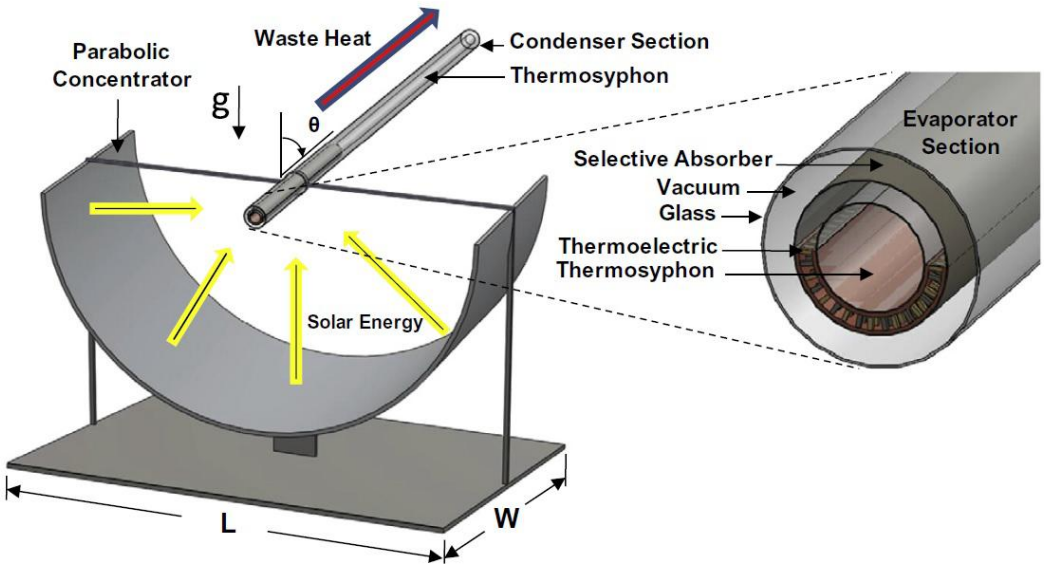

Figure 2.10 Schematic diagram of the concentrated solar thermoelectric system de- signed by Miljkovic et al [30]***.***

X.F Zheng et al[31], has designed a co-generation system for domestic use. The system get advantages of a hot water comes from solar collector mounted on the roof and supply it to the hot side of the thermoelectric module. A prototype of the co- generation thermoelectric module was constructed, and the performance was measured, a Bi2 Te3 semiconductor based thermoelectric module with dimension of 40 mm *40 mm * 3.8 mm consist of 127 thermo-elements was used. The result shows that the maximum temperature difference was 130 °C and the efficiency was 3.9%.

Kraemer et al [32], has introduced a new way to improve the efficiency of the thermoelectric generator using conventional thermoelectric material and what he called a thermal concentration instead of optical concentration. an experimental study has been conducted ,the results then compared the results of the simulation , it is been found that the maximum efficiency of the system is 4.6% and 5.2% at solar radiation 1 kW/m2 and 1.5 kW/m2 respectively, the vacuum adds more stability of the power supply from the system when the sky is partially blocked by the clouds, this because to the elimination of the convection heat transfer losses from the system.

He et al [33] integrated the thermoelectric generator with a heat pipe evacuated tube, the thermal efficiency is predicted by a mathematical model as well as the electrical efficiency of the thermoelectric generator. An experiment to obtain the thermal and the electrical efficiency of the system has been also conducted. For the experiment setup a commercial thermoelectric generator has the dimension of 40mm*40 mm*4 mm has been used, the results obtained from the experiment shows that the system has a maximum power generation of 0.98 W achieved at 850 W/m2 solar radiation and cooling water temperature of 30 °C. at solar radiation 780W/m2 a maxi- mum power generation achieved was 0.78 W when the cooling water temperature was 40 °C.

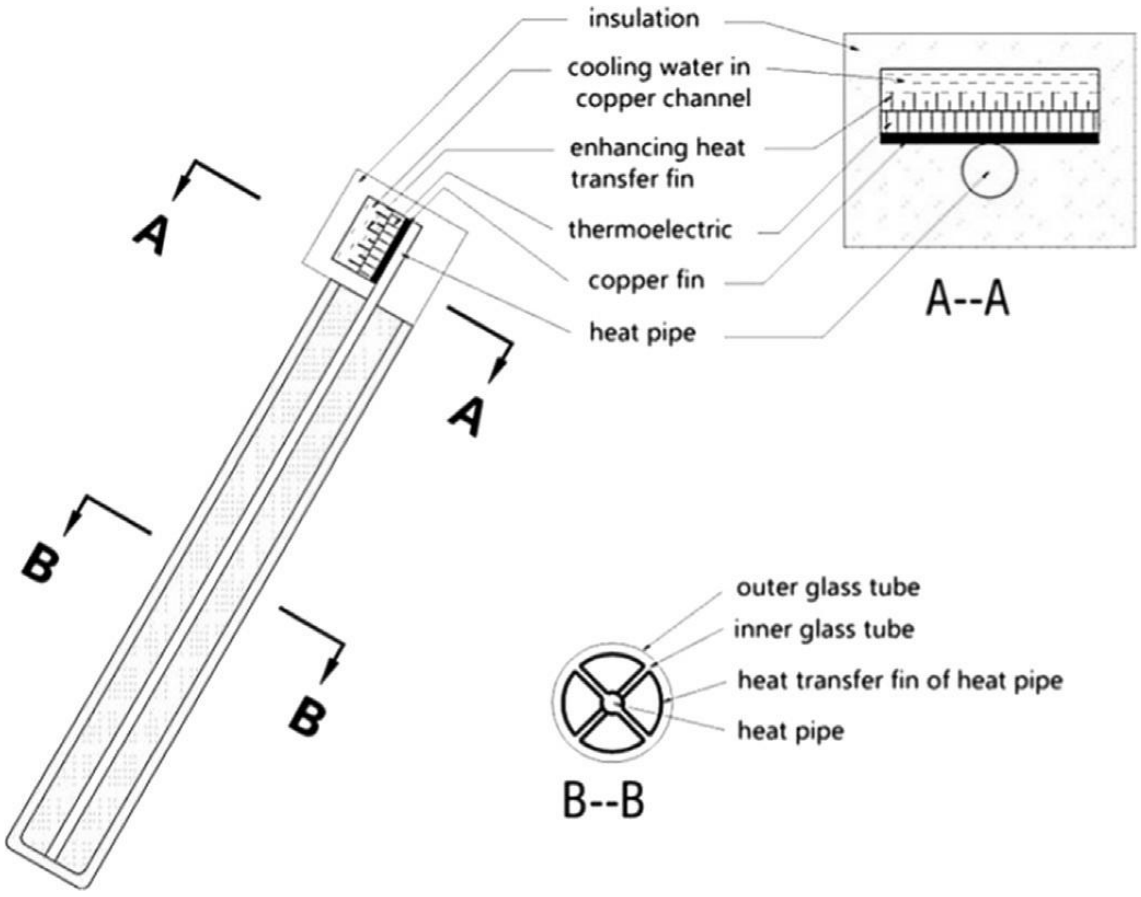

Figure 2.11 the integrated thermoelectric generatior with heat pipe evacuated tube designed by He et al[32].

Singh et al [34], integrated thermoelectric system with a solar pound for power generation, in his study the thermal energy stored in the bottom of the solar pound that has been collected from the sun is suggested to be used for power generation from thermoelectric device. the thermoelectric system gain the temperature difference from the temperature difference between the lower convective zone (LCZ) and the upper convective zone (UCZ) the solar pond, where the hot side of the thermo- electric module uses the high temperature in the lower convective zone, and the cold side temperature uses the low temperature in the upper convective zone. The heat is transferred from the bottom of the solar pond to the top of the solar pond where the thermoelectric module installed using a thermosyphon. Out an indoor test for the proposed system has been carried out, a test rig to simulate the thermosyphon thermoelectric integrated system has been built. The result of the test shows that a maximum output of 3.2W has achieved at a temperature difference of 27 °C from the 16 thermoelectric modules, the short circuit current and the open voltage circuit are 0.4A and 26V respectively.

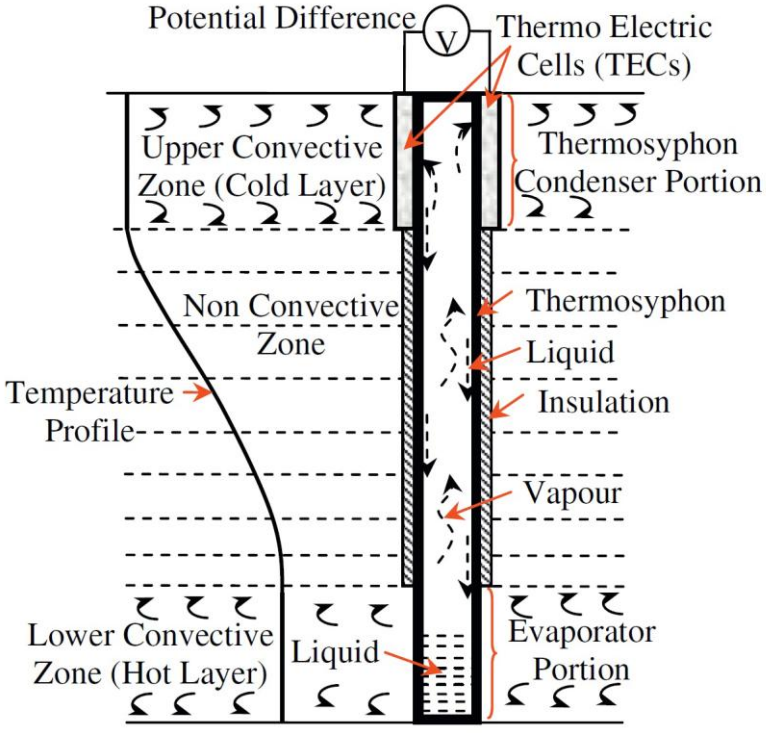

Figure 2.12 Thermoelectric Thermosyphom system proposed by Singh [34]

Xiao et al developed a 3-D finite element model to predict the performance of thermoelectric power generators, two thermoelectric materials have been studied, Bismuth telluride and filled-skutterudite. a comparison of the change of the efficiency with the change of the temperature difference of both materials over the range of the temperature each material can stand, figure 13 shows how the efficiency of Bismuth telluride and filled-skutterudite change with the temperature difference [35].

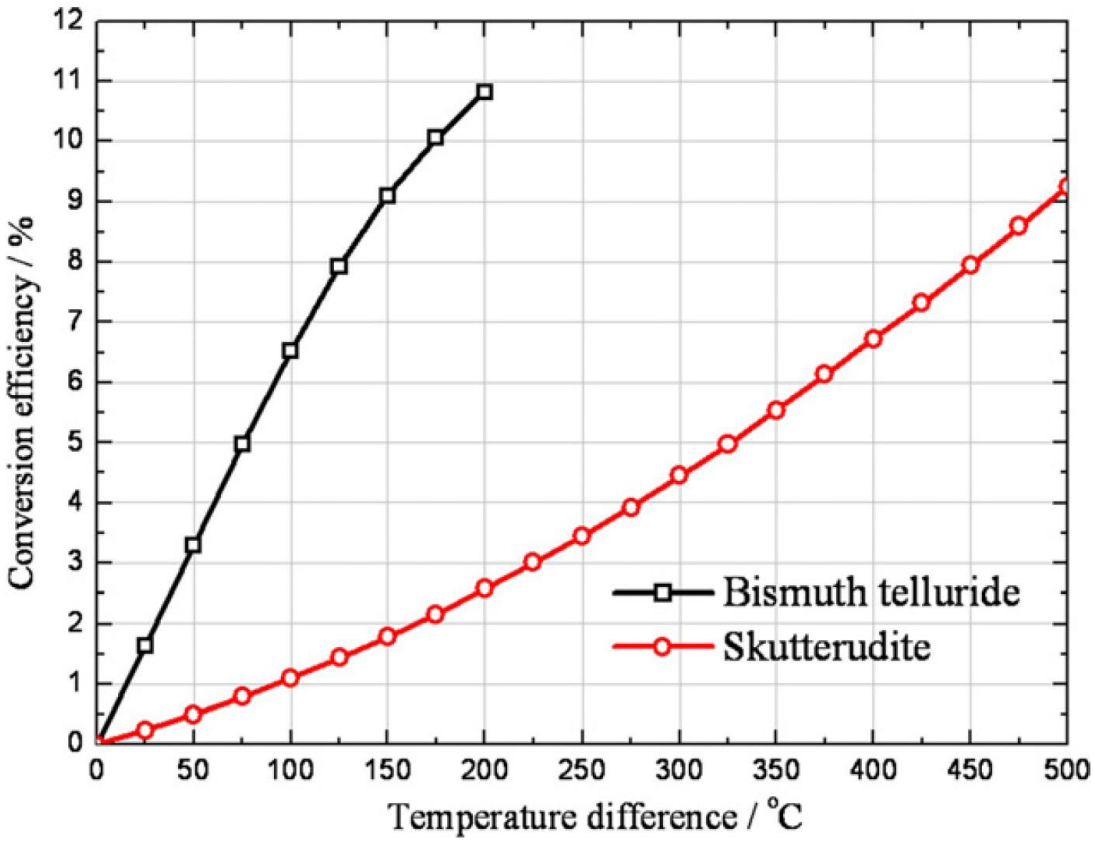

Figure 2.13 Efficiency of Bismuth telluride and filled-skutterudite as a function of the temperature difference [35]

Verma et al [36], developed a mathematical model to a hybrid integrated photo-voltaic thermoelectric generation system. The modelling of the co-generation system done using MATLAB/Simulink. The system consists of a thermoelectric

module attached to the back of PV panel, the system uses the temperature difference between the ambient temperature and PV panel to generate power from a thermoelectric generator. In additional benefit to the power generation from the thermoelectric module, a rise of the conversion efficiency of PV panel is achieved by lowering the temperature, as the efficiency decreases with the increase of the temperature of the PV module.

2.2.5 Thermoelectric cooling

Thermoelectric cooling systems has many advantages over conventional ways, such as lightweight, reliable, noiseless, absence of refrigerant [37], and it has been proposed for wide range of application, from a small cooling box to a space conditioning system.

Dai et al[38], has designed and constructed a solar thermoelectric refrigeration system to be used for outside cooling purposes. Two principles taken in account when the system has been designed, firstly to be light weight (portable), secondly to be cost economic. the result of the experiment conducted show that the system is able to maintain a temperature between 5 and 10 C, and the COP is 0.3.

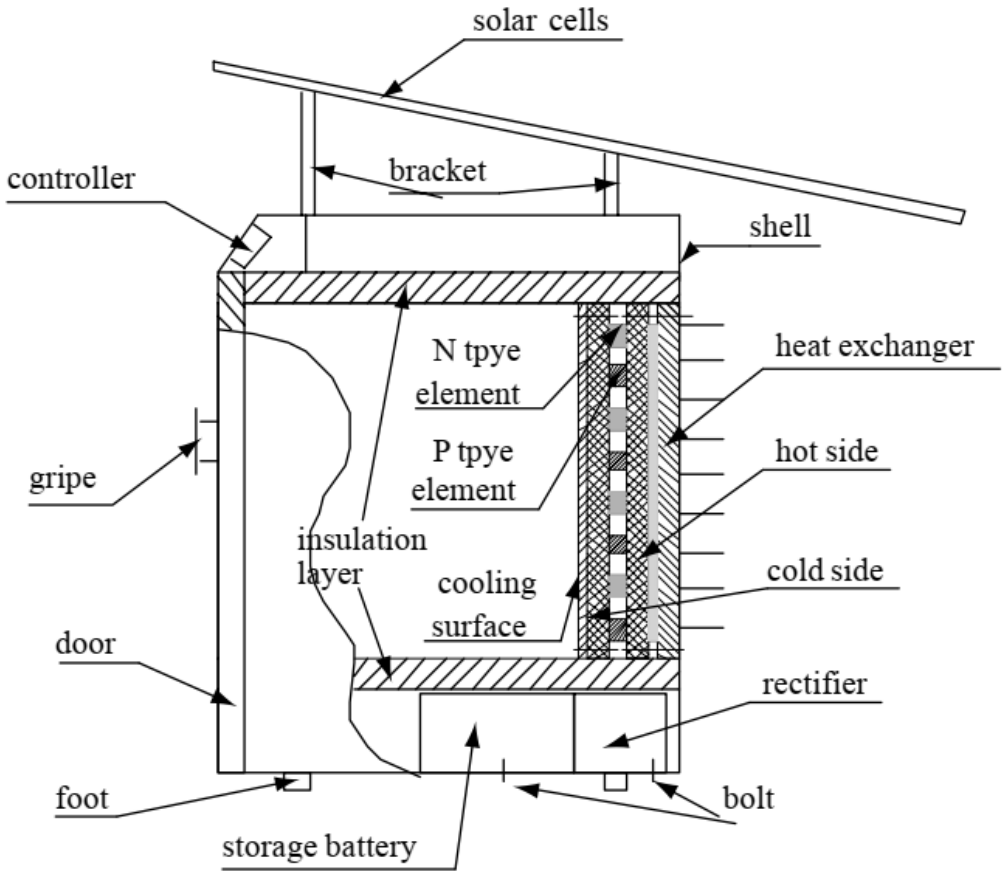

Figure 2.14 Schematic of solar cell driven, thermoelectric refrigerator designed by Dai et al[38]

Min et al [39], studied a various thermoelectric refrigeration system for domestic use, the COP found to be from 0.3 to 0.5 for operation temperature of 5 °C and outside environment temperature of 25°C.

Sabah et al [40], designed a solar thermoelectric refrigeration system for rural area where electricity is not accessible in Oman, the volume of the refrigerator is 0.5 Liter, heat sink and cooling fan are used to enhance the heat transfer to the environment from the hot side of the thermoelectric, the results show that the temperature dropped from 27 to 5 inside the refrigerator in just 44 minutes, and the COP of the system was 0.16.

Putra [41], investigated the use of thermoelectric refrigeration for vaccine carrying the system uses heat pipe and cooling fan to help in heat dissipation from the hot side of the thermoelectric module to the environment. According to Putra the temperature required for maintaining vaccine is ranged between 2 and -8 °C, and the system reached a minimum temperature of -10 °C which indicate that the system is able to maintain the vaccine at the desired temperature.

Adeyanju et al [42], designed and manufactured a thermoelectric refrigerator for fast beverages chilling. it has been found that to cool 474 ml of water to the desired temperature of 6 C in 2 minutes 6 Thermoelectric module are needed, by increasing the cooling time to 4 minutes only 4 thermoelectric modules are needed.

Lertsatitthanakorn et al [43], studied the cooling performance of thermoelectric ceiling cooling panel (TE-CCP). the system consists of 36 thermoelectric modules attached to an aluminium ceiling panel, active cooling using water and copper heat ex- hanger is used to extract the heat released from the hot side of the thermoelectric modules. the system used to cool a test chamber of 4.5 m3, and the system is tested to identify if it is meet the ashrea standard-55, the results show that the standard was met when the system operating at 1 A current with cooling capacity was 201.6W, and COP of 0.82.

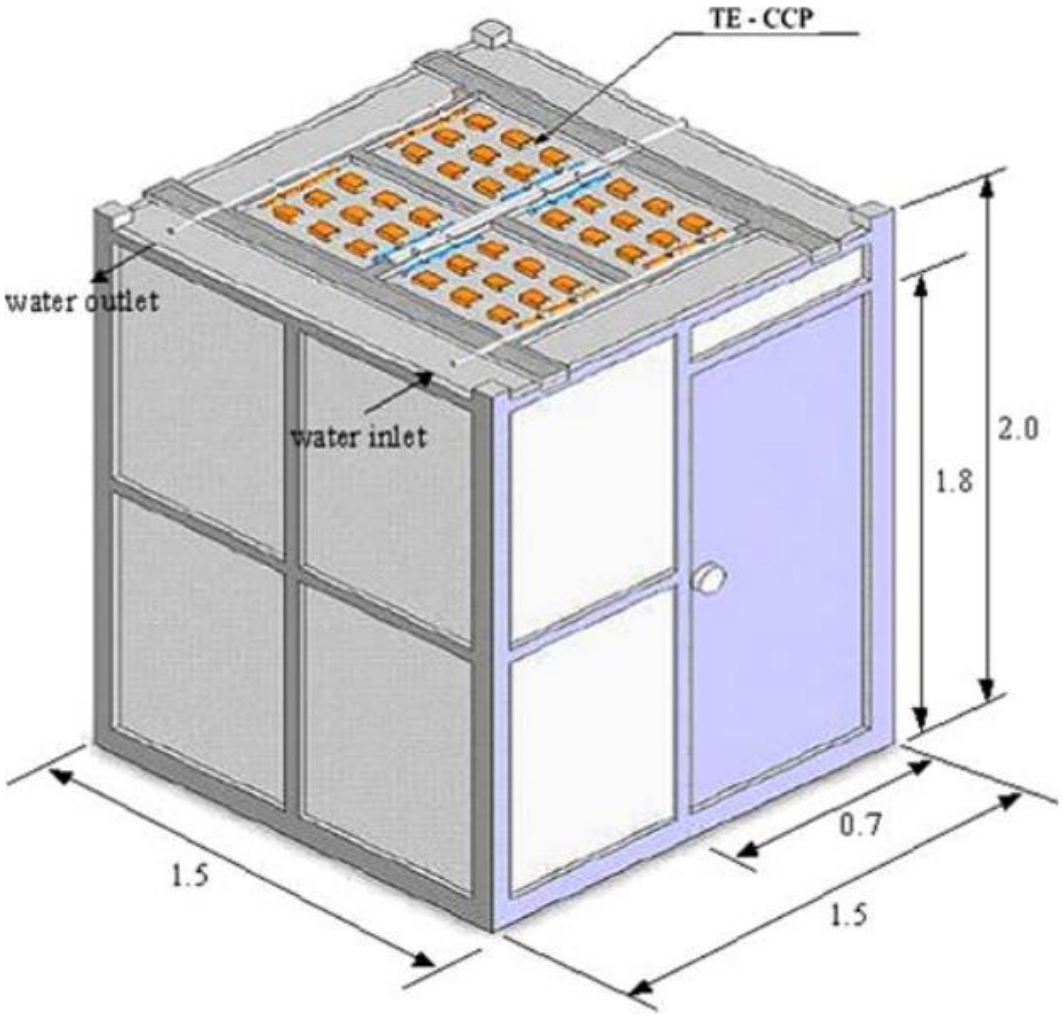

***Figure 2.15 Position of the TE-CCP on the test chamber designed by Lertsatitthanakorn et al** [43].*

Liben et al [44], designed and experimentally evaluated a thermoelectric cooling device for small-scale space conditioning applications in buildings. A theoretical study was conducted first to identify the optimum operation condition, the condition obtained then applied to the laboratory experiment. the system designed contain 8 thermoelectric modules, at a current of 4.8A the system was producing up to 220W of cooling and the COP of the system was 0.46. using solar energy was also investigated, it has been found that for the system with PV panel to be able to compete with the system use electricity from the main, the cost of PV panel should be less than £1.25 per Watt.

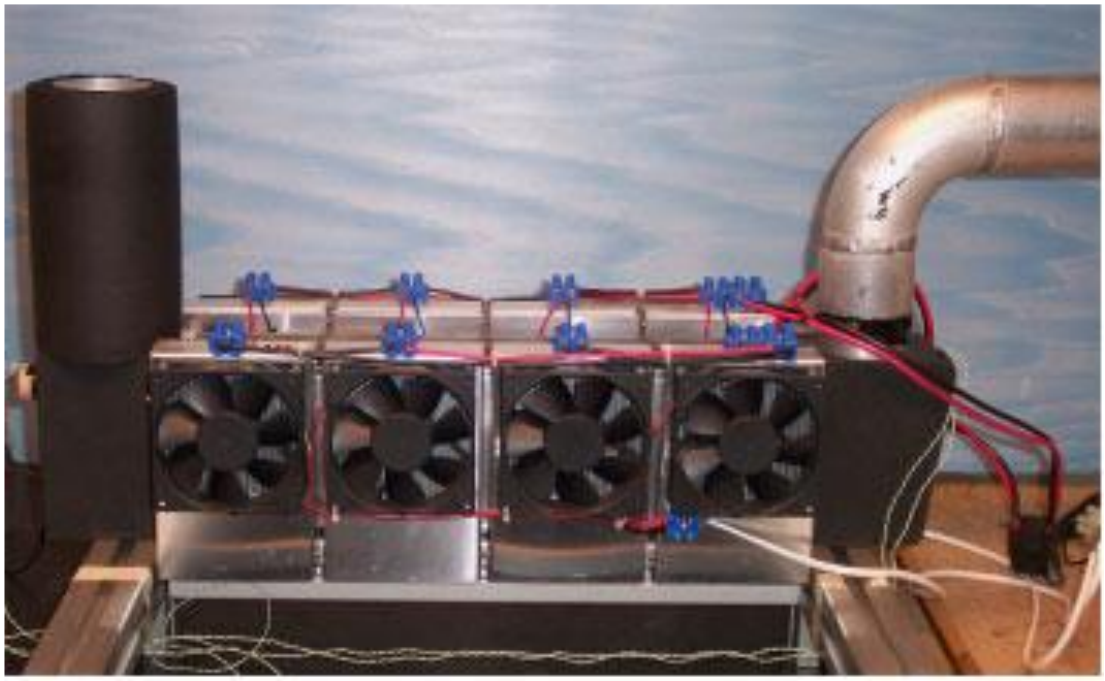

Figure 2.16 Photo of thermoelectric unit for small-scale space conditioning applications designed by Liben et al*[44].*

Bansal et al [45], compared thermoelectric refrigeration unit with identical capacity vapor compression and absorption refrigeration systems. the volume of each system is 50 litres, the results reveal that the most energy efficient system is vapor compression refrigeration with COP of 2.59, then comes the thermoelectric refrigeration with COP of 0.69, and finally the absorption system with COP pf 0.47. cost analysis also conducted for the total cost of the systems over the life time, the vapor compression system found to be the cheapest with cost only $506, followed by the thermoelectric system ($1382) and lastly the absorption system ($1387.4).

2.3 Water Desalination Technologies

Despite the fact that water cover almost 71%of earth surface, water shortage is becoming a serious problem for many countries around the world [46]. It is estimated that one third of the world population currently live in severe water stress areas [47]. Desalination of water is one of the most effective ways to desalinate salt or brackish water and provide clean drinkable water desalination can be divided into two categories:

1. Thermal technologies

- Multiple-stage flash distillation (MSF)
- Multiple effect distillation (MED)
- Vapor compression (VC), mechanical Vapor compression (MVC) and thermal Vapor compression (TVC).
- Solar Distillation

2. Membrane technologies

- Reverse osmosis (RO)
- Electrodialysis (ED)

2.3.1 Multiple-stage flash distillation (MSF)

In MSF desalination technology the evaporation of the water takes place within the liquid bulk not on the hot surface of heat exchanger tubes [48]. Water is heated under pressure to prevent it from boiling, then it is released in the first chamber (flash chamber) where the pressure is lower than the vapor pressure of the water and sudden evaporation occur (flashing). The water then enters the second stage where the pressure is lower, and flash evaporation takes place. the

evaporated water is condensed, and the heat is transferred to the feed water[49]. the capacity of MSF unit ranges from 10000 to 35000 m^3/day [50] , and the cost of water produced is between 0.84 to 1.6 $/$m^3$.day [51].

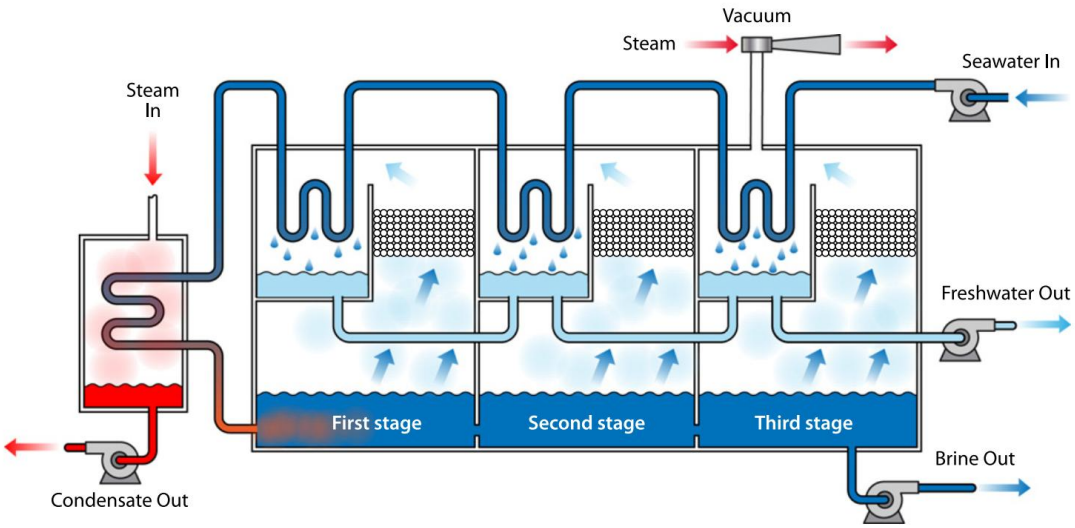

Figure 2.17 Multiple-stage flash distillation (MSF) [16]

2.3.2 Multiple effect desalination (MED)

MED is a combination of multi single effect evaporation, the vapor produced in the first effect is used as a heating medium in the next effect. it works on the principle of reducing the pressure in every effect to allow the feed water to boil multiple times without the need to supply any additional heat after the first stage[52]. the energy to heat the water can come from different sources like solar, power plant waste heat, and fossil fuels. MED capacity ranges from 600 to 30000 m^3/day, and the cost of water produced is between 1.21 to 1.59 $/$m^3$.day [51].

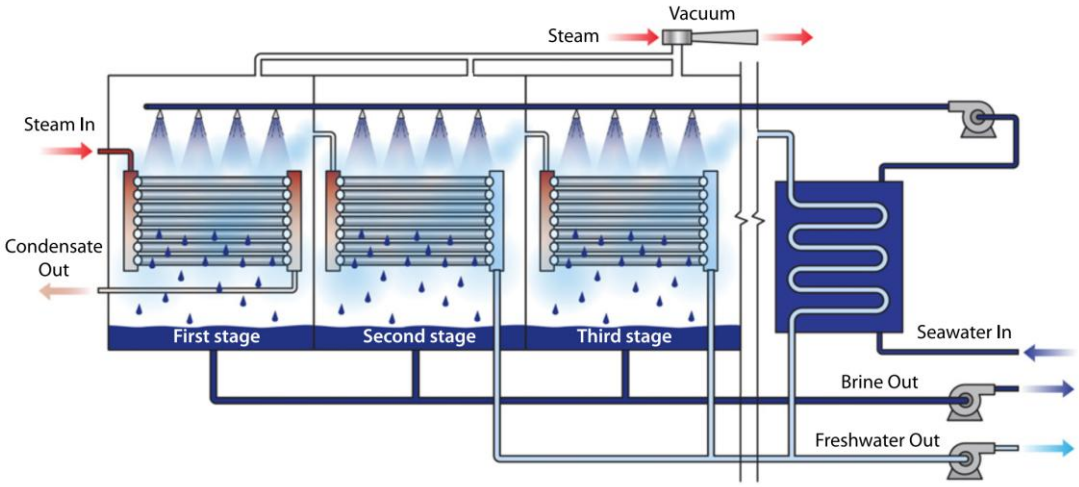

Figure 2.18 Multiple effect desalination (MED) [16]

2.3.3 Vapor compression.

Vapor compression process can be achieved by two methods, Mechanical (MVC) or thermal vapor compression (TVC). The process itself is similar to MED, the only difference is that the steam generated in the stage is compressed, then returned to the same stage where it is generated to condenses and give it is latent heat to evaporate additional amount of the brine[52]. Vapor compression processes are especially useful for small to medium installations [60] the capacity of MVC ranges between 100 and 3000 m3/day, and for the (TVC) from 10000 to 300000 m3/day [50]. The energy consumption is 12 kWh/m3 and 16 kWh/m3 for (MCV) and (TVC) respectively[50], [53].

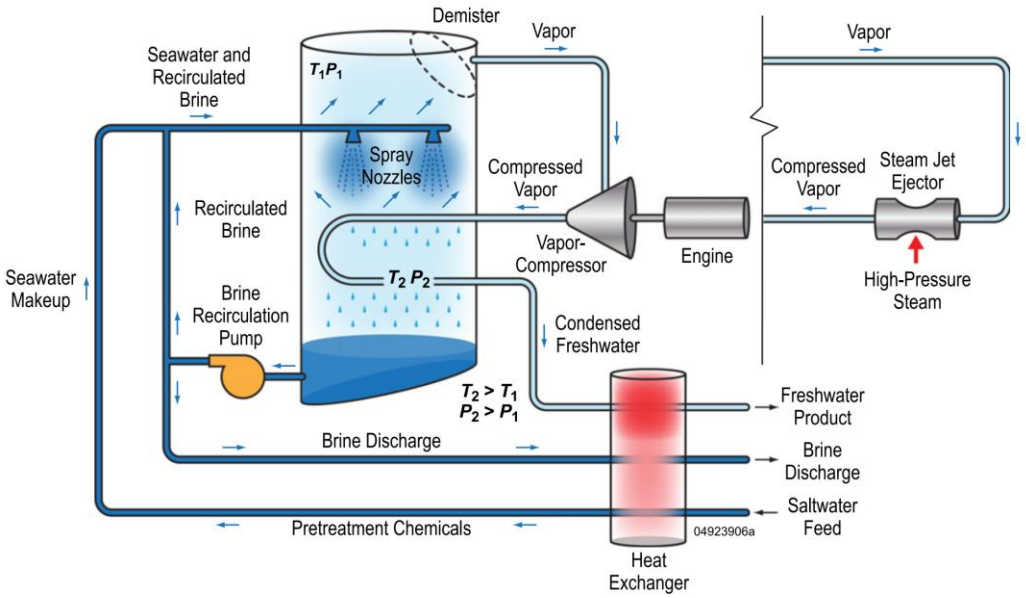

Figure 2.19Vapor compression [16]

2.3.4 Reverse osmosis (RO)

Osmosis is a natural processes happen when water flow through a semi-permeable membrane because of a difference in solute or Dissolved mineral concentration across the membrane, naturally the osmosis occurs when water flows toward the saline solution through a semi-permeable membrane, by applying pressure to the compartment that contains the salt water the process can be reversed, and water will flow from the saline solution to the unsalted water, this is the process of Reverse Osmosis (RO) [49], [52] The average reported energy consumption ranges from 3.7 to 8 kWh/m3 [50], [54]. the cost of water produced by (RO) is ranged between 1.06 to1.36 $/m3.day[51].

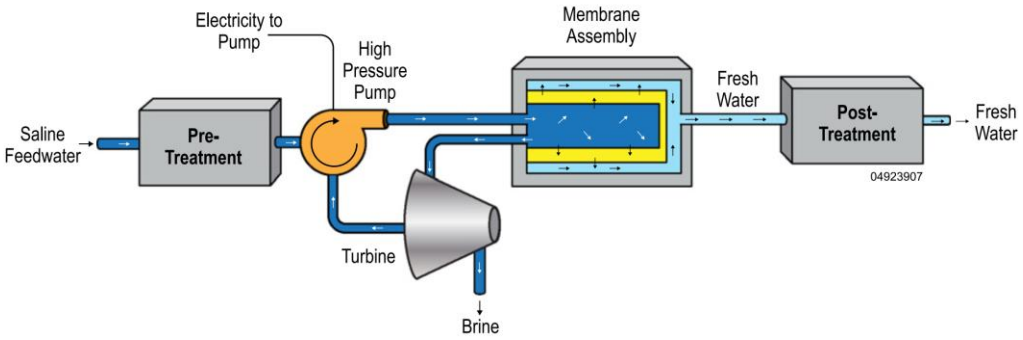

Figure 2.20 Reverse Osmosis (RO) [16]

2.3.5 Electrodialysis (ED)

Electrodialysis (ED) is an electrochemical process uses electrical potential difference as driving force to move salt ions from water through a membrane [55]. electrodialysis cell compromise of a number of small compartments which water is pumped through, these compartments are separated by membranes that either anion-permeable or cation- permeable electrodes are placed on the sides of the compartments, when electricity applied to the electrodes, negative salt ions move through the anion-permeable membrane to the positive electrode, and positive salt ions move through the cation- permeable membrane toward negative electrodes [52].

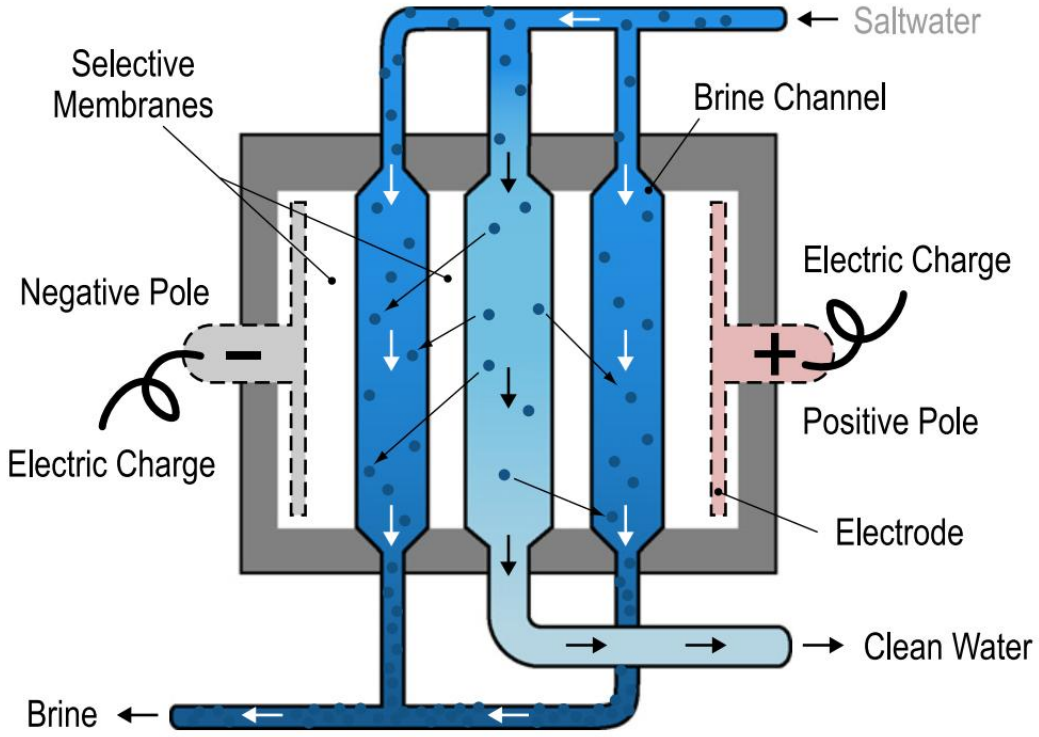

Figure 2.21 Electrodialysis (ED) [16]

2.3.6 Solar Distillation

Solar distillation considered one of the most common distillation system due to it is simple design, no pollution, and maintenance free. Solar distillation is suitable for sunny region of the world, such as North Africa, and the southern region of the US. There are number of solar distillation system have been developed over the years, Sadineni et al [56] developed a design to increase the water surface area that can be exposed to the solar radiation, the weir-type design tested in Las Vegas and it shown in Figure 2.22. an insulation is used to minimize the heat loss from the sides and the bottom of the unit. The water production from both single and double glass pane measured during August and September was 5.5 L/m^2 and 5.5 L/m^2 per day respectively.

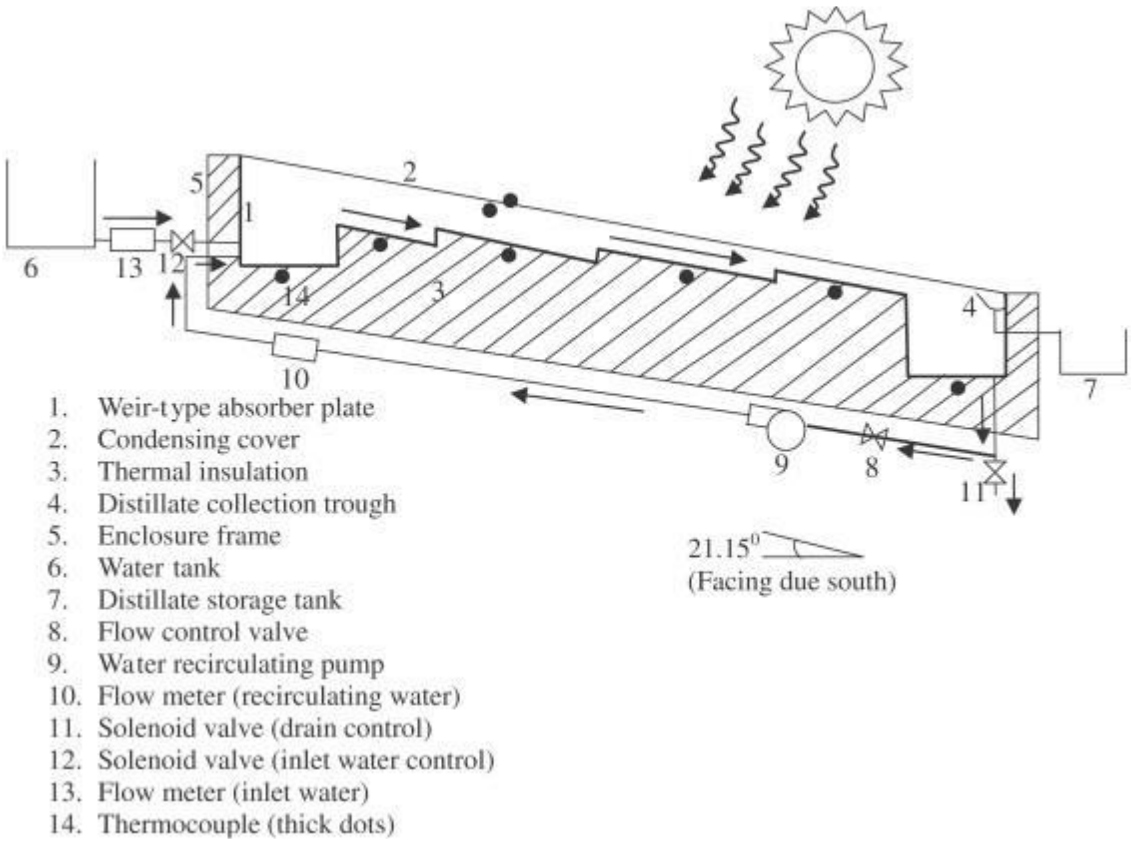

Figure 2.22 Schematic of the weir-type distillation unit and its components [56]

Kumar et al [57] Combined the use of PV-T with convenstional solar still, the designed system uses the PV-T to power a pump and heat the water to increase it is temperature. Two configuration where investigated, Passive design where the water is heated directly by the solar radiation, and a hybrid design where the sample water is heated by direct solar radiation and by the heat dissabated from the back of the PV panel, this allow to use the thermal energy that usually wasted from the PV panel. this technique allows the designed system to have more than 3.5 times the productivity of the passive one. Also the power consumption can be reduced by operating the pum less hours, it is found that sves 43% of the power consumption hen the operating hours reduced from 9 to 5. The maximum distilation yeild of the hybrid active solar still was 0.68 L/m^2h.

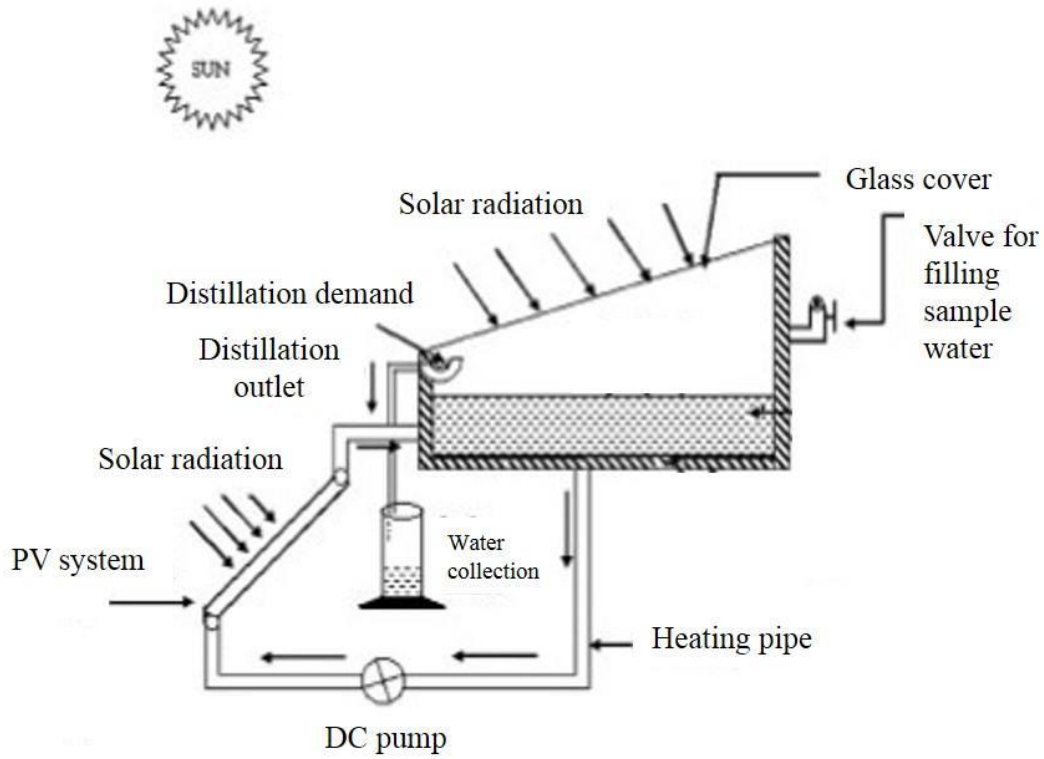

Figure 2.23 Schematic diagram of an integrated hybrid PV active solar still[57]

Tiwari et al [58], evaluated the heat transfer coefficient for three different water depth for both solar still types (single slope, double slope), in both season Summer and winter. The water depths investigated was (0.01 m, 0.02 m, 0.03 m) using various thermal models. Figure 2.24 and Figure 2.25 show the cross-sectional view of the single slope solar still and the double slope solar still.

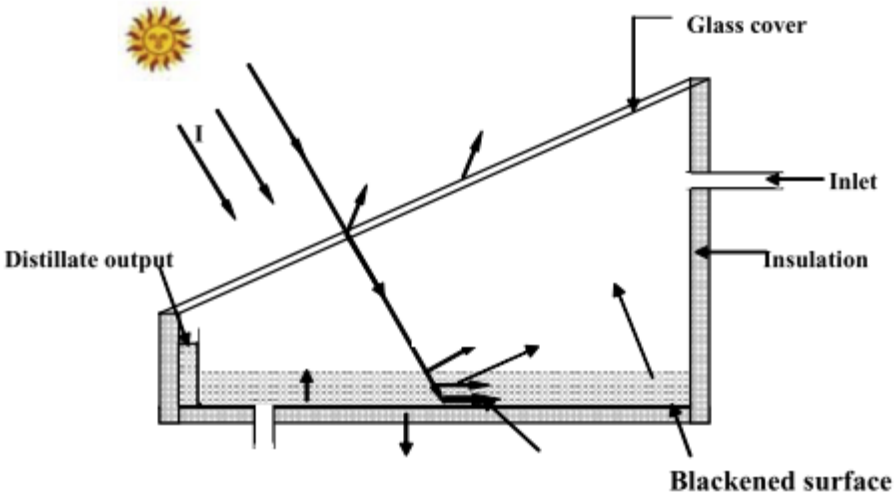

Figure 2.24 Cross-sectional view of a single slope passive solar still [58]

The experiment was carried in composite climate of India (New Delhi). The study concluded that the average value of the internal heat transfer coefficient are 8.837 W/m^2.K and 8.19 W/m2.K for single and double slope solar still, respectively. The annual yield of the single slope solar still is 499.41 L/y and for the double slope solar still is 464.68 L/y.

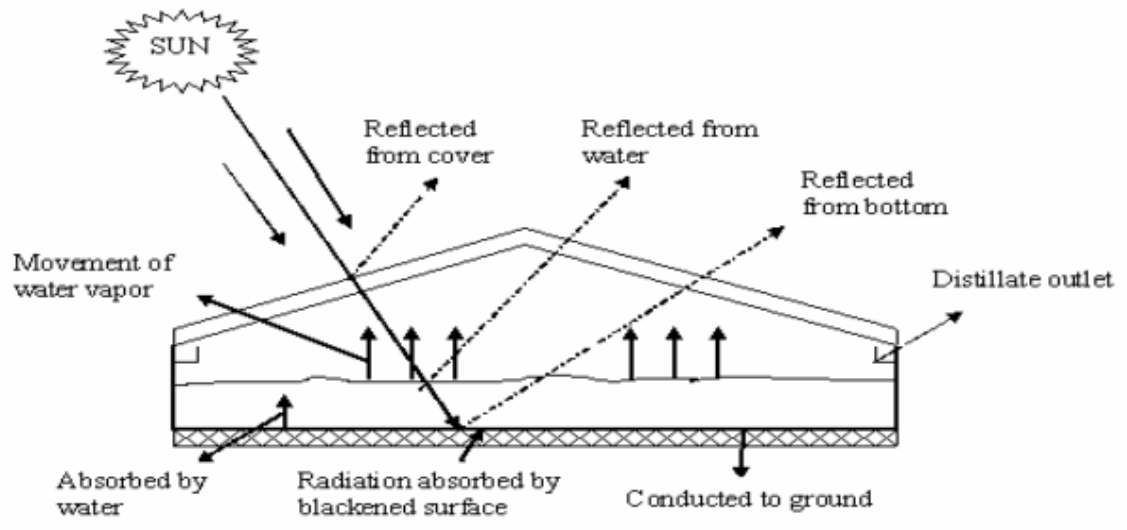

Figure 2.25 Cross-sectional view of a double slope passive solar still [58]

Two processes that the solar thermal distillation system depends upon, evaporation and condensation. Both processes rate depends on convictive heat transfer. The rate also changes with the interface area, the temperature difference between the fluids and the condensing surface, and the heat transfer coefficient[59], [60], [61].

2.3.7 Thermoelectric Distillation

The use of thermoelectric in freshwater generation can be divided into three ways, to enhance the condensation, as an auxiliary heating to assist solar distillation, and in Humidification Dehumidification system to extract water from humid air. In this section a review of some of the work done to employ the thermoelectric in freshwater application will be presented.

Esfahani, et al [62], designed and constructed a small portable solar distillation, many ways to improve the system were investigated in this study. due to the

small area of the absorbed, an active solar heating system is used in order to increase the water temperature. The system is divided into two section, evaporation zone and condensation zone, the water is circulated between the evaporation zone and the parabolic solar collector by a small pump. A sprinkling system is used also to increase the evaporation rate inside the system, thermoelectric cooling is used to enhance the water condensation. The maximum efficiency of the system was 13%, and the daily productivity of the system was 1.2 L/m2 over the period of the test .

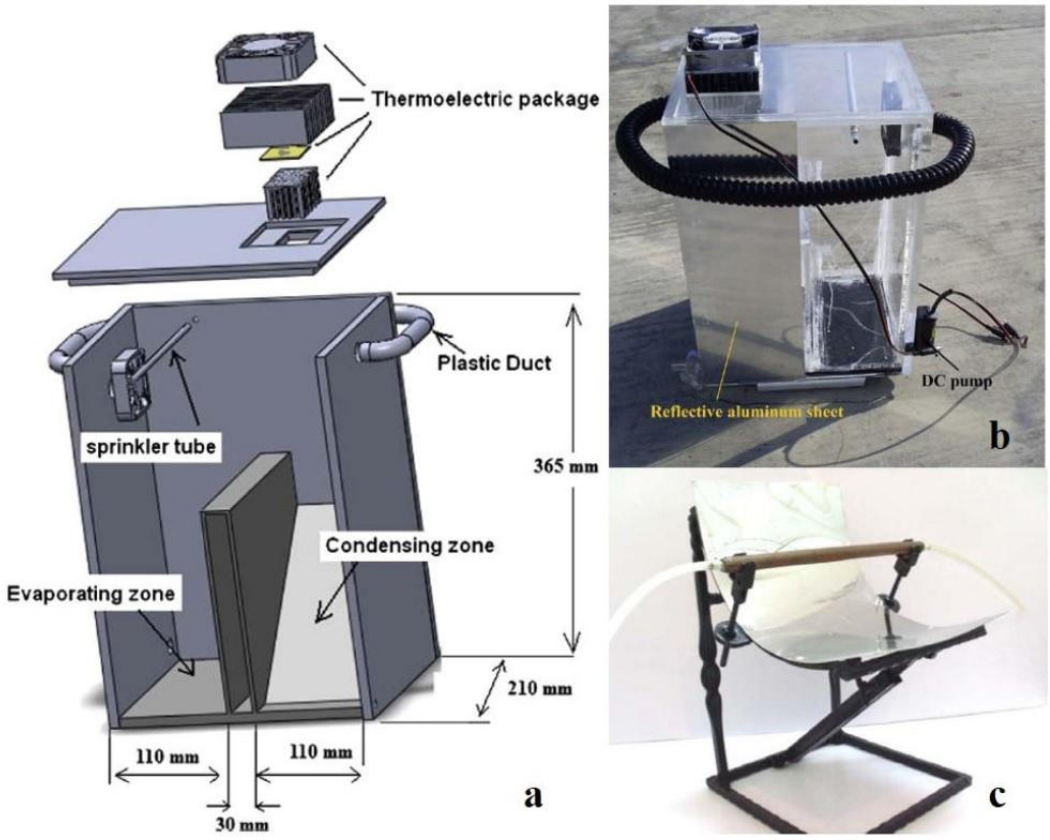

Figure 2.26 a) a schematic of the distillation system, b) photo of the system, c) parabolic solar collector used to heat the water *[62].*

Joshi et al [63] investigated the use of thermoelectric in HDH system to generate fresh water, the claim was made is that this system will be suitable for people living on coastal area whcostalere the relative humidity of air is above 60%. Ten thermoelectric modules of a dimension 0.04 * 0.04 m^2 are attached to a 0.7 m cooling channel, heat sinks are attached on both sides of the thermoelectric to

enhance heat transfer rate, 4 axial fans are also used on the hot side, the cooling channel is placed in air conditioning test rig to control the relative humidity. the study conducted to investigate three parameters, relative humidity, air flow rate, and the current supplied to the thermoelectric. the result shows that the productivity of fresh water is directly proportional to all the three parameters, the use of heat sink on the cold side enhanced the productivity of the system by almost 81% compared to the system without it.

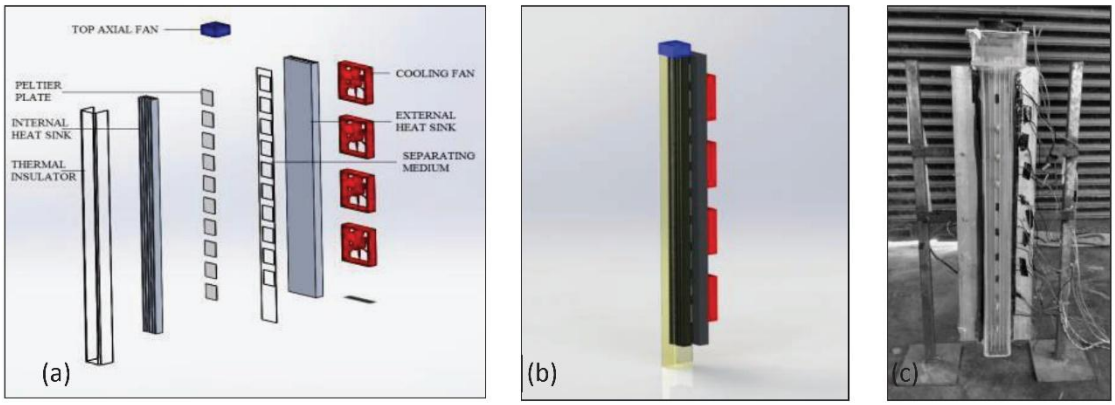

Figure 2.27 a) schematic of the system component, b) schematic drawing of the system,c) photo of the system *[63]*

Nazari, Safarzadeh, et. al. [64]. carried out study to improve the performance of single slope solar still by employing thermoelectric cooling channel. It was found that when the thermoelectric glass cover cooling channel is employed, the distillated water rises 41.8% compared with the conventional solar still.

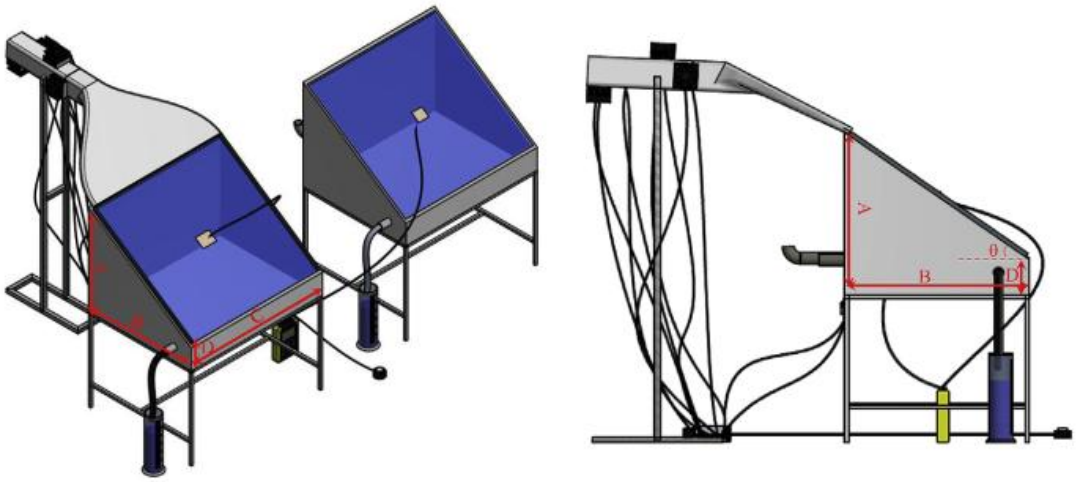

Figure 2.28 Solar distillation systems with and without cooling channel [64]***.***

Yildirim et. al [65]. designed a humidification dehumidification desalination unit (HDH) using the hot and the cold side of thermoelectric cooler, water is heated using the hot side of the thermoelectric then it is distributed in inside the humidifier by spreader where it comes into contact with air forced by a fan. The humidified air enters into the dehumidifier and water vapor condensed by aluminium heat sink fixed on the cold side of the thermoelectric. The daily water output of the system was 143 g, and the COP of the system was 0.78.

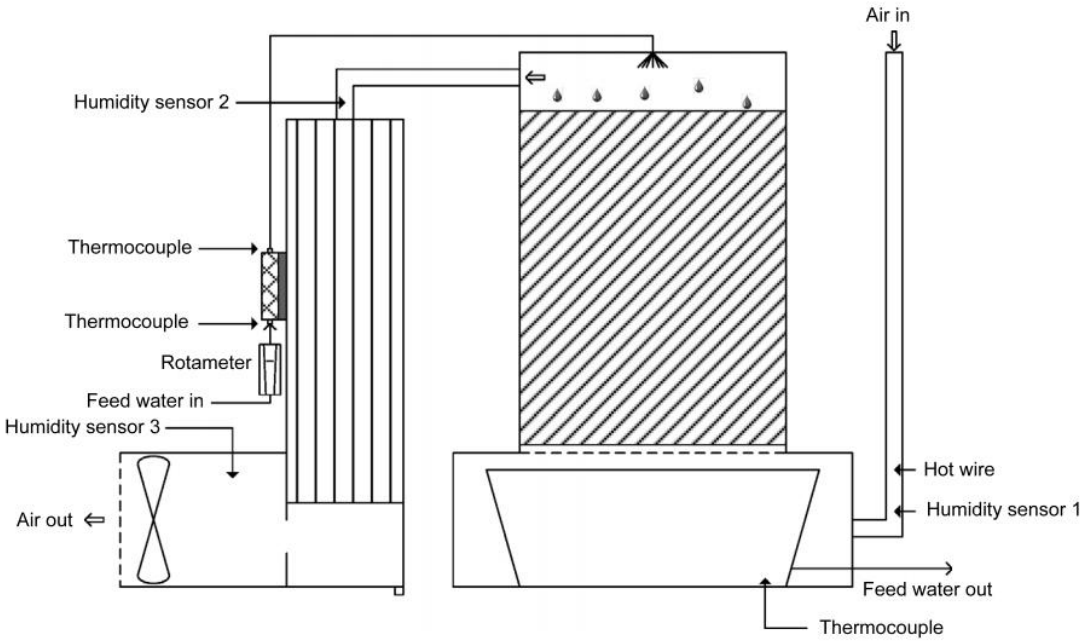

Figure 2.29 A schematic diagram of HDH experimental [65].

Al-Madhhachi et al [66]. designed and constructed a novel thermoelectric distillation system with effective use of both sides of the thermoelectric. The evaporation zone made from 8mm Plexiglas, the condenser which mounted inside the evaporation zone and on the cold side of the thermoelectric made from aluminium heat sink has an area of 0.041 m2 with 10 fins, which are 25 mm long and 1.5 mm thick. The hot side of the thermoelectric is used to heat the water through a copper heat exchanger, the thermoelectric module has an area of 62* 62 mm and manufactured using Bi2 Te3 alloys. A small pump is used to circulate the water between the evaporation zone to the hot side heat exchanger, two power supply used to power the pump and the thermo- electric module. The results of experiments show that the average water production is 28.5 mL/h with a specific energy consumption of 0.00114 kW h/mL.

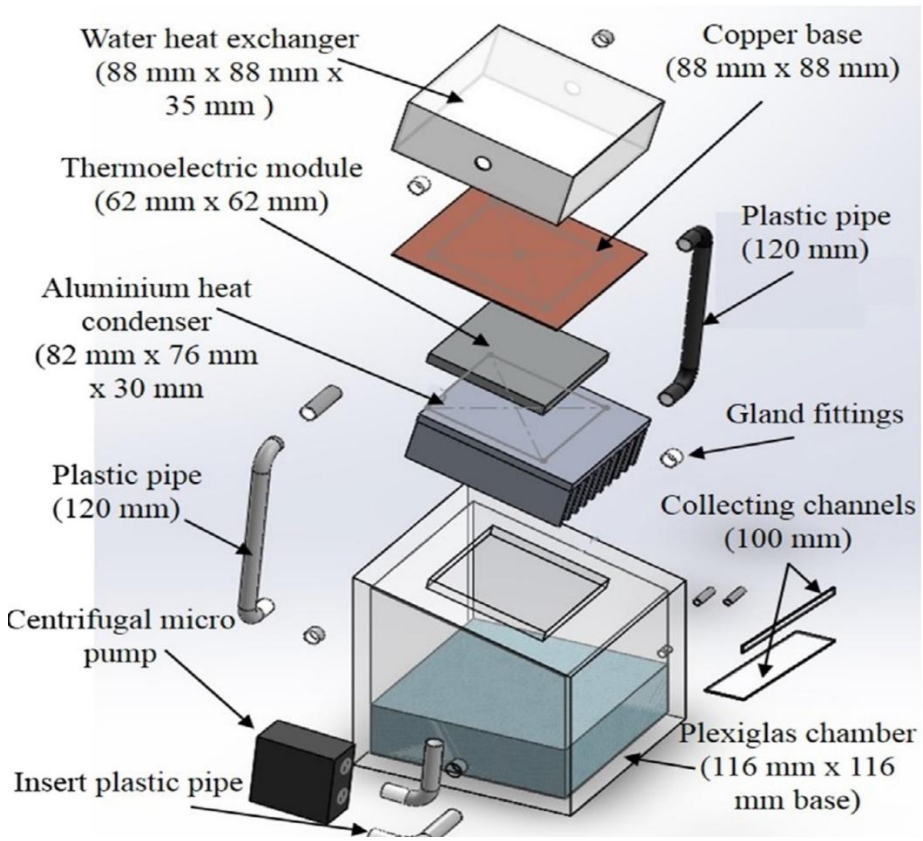

Figure 2.30 schematic drawing of the thermoelectric distillation system designed by Hayder[66] ***.***

Al-Madhhachi et al [67]. studied the factor that affect the productivity of the thermoelectric distillation, an experimental investigation was performed to investigate the influence of evaporation temperature, vapour volume, Peltier current and input power on the water production rate. The results of the experiment show that an in- crease in the sample water temperature from 30 °C to 60°C led to an increase in total water production by 47%. In addition, an increase in total water production by 58% was obtained by reducing the vapour.

Rahbar et al [68]. designed asymmetrical solar still that uses thermoelectric modules to cool the vapor. The designed system uses three thermoelectric modules (TEC-12708) mounted on aluminium plates act like a condenser, thermal paste is used to help with the heat transfer between the aluminium condenser and the thermoelectric modules. Heat sink is attached to the hot side of the thermoelectric module to help dissipate the heat using forced conviction by employing three fans each has power rating of 2 W. the daily rates of water production were 500 and 225 ml corresponding to solar intensities of 25500 j/m^2 and 20500 j/m^2 , respectively.

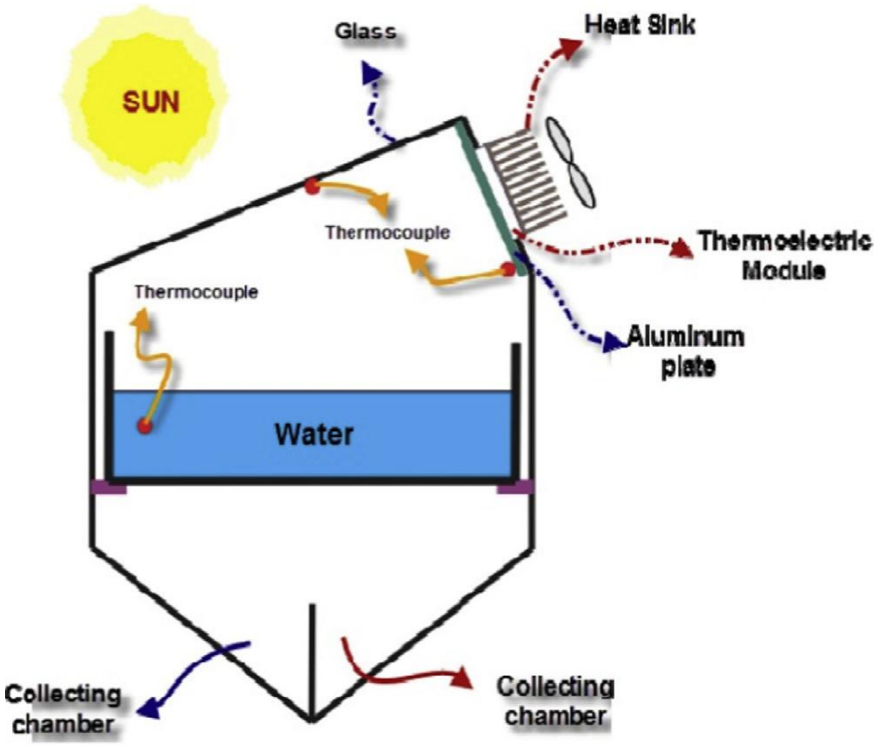

Figure 2.31 schematic drawing of the asymmetrical solar still *[68]*

The advantages and disadvantages of the desalination technologies described in the previous section is summarised in Table 2-1 [69], [70], [71], [72], [73], [74]

Table 2-1 The advantages and disadvantages of current desalination technologies

Technology	Advantages	Disadvantages
Multi-Stage Flash (MSF)	- High water productivity - High water quality - Reliable and long operational life	- High energy consumption - Requires large space - High maintenance due to corrosion issues - High greenhouse gas emissions
Multi-Effect Distillation (MED)	- High water productivity - High water quality - Can use waste heat for energy	- High capital and operational costs - High energy consumption - Vulnerable to high temperatures and corrosion
Vapor Compression (VC)	- High water productivity - Small system size - Lower operational cost compared to MSF and MED	- High energy consumption - Not portable - Requires a heating source and compressor maintenance
Solar Distillation (SD)	- Low cost - No pollution - Portable and efficient with solar modules	- Low water production rate - Slow distillation process (2-5 hours per

		liter) - Glass cover attracts insects
Reverse Osmosis (RO)	- No need for thermal energy - Reduced energy costs compared to MSF, MED, and VC - Automation feasible	- High maintenance costs (membrane replacement) - Complicated feed water pre-treatment - Wastes water during operation
Electrodialysis (ED)	- High water productivity - Low energy consumption compared to RO - Effective for low-salinity water	- Not portable - Requires pre- and post-treatment - Works best with low-salinity water

2.4 Superhydrophobic surface

Surface wettability usually characterised by the contact angle between liquid droplet and the surface, in general contact angle smaller than 90 degrees means the surface is hydrophilic and contact angle smaller than 10 degrees considered super hydrophilic. If the contact angle reaches above 90 degrees this means that the surface is hydrophobic, and a contact angle bigger than 150 degrees with sliding angle below 5 degrees are called superhydrophobic [75], [76]

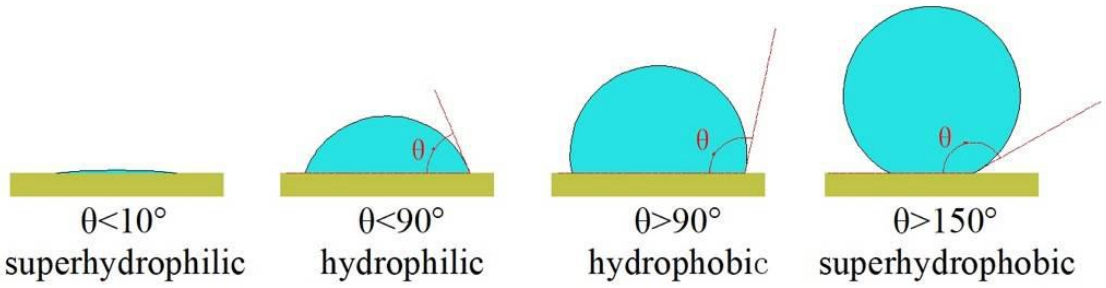

Figure 2.32 Droplet state on the surface

The idea of super hydrophobic surface came from nature, many plants and insects exhibit superhydrophobic properties, for example rice leaf, lotus leaf, butterfly wings, and mosquitos' feet. The contact angle is the most important parameter for wettability characterisation of any surface, usually measured by contact angle meter using 2 to 5 µL water drop on the surface. The first correlation between the contact angle and the surface tension was developed by Thomas Young in 1805, it assumes that the surface is ideally smooth. Because the theory is valid only on smooth surfaces, two other models was introduced by Wenzel and Cassie Baxter to take into account the wetting state on rough surfaces.

A dynamic contact angle refers to the contact angle formed when the three-phase contact line (where solid, liquid, and vapor meet) is in motion. This occurs when a liquid is either advancing or receding on a solid surface, typically observed by expanding or contracting the liquid. The advancing contact angle (θa) is measured as the liquid spreads, while the receding contact angle (θr) is observed as the liquid retracts. The difference between these two angles is called hysteresis (H) [77].

In recent years scientist developed various methods to introduce the superhydrophobic coating or layer on metal surfaces, fabrication the superhydrophobic layer on metals usually done in two steps, firstly by fabrication the nano-micro roughness structure, secondly by lowering the surface energy with chemical materials. There are mainly three methods used to achieve the super hydrophobic surface on metals:

1. Etching
2. Sol-gel
3. Electro-chemical deposition

2.4.1 Etching

Mainly done by three methods, laser ablation, plasma etching, and chemical etching. Qian et al [78], used picosecond laser ablation method to fabricate superhydrophobic surface on nickel - aluminium bronze, the contact angle achieved was more than 163 degrees and the sliding angle of only 3 degrees. To study the stability of the hydrophobic surface, the surface was exposed to atmospheric condition for 14 days, the surface found to be stable and maintained high contact angle.

Wang et al [79] used nanosecond laser ablation to fabricate a bionic-fish scale structure with four zoom ratios (30%, 50%, 80%, 100%), the substrate used was an Al alloy. It has been found that when the zoom ratio is less than 50%, the fabrication of the superhydrophobic surface was not successful, as the zoom ratio become higher than 50% the desired pattern was successfully fabricated. At 100% zoom ratio the contact angle between the water droplet and the surface achieved was 154.9 degrees.

Subeshan et al[80] used plasma etching technique to fabricate a super hydrophobic coating on aluminium alloy. The surface was heat treated for 60min at a temperature of 150C before the applying the self-cleaning application. The contact angle achieved by this plasma-treated super hydrophobic coating was 165 degrees.

Sharifi et al[81], compared two plasma technique to fabricate superhydrophobic coating on stainless steel substrate, the results shows that the method using suspension plasma spraying gives higher water repellence properties than using atmospheric plasma spraying. The contact angles achieved were 167 degrees and 145 degrees respectively.

Chemical etching is simple and cheap technique to fabricate a superhydrophobic surface on metal, it involves submerging the metal in strong acid or a base solution to create binary micro-nano structure on the metal surface, then low surface energy material can be applied to the surface to create the superhydrophobic surface. Saleh et al [82] fabricated a superhydrophobic on stainless steel mesh using sulfuric acid, the stainless-steel mesh then treated with octyltrichlorosilane to lower the energy of the surface to get the superhydrophobic effect. The contact angle achieved with this method was 166.8 degrees.

Kim et al [83]achieved a superhydrophobic on stainless-steel by using an HF solution and low surface energy material. The contact angle achieved was 166 degrees and sliding angle of 5 degrees.

2.4.2 Sol-Gel

The sol-gel technique used low temperature and low-pressure method to achieve the surface roughness desired for superhydrophobic coating. It requires two steps to prepare the surface, first the sols are prepared by hydrolysis and condensation of oxides in the presence of solvent, then the gel fabricated by immersing the sols in a solvent. Caldarelli et al [84] used alcoholic alumina sol to fabricate a superhydrophobic Cu surface, after the Cu submerged in the alcoholic alumina sol is treated thermally and dipped in low free energy solution. The contact angle of the water droplet reached nearly 180 degrees and sliding angle less than 4 degrees.

Xia et al [85]deposited CuO/Ti02 coating on steel surface using chemical deposition and sol-gel method. The contact angle achieved by this method was 160 degrees and sliding angle of 2.5 degrees.

2.4.3 Electrochemical deposition

The electrochemical deposition method is less complex than the other methods, the superhydrophobic surface can be fabricated in one step only. Li et al [86] fabricated a superhydrophobic film on a copper substrate using one step electrochemical deposition method, the contact angle between the water droplet and the surface of the copper substrate was 159.2 degrees and sliding angle of 1.7 degrees. The method used two copper plates to work as a cathode and anode, the solution used as an electrolyte is ethanol solution containing Fe-myristic acid.

Zhang et al [87] fabricated anti-corrosion superhydrophobic surface on aluminium substrate using one-step electrochemical deposition method, ethanol solution of cerium nitrate hexahydrate and hexadecenoic acid is used as electrolyte solution. The cathode and anode were Al foil and pt plate, respectively. This method achieved astatic water contact angle of 167.4 degrees and sliding angle of 2 degrees.

Chapter 3: Experimental Investigation of factors affecting evaporation and condensation processes

3.1 Introduction

In this chapter, the primary objective is to develop a comprehensive understanding of the processes of condensation and evaporation. The knowledge gained from this understanding will be applied in the design of the PV-T thermoelectric distillation system. To achieve this, two experiments were conducted to specifically examine the influence of water temperature on the rate of evaporation, as well as the impact of both water and surface temperature on the rate of condensation. These experimental investigations were then compared with a mathematical model.

By conducting these experiments and validating the results with a mathematical model, the chapter aimed to establish a strong foundation of knowledge regarding the mechanisms of condensation and evaporation. This knowledge would then serve as a basis for the design of the PV-T thermoelectric distillation system, which relies on these processes.

3.2 Experiment to investigate factors affecting the evaporation process.

Evaporation is the process by which a liquid, such as water, transforms into a gas, such as water vapor. The rate of evaporation depends on several factors, including temperature, surface area, and the concentration of water vapor in the air.

3.2.1 Experimental setup

The system will use Neslab GP-300 shown in Figure 3.1 to maintain the water at a constant temperature. The Neslab heating bath has a heating element that can supply 1200 W of heat to the water, it is dimension are 25.5x26.4x21.6 cm and it can hold 20 litre of water. The temperature of the water can be controlled precisely using a knob.

Figure 3.1 Neslab GP-300

A RS PRO Type K thermocouples were used to monitor the temperature of the water as well as the ambient temperature, The specifications of the K-type thermocouples used are shown in Table. the humidity of the lab was monitored using Komodo Digital Humidity Meter. Figure 3.2 shows the RS PRO Type K Thermocouple, and the digital humidity sensor.

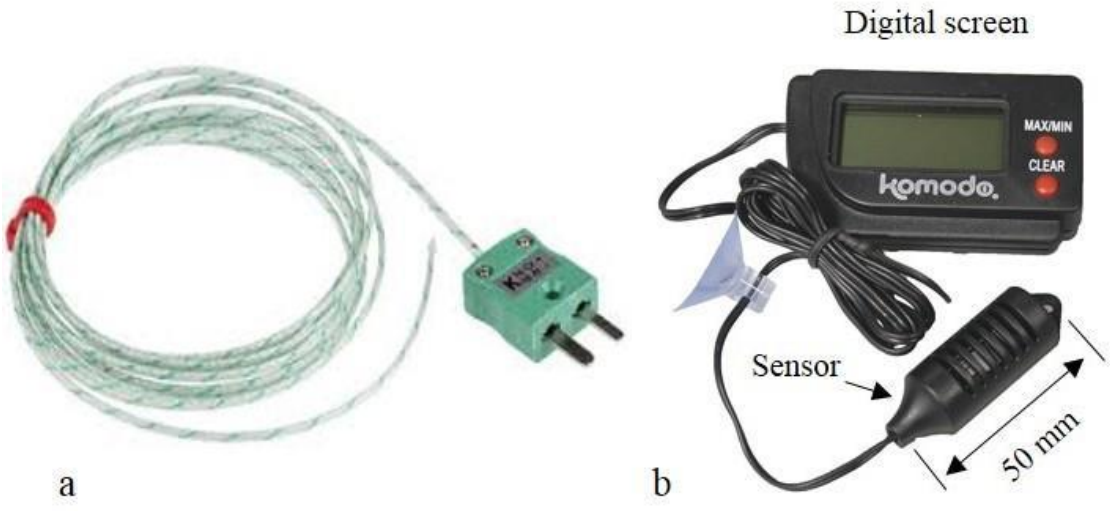

Figure 3.2 a) RS PRO Type K Thermocouple, b) digital humidity sensor

Table 3-1The specifications of K- type thermocouple used in the experiments [88].

Characteristic	Type K
Maximum and minimum temperature sensed	From – 60 °C to 350 °C
Termination type, Cable length	Miniature plug, 1m
Accuracy	±1.5°C

For automatic data acquisition the thermocouples were connected to Pico Log TC-08 data logger, the TC-08 support a wide temperature range (from -270 C to 1800 C), and using the software provided with it the temperature values were stored in the computer with interval of three seconds. Figure 3.3 shows a photograph of the Pico data logger.

Figure 3.3 Pico Log TC-08 data logger

To measure the change of water depth a steel ruler was attached to the side of the Neslab GP-300 water circulating pump. The complete experiment setup is shown in Figure 3.4.

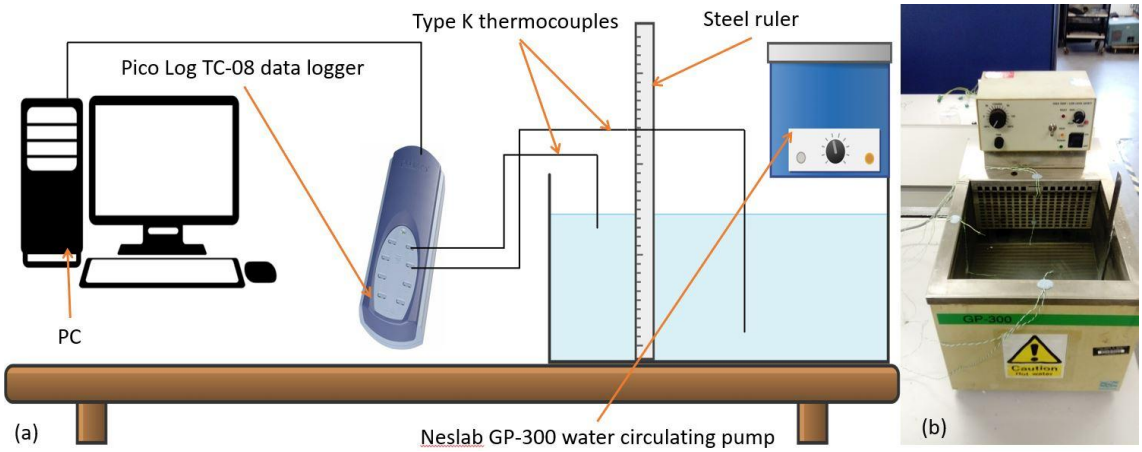

Figure 3.4 (a) scematic diagrame of the evaporation rate experiment setup, (b) the Neslap GP-300 with ruler and the thermocouples attached .

3.2.2 Experimental Procedure

In this experiment, the objective is to investigate the amount of water that evaporates at different temperatures. To maintain a constant temperature, a NESLAP GP-300 device was used. The experiment involved placing six

thermocouples in the water, with three positioned on the surface and the other three at the bottom.

To achieve the desired temperature, the knob on the NESLAP GP-300 was carefully adjusted. Once the temperature was set, the water was left undisturbed for approximately half an hour after it reached the desired temperature to ensure that it stabilized at the desired temperature.

At the beginning and end of each experiment, the water level was measured to determine the change in water depth. By measuring the difference in water volume between the start and end of the experiment, the evaporation rate could be calculated. Each experiment lasted for four hours.

The following temperatures were investigated: 40°C, 50°C, 60°C, 70°C, and 80°C.

To summarize the experimental procedure:

1. Set the desired temperature using the NESLAP GP-300 device.
2. Allow the water to stabilize at the desired temperature for approximately half an hour.
3. Measure the initial water level.
4. Start the experiment and allow the water to evaporate for four hours.
5. Measure the final water level.
6. Calculate the difference in water volume between the start and end of the experiment.
7. Repeat the procedure for each temperature (40°C, 50°C, 60°C, 70°C, and 80°C).

By following this experimental setup, the evaporation rates at different temperatures can be determined.

as we have no means of controlling the humidity thus, we cannot repeat the experiment with the same exact humidity and surrounding air conditions, the humidity and the temperature of the surrounding air only monitored in order to use it to verify the result using a mathematical formula.

3.2.3 Results

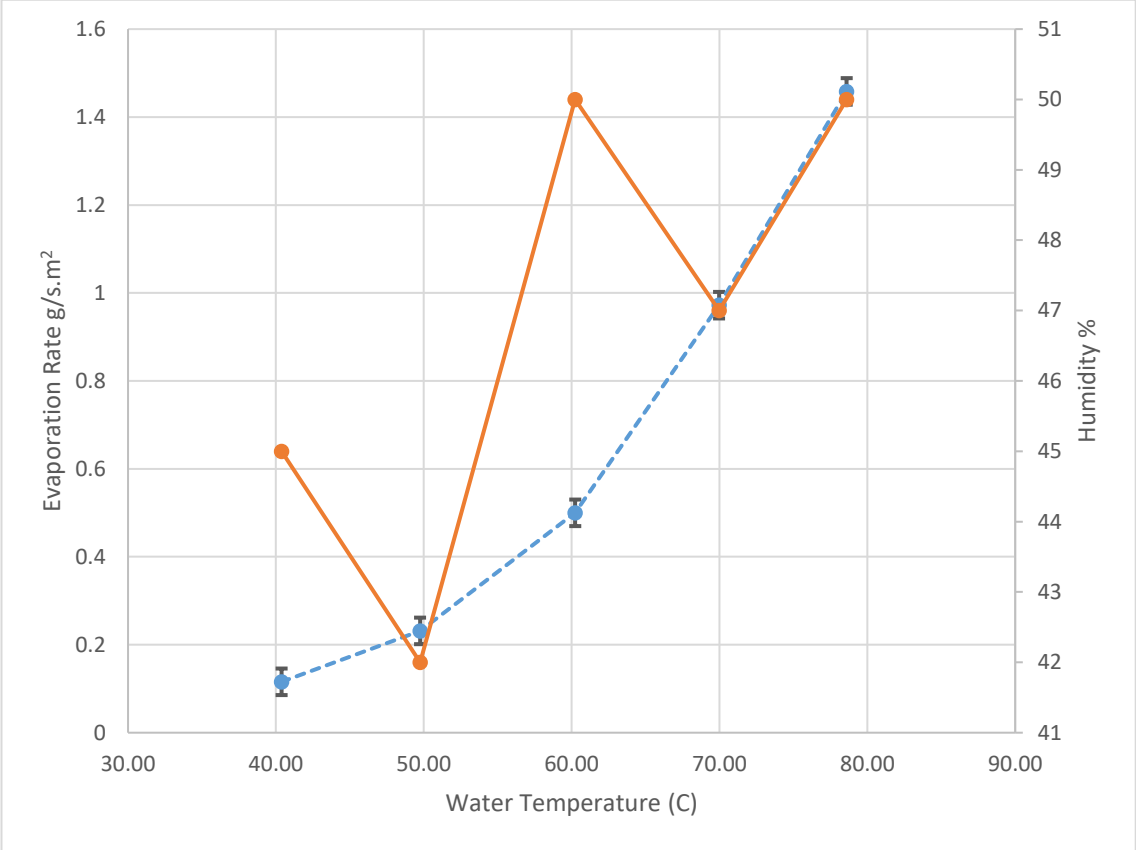

Figure 3.5 Evaporation rate change with the water temperature obtained from the experiment

The results clearly show that the evaporation rate increases dramatically with the increase of temperature. At 40°C, the evaporation rate was 0.115 g/m².s. This increased to 0.185 g/m².s. at 50°C, representing an increase of around 60% for a water temperature increase of 10°C. At 80°C, the evaporation rate increased to 1.458 g/m².s.

As the water temperature increases, the water molecules move faster. This results in more collisions between water molecules, which can break the hydrogen bonds that hold the water molecules together. When the hydrogen

bonds are broken, the water molecules are free to escape into the air from air-water interface.

It has been found that the break of the hydrogen bond is essential in the evaporation process [89]. Analysis of molecular dynamic trajectories of the evaporation of the water molecule from water droplet shows that evaporation happens as a result of a collision of two water molecules [90]. It has been estimated that the energy required for water molecules to escape from water interface to the air is between 25 to 30 Kj/kmol at room temperature [91].

However, Nagata et al. [92], claim that all these studies have not explained in detail how water molecules gain this amount of energy to escape from the water interface. They observed that the energy from the collision is not enough alone to evaporate the water molecule. In order for molecule A to evaporate, it must collide with a molecule B that has just formed a bond with a third molecule C.

Another big factor that affects the evaporation rate is the relative humidity, the humidity effect studied by repeating one point in different days to get different humidity values as there were no means of controlling it. The result shows that the evaporation rate increased with the decreases of humidity. The evaporation rate changed from 0.0251 g/m.s when the humidity was at 42% to 0.0201 g/m.s when the humidity was 57%. A fall of around 20%.

The higher the relative humidity, the closer the air is to being saturated with water vapor. When the relative humidity is high, the air is already close to being saturated with water vapor, which means that the concentration of water vapor in the air is high. As a result, the rate of evaporation is slower because there is less room in the air for additional water vapor. Conversely, when the relative humidity is low, the air is relatively dry, which means that the concentration of water vapor in the air is low. This creates more room in the air for additional water vapor, which speeds up the rate of evaporation. In summary, high relative

humidity slows down evaporation, while low relative humidity speeds up evaporation.

There are many formulas that can be used to predict the amount of water evaporated from a free water surface, mainly empirical formula. The one used to validate the result is developed by Smith et al [93].

The result then validated using a Mathematical formula

$$\dot{m} = \left(P_{sat.water} - P_{sat.vapor \in air}\right) * (0.089 + 0.0782 * V)/h_{fg} \quad \textbf{3-1}$$

Where $P_{sat.water}$= the saturation vapor pressure at water surface in (pascals (Pa))

$P_{sat.vapor \in air}$= the saturation vapor pressure in the surrounding air in (pascals (Pa))

V = air velocity above the water surface in (m/s)

h_{fg}= enthalpy of evaporation in (kJ/kg)

$P_{sat.water}, P_{sat.vapor \in air}$ and h_{fg} are all water properties which are determined using the water and air temperature and the steam table.

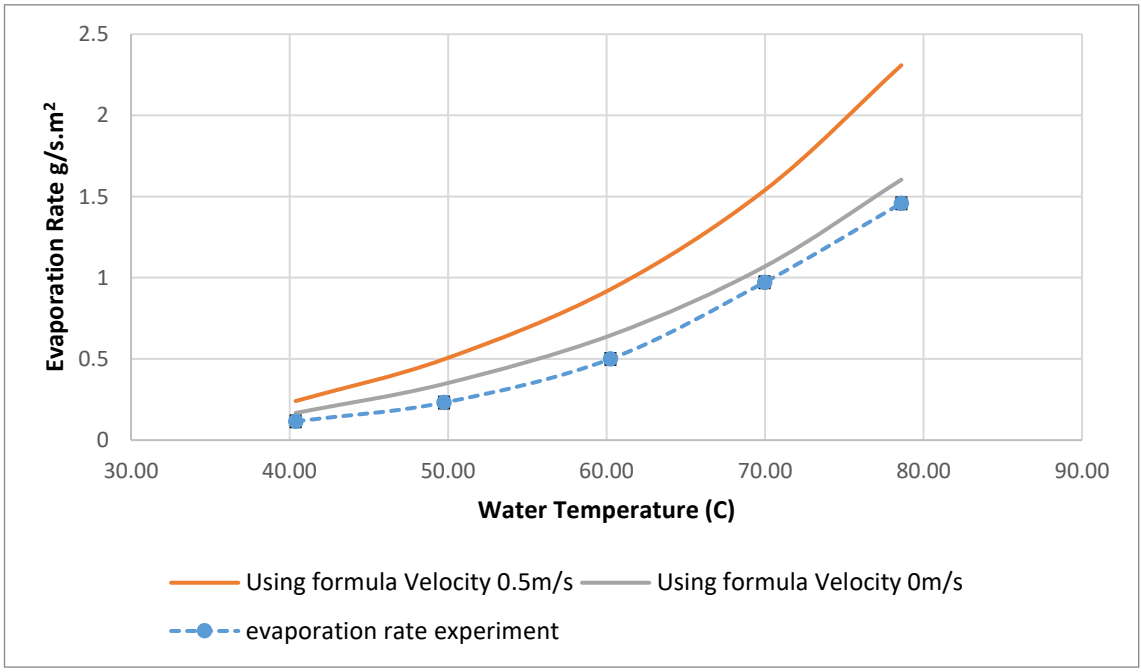

Figure 3.6 comparison between the evaporation rate obtained from the equation and the experimental results.

The experimental results have the same trend as the result obtained from the formula, however, even when the velocity assumed to be zero, the evaporation rate obtained from the equation is overestimated and higher than the result from the experiment.

To understand the energy required to for the evaporation process to accrue, the evaporation rate is compared to the heat of vaporisation (enthalpy) in Figure 3.7.

The enthalpy is determined using the water temperature and the steam table. it is clearly seen that as water temperature increases the enthalpy of vaporization decreases. And the evaporation increases.

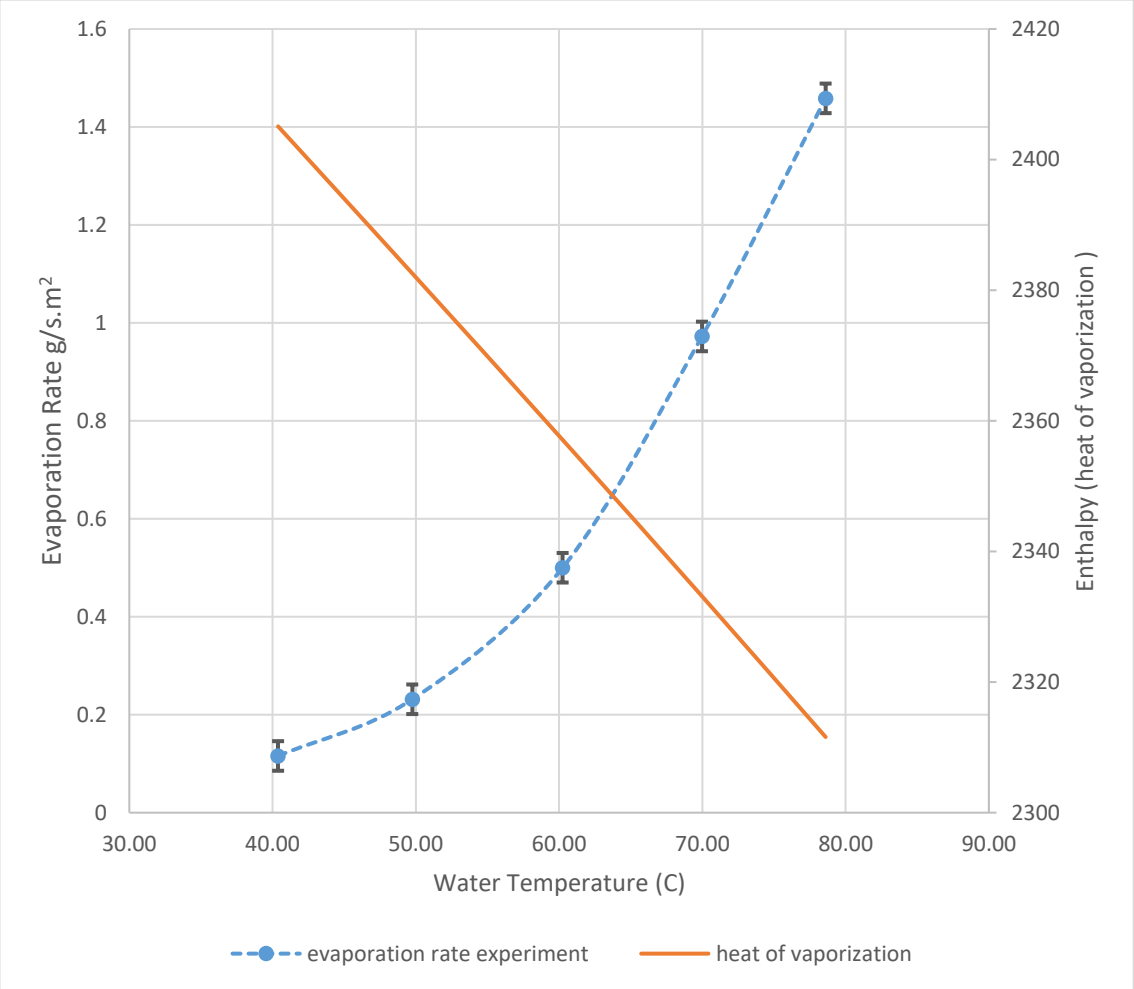

Figure 3.7 Comparing the change of evaporation rate to the heat of vaporization with water temperature

This occurs because at higher temperatures, the molecules of the liquid have higher kinetic energy, which means that they are moving faster and have more thermal energy. As a result, the intermolecular bonds between the molecules are weaker, and it requires less energy to break them and transform the liquid into a gas. In other words, the heat energy required to evaporate a liquid at a higher temperature is lower than the heat energy required to evaporate the same liquid at a lower temperature.

3.3 Experiment to Investigate the Effect of Water Temperature, Condenser Temperature and Angle on the Condensation Rate

Condensation is the opposite of evaporation; it happens when one gas molecule return to it is liquid phase when it meets cold surface. condensation can happen in one of two ways [94], [95]:

1. Filmwise Condensation

2. Dropwise Condensation

In film wise condensation the vapor forms a film on the condensing surface, film wise condensation results in low heat transfer rates. The thickness of the film depends on many parameters including orientation of the surface, viscosity, and rate of condensation.

Dropwise condensation takes place when the condensing surface is coated with a material that prevent wetting. the drops formed cover more than 90% of the surface, and the size of the drops range from micrometre to a visible to the naked eye. In drop wise condensation, high heat transfer rates are achieved [95].

3.3.1 Experimental Setup

An experiment conducted to identify the effect of the condenser temperature on the condensation rate, the setup consists of heat path that used to maintain the water temperature at a constant temperature, and a cover with inclined plate to use as a condenser. the condenser area is 62*62 mm and chosen to be the same area of the thermoelectric in order to get uniform temperature across the condenser, two different angles will also be tested, 65, and 45 degree.

The chamber is designed from plexiglass in order to have a visibility to the condenser, and act as insulator from the alumni cover that cover the water path, the channel is made from a thin aluminium plate (0.2mm thick), the NESLAP GP-300 is used as the hot water path to control the water temperature.

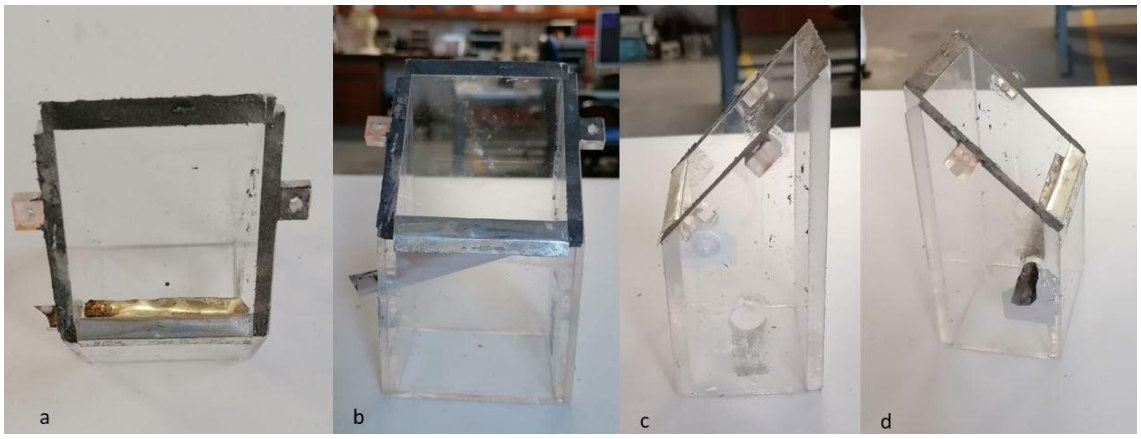

Figure 3.8 The plexi glass chamber :(a) top view, (b) front view, (c)and (d) side views

The cold side of the thermoelectric will face the condenser, and the hot side will be cooled by a fin and a fan, the temperature will be controlled by increasing and decreasing the current supplied to the thermoelectric module, the experiment will be conducted for a certain amount of time and the condensed water will be collected using a collecting channel underneath the condenser, then the water will flow through to a container. the weight of the water will be measured at the end of each experiment, and the condensation rate will be calculated.

The experiment run at water temperature of 50, 60, and 70 C. Meanwhile the condenser temperature was kept at three degrees, 15, 10, 5 C.

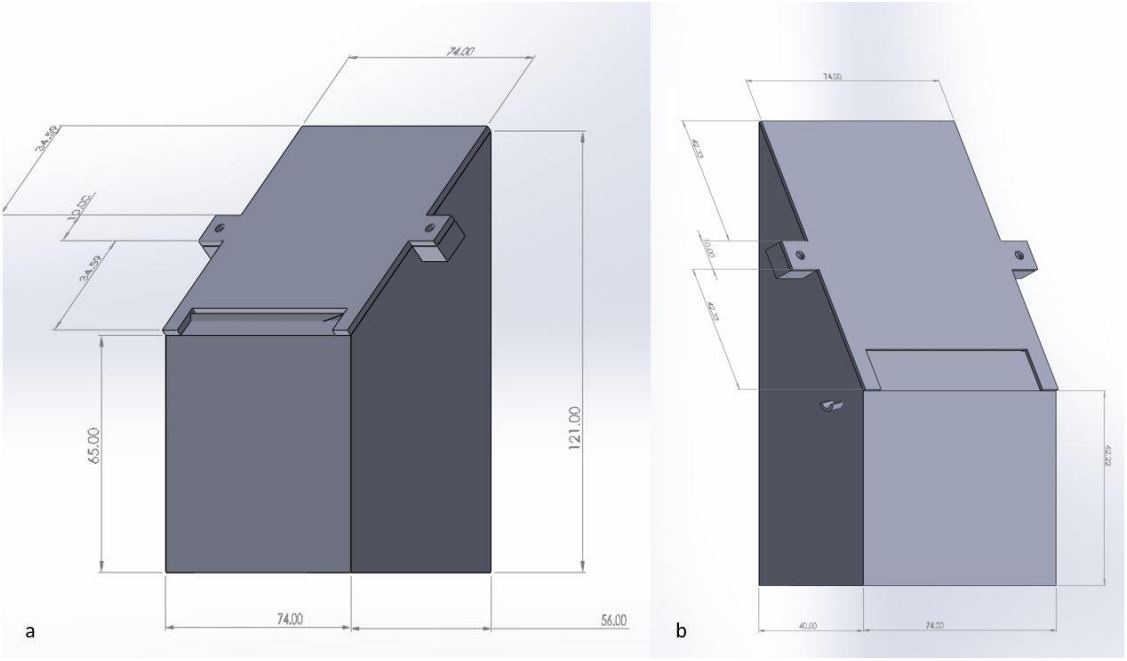

Figure 3.9 The desinged chamber with the aluminum condenser . (a) for 45 degree angle, (b) for 65 degrees angle.

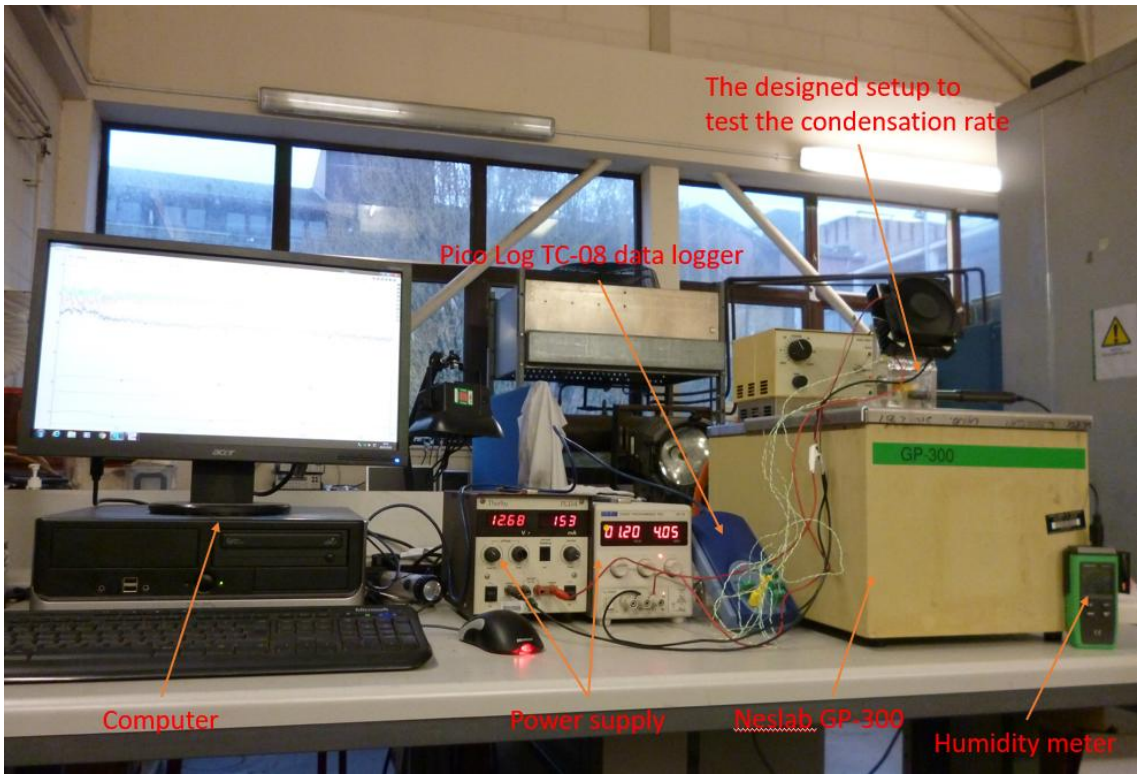

Figure 3.10 the condensation experiment setup

3.3.2 Results

The result of the experiment is shown in Figure 3.11, it can be clearly seen that the condensation rate increases by increasing the water temperature and decreasing the condenser temperature. It also shows that increasing the water temperature has more effect on the condensation rate than decreasing the condenser temperature. For example, the condensation rate rise around 96% when we change the water temperature by 10 C° from 50 C° to 60 C° and keep the condenser temperature at 5 C°. compared to lowering the condenser temperature buy 10 C° from 15 C° to 5 C°, when the water temperature kept at 50 C° this resulted in a rise of only 38% of the condensation rate. And when the water temperature kept at 60 C° it rises by around 34%.

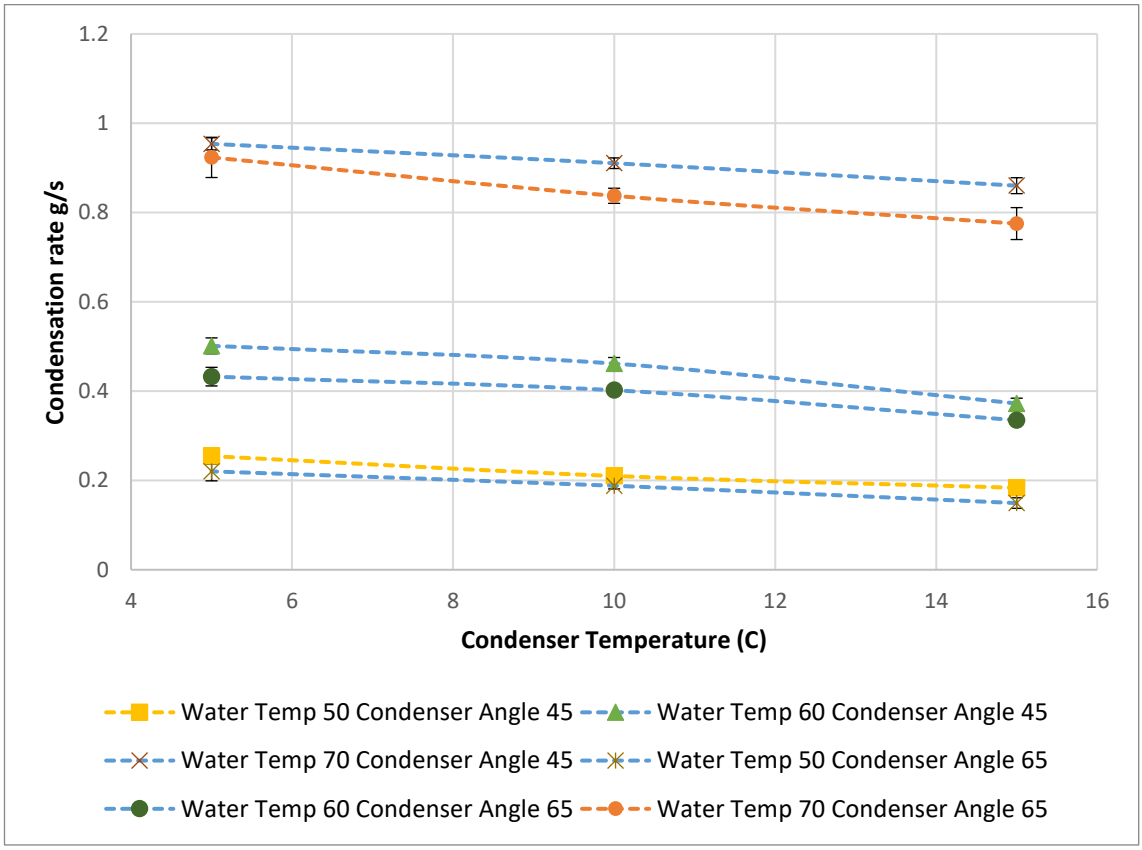

Figure 3.11 Condensation rate change with condenser temperature and water temperature

The power supplied to the TE module to keep the condenser at the constant desired temperature is shown in Figure 3.12. the power required to keep the condenser at certain temperature increases dramatically with the increase of water temperature. For example, the power required to keep the condenser temperature at 5 C° increases by 87% when water temperature increases from 50 C° to 60 C° and 172% when water temperature increases from 60 C° to 70 C°.

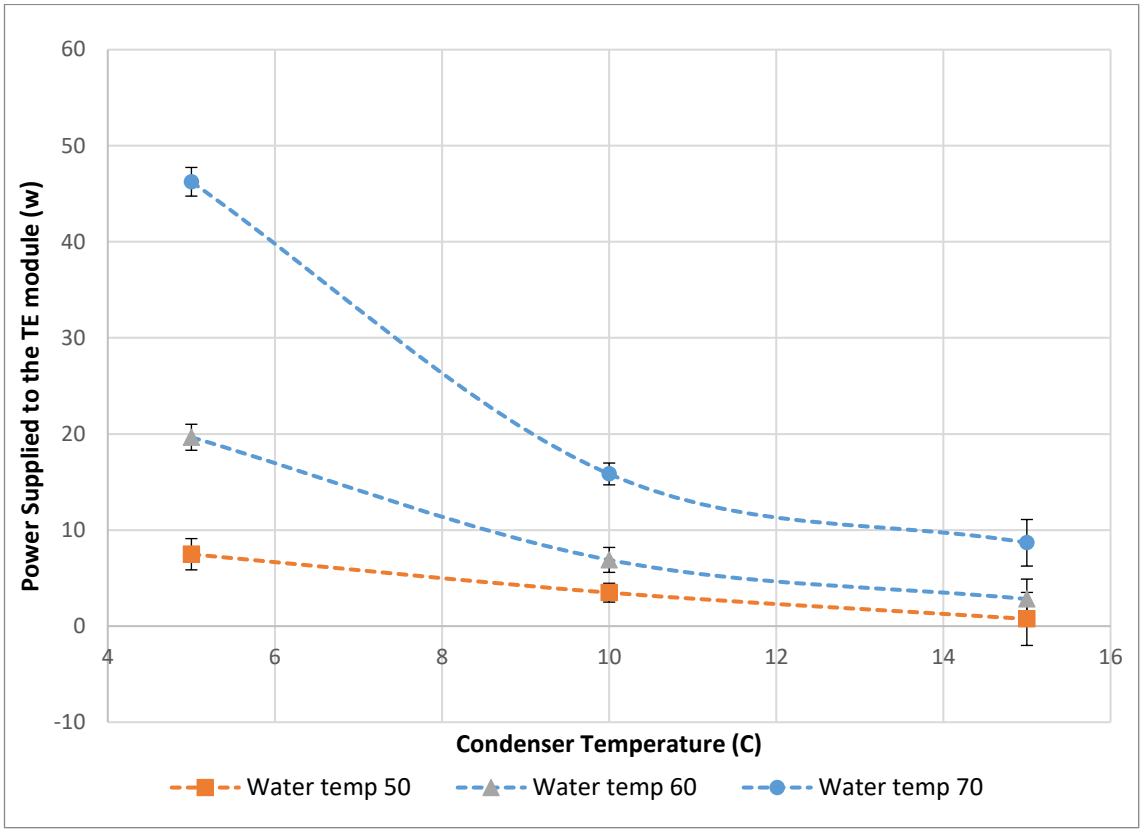

Figure 3.12 The power supplied to the TE module

As it can be seen from Figure 3.11, the condenser angle of 45 degree always gives higher condensation rate than the 65 degrees by around 10%. This is possibly caused by the smaller cross-sectional area of the 65 degrees chamber as shown in Figure 3.13. the cross-sectional area of the 45 degrees chamber is 36% larger than the 65 degrees chamber. This can have great impact on the flow of vapour from the hot water underneath to reach the condenser and affect in return the

condensation rate. This has been confirmed by the relative humidity. The relative humidity inside the 45 degrees chamber stays at around 96% in all 9 experiments, and around 90% inside the 65 degrees chamber.

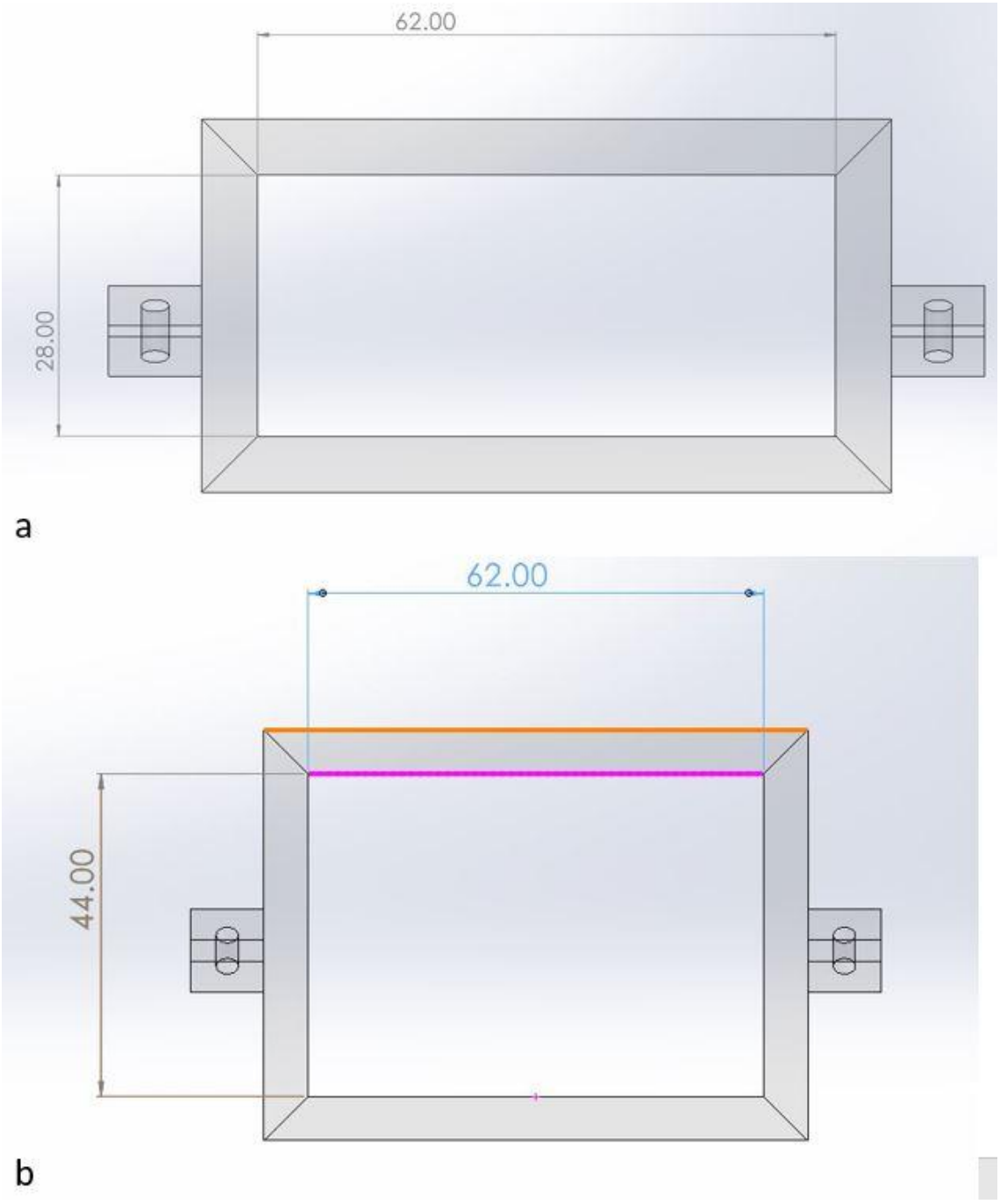

Figure 3.13 the cross sectional area of both chamber :(a) 65 degree, (b) 45degree.

The result obtained from the experiment was compared to the result obtained from Nusselt theory of condensation.

the rate of condensation of film wise condensation on vertical flat plate can be calculated by equation 3-2 [96]:

$$\dot{m} = \frac{q}{h_{fg}} \quad \text{3-2}$$

where ˙m is condensation rate kg/s, q is the heat transfer to the surface, h_{fg} is the latent heat of water.

the total heat transfer can be calculated by using equation 3-3:

$$q = h_L * A_s * (T_{sat} - T_s) \quad \text{3-3}$$

where h_L is the average convection heat transfer coefficient for the entire plate, $W/m^2 \cdot °C$

T_{sat} is the saturation temperature of the vapor, · °C

T_s is the surface temperature of the plate, · °C

A is the area of the plate. m^2

now by substitute equation (4) in (3) we obtain equation 3-4 [96]:

$$\dot{m} = \frac{h_L * A_s * (T_{sat} - T_s)}{h_{fg}} \quad \text{3-4}$$

Where As is the condensing area in (m^2)

hfg is the enthalpy of vaporization in (kj/kg)

In order to calculate the average convection heat transfer coefficient Nusselt made and assumptions to simplify the analysis:

1. Constant properties are assumed for water film at a specific temperature.

2. The flow is laminar.

3. The vapor is assumed to be pure vapor at a uniform temperature equal to saturation temperature with no temperature gradient in the vapor.

4. Heat transfer at the water–steam interface can occur only by condensation at the interface. and the Nusselt number can be calculated from equation 3-5 [96]:

$$\boldsymbol{Nu_L = \frac{h_L * L}{kl} = 0.943 * \left[\frac{g * \rho_l * (\rho_l - \rho_v) * h_{fg} * L^3}{\mu_l k_l (T_{sat} - T_s)}\right]^{1/4}} \quad \ldots\ldots\ldots\ldots\ldots\ldots\ldots\ldots 3\text{-}5$$

Where g is gravitational acceleration, m/s2

$\rho_l \; and \; \rho_v$ densities of the liquid and vapor, respectively, kg/m3

μ_l is the viscosity of the liquid, kg/m · s

$\boldsymbol{h_{fg}}$ is the latent heat of vaporization, J/kg

k_l is the thermal conductivity of the liquid, W/m · °C

L is the height of the vertical plate, m

$\boldsymbol{T_s}$ is the surface temperature of the plate, °C

$\boldsymbol{T_{sat}}$ is the saturation temperature of the condensing fluid, °C

therefore the average convection heat transfer coefficient is calculated by equation 3-6

$$\boldsymbol{h_L = 0.943 * \left[\frac{g * \rho_l * (\rho_l - \rho_v) k_l^3 * h_{fg}}{\mu_l * (T_{sat} - T_s) * L}\right]^{1/4}} \quad \ldots\ldots\ldots\ldots\ldots\ldots 3\text{-}6$$

In order to take into account, the effect of humidity, the vapour temperature will be replaced with the dewpoint temperature which can be calculated using equation 3-7 :

$$\boldsymbol{T_{dew} = \frac{243.04 * \left[ln\left(\frac{RH}{100}\right) + \frac{17.62 * T_{sat}}{243.04 + T_{sat}}\right]}{17.62 - ln\left(\frac{RH}{100}\right) + \frac{17.62 * T_{sat}}{243.04 + T_{sat}}}} \quad \ldots\ldots\ldots 3\text{-}7$$

Where $\boldsymbol{T_{dew}}$ is the dew point temperature °C

RH is the relative Humidity %

the result for both condenser angles (45 and 65 Degrees) are shown in Table 3-2 Table 3-3.

Table 3-2 Comparision between the condensation rate obtained from the mathematical model and the experiment condenser angle 65 degrees

Condenser Temp (°C)	Water Temp (°C)	Condensation rate Model (g/s)	Condensation rate Experiment (g/s)	Error %
14.93	51.05	0.83	0.15	138.93
10.18	50.87	1.04	0.19	138.78
4.92	50.09	1.33	0.22	143.00
14.98	60.89	1.11	0.33	107.57
9.95	61.01	1.32	0.40	106.77
5.24	60.18	1.53	0.43	112.00
14.97	70.35	1.38	0.78	56.06
10.12	70.71	1.57	0.84	61.09
5.11	70.04	1.80	0.92	64.51

Table 3-3 Comparision between the condensation rate obtained from the mathematical model and the experiment condenser angle 45 degrees

Condenser Temp (°C)	Water Temp (°C)	Condensation rate Model (g/s)	Condensation rate Experiment (g/s)	Error %
15.16	50.00	0.78	0.18	123.73
10.08	50.32	1.12	0.21	136.81
4.93	50.55	1.31	0.25	134.77
15.21	60.35	1.14	0.37	101.80
10.50	60.39	1.39	0.46	100.30
5.12	60.33	1.67	0.50	107.72
14.93	70.36	1.40	0.86	47.96
10.09	70.31	1.62	0.91	56.32
5.03	70.20	1.81	0.95	62.17

The results obtained from the mathematical model is always higher for both condenser angles, however, the error or the difference does not change much by changing the condenser temperature. As it can be seen from the tables, when

water temperature is 50 C the difference between the mathematical model and the experimental result hovers around 130%. As the water temperature increases the difference gets smaller, at water temperature 60C the difference was around 100% for both condensing angles. And around 60% when the water temperature was 70 C.

This difference is a result of the presence of the non-condensable gases, it has been found that the non-condensable hinder the process of condensation.

3.4 Conclusion

The evaporation rate increases dramatically with the increase of the temperature, humidity also affects the condensation rate, it been found that The evaporation decreased from 0.0251 g/m^2.s to 0.0201 g/m^2.s when the humidity increased from 42% to 57%. A fall of around 20%. The mathematical formula used for evaporation rate calculation gave a result around 10% higher than the experimental results.

The condensation rate increases by increasing the water temperature more than by decreasing the condenser temperature for the same amount. In other words, the condensation rate is more sensitive to the water temperature change than the condenser temperature change.

Mathematical model for condensation process does not represent the real results due to the limitation of the theory developed by Nusselt, which includes the assumption of thin film, laminar flow, pure vapor, and finally constat properties of water film [97], [98], [99].

The presence of the NCG (non-condensable gases) also affected the results, NCG forms a boundary layer which works like a thermal resistance and in return reduce the overall heat transfer coefficient [99].

Chapter 4: Design, fabrication, and test of the hybrid PV-T thermoelectric distillation system.

4.1 Introduction

This chapter start with the testing the solar simulator that will be used to perform the experiments on the designed hybrid PV-T thermoelectric distillation system to insure it is readiness. The simulator will be tested according to the E927-10 standards. Three tests will be performed to identify the class of the light source of the simulator, Spectral Match, Non-uniformity, and Temporal Instability. then the designed hybrid PV-T thermoelectric distillation will be tested systematically in different configurations. First using the thermoelectric as a heat source to heat the water and cool the condenser, in second configuration the PV-T is added to the system so the water will be heated by both the TE module and PV-T. last configuration involves replacing the condenser with smaller one that cover only the 65 degrees slope and submerge a black coated aluminium plate in the water to heat the water by three way.

4.2 Solar Simulator Test (Calibration)

The simulator used in this study is installed at the solar and environmental research laboratory. Figure 4.1 shows the simulator, and it is component. The light source ARRISUN 60 from ARRI is installed in walk through environmental chamber manufactured by THERMOTRON and has a model number WP-563-THCM1-5-5-AC. The light source installed at the top of the chamber, and it is facing downward. A shutter is also installed that allow the blockage of the light. It is operated remotely with 12V DC linear actuator.

The light source uses a Philips lamp model MSR 6000 HR UNP, the power rating of this lamb is 6000 W with lifetime to 50% failure of 300 hours. An electronic

ballast 6000 EB manufactured by ARRI is used to control the light intensity using a knob.

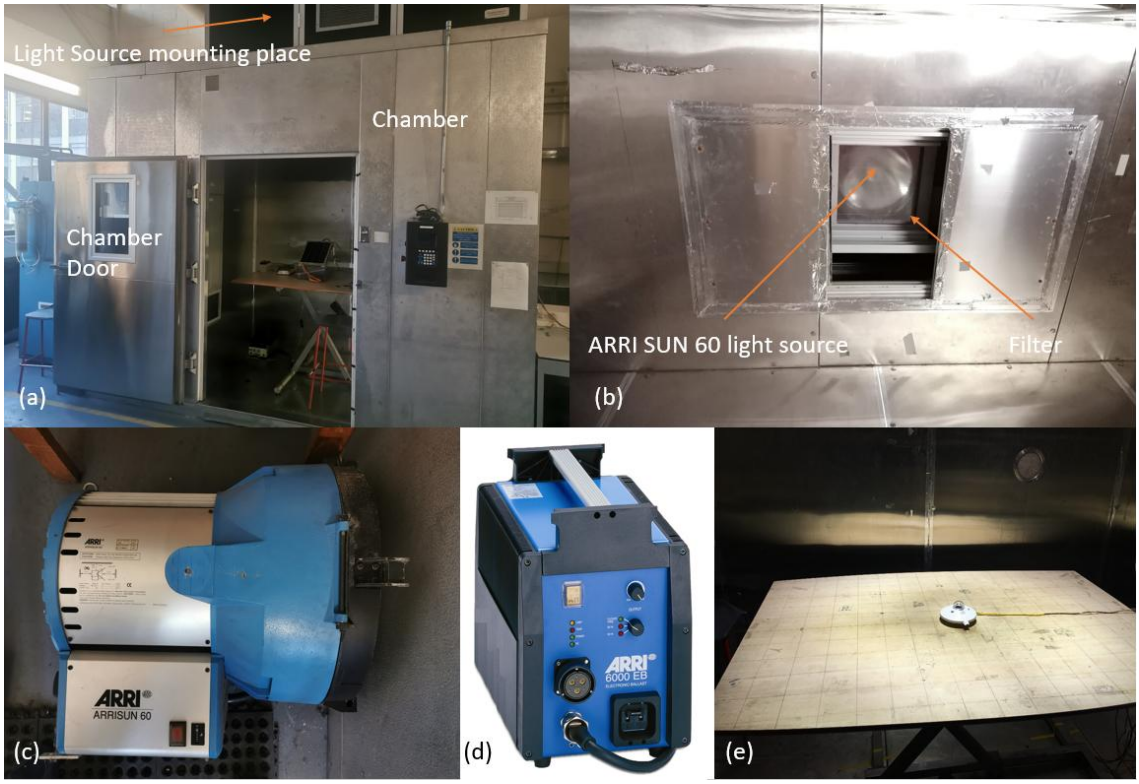

Figure 4.1 The solar simulator system: (a) environmental chamber from outside, (b) ARRISUN 60 light source viewed from inside the chamber, (c) ARRISUN 60 light source, (d) electronic Ballast and (e) adjustable test table.

A bench is located inside the environmental chamber underneath the light, it is approximately in the center of the light source. The height of the table is adjustable. The table is 160*100 cm^2 and it is divided into 10*10 cm^2 areas to investigate the non-uniformity of the light source which will be discussed in Section 4.2.2.

The simulator will be tested to unsure that it meets the E927-10 standards issued by the American Society for Testing and Materials (ASTM). According to the standard specification for solar simulation for photovoltaic testing, there are three parameters used to identify the class of the solar simulator, Spectral Match, Non-uniformity, and Temporal Instability. Table 4-1 shows the Classification of large area solar simulators according to their performance.

Table 4-1 Classification of large area solar simulators according to their performance .

Performance measure	Solar simulator class		
	A	B	C
Spectral match (%)	0.75 to 1.25	0.6 to 1.4	0.4 to 2
Spatial non-uniformity (%)	3	5	10
Temporal instability (%)	2	5	10

4.2.1 Spectral Match

The spectrum of the ARRISUN 60 light source was assessed and compared against both the Sun's spectrum and the limits outlined in the E927-10 standards. This was done to determine its spectral compatibility class. Figures 3.2 and 3.3 show the setup used to measure the spectrum. The spectrometer employed in this study originates from StellarNet and comprises of two devices designed to swiftly measure the electromagnetic spectrum across wavelengths spectrum.

A dual super range Spectroradiometer system to cover 200-1700nm of the wavelength is used to conduct the experiment, the system compromises from two Spectrometers, a Blue Wave Spectrometer (UV-VIS) covers the wavelength from 200 to 1050nm and a Dwarf Star Spectrometer (NIR) covers wavelength from 900 to 1700nm.

(a) **(b)**

Figure 4.2 (a) Blue Wave Spectrometer (UV-VIS) and (b) Dwarf Star Spectrometer (NIR)

The Receptor placed in the centre of the light area (Cosine receptors provide relative and absolute spectral intensity measurements for emissive color applications and for evaluation of light sources such as the Sun, Lamps, LEDs and Lasers), it is connected to the Spectroradiometer by Y-Fibre Optic Cable SMA 905, both Spectroradiometer connected to a PC by USB cables, where the software SpectraWiz installed to record the spectrum. Figure 4.3 shows the experiment setup to measure the spectrum.

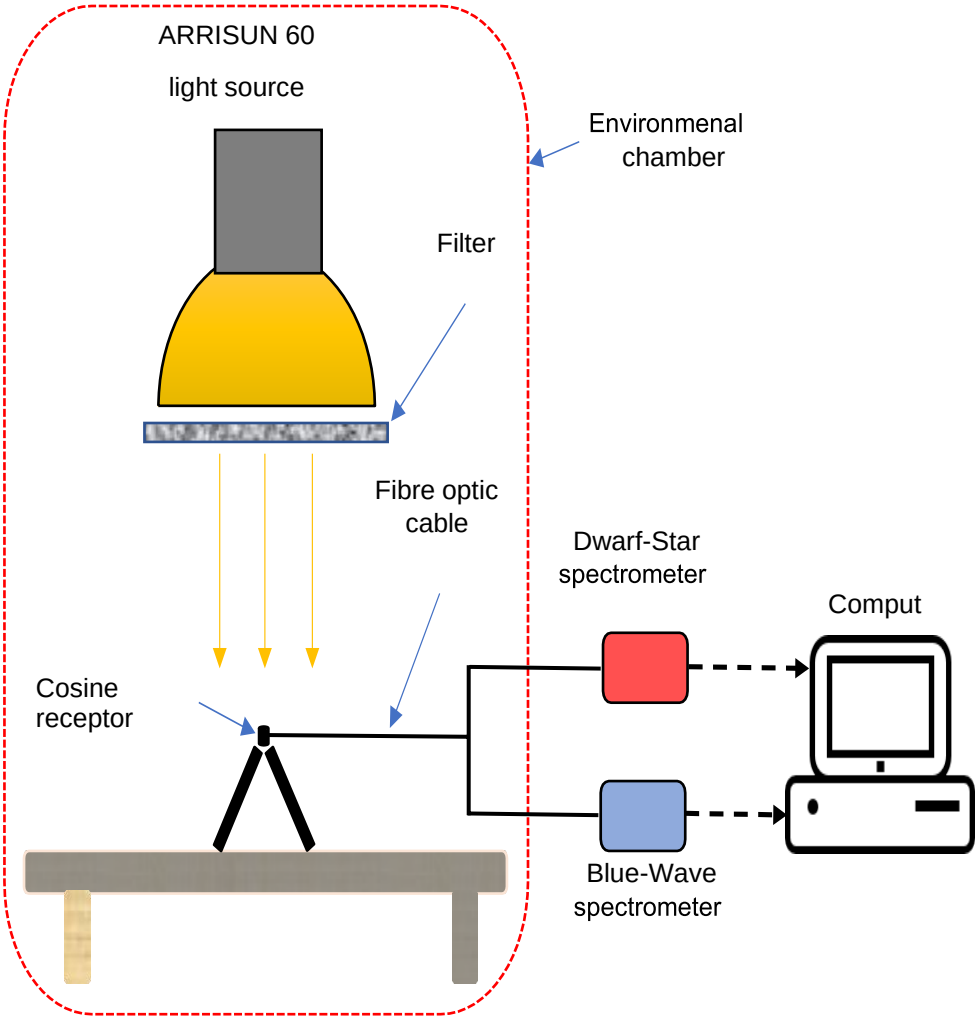

Figure 4.3 Schematic diagram of light source spectral measurement.

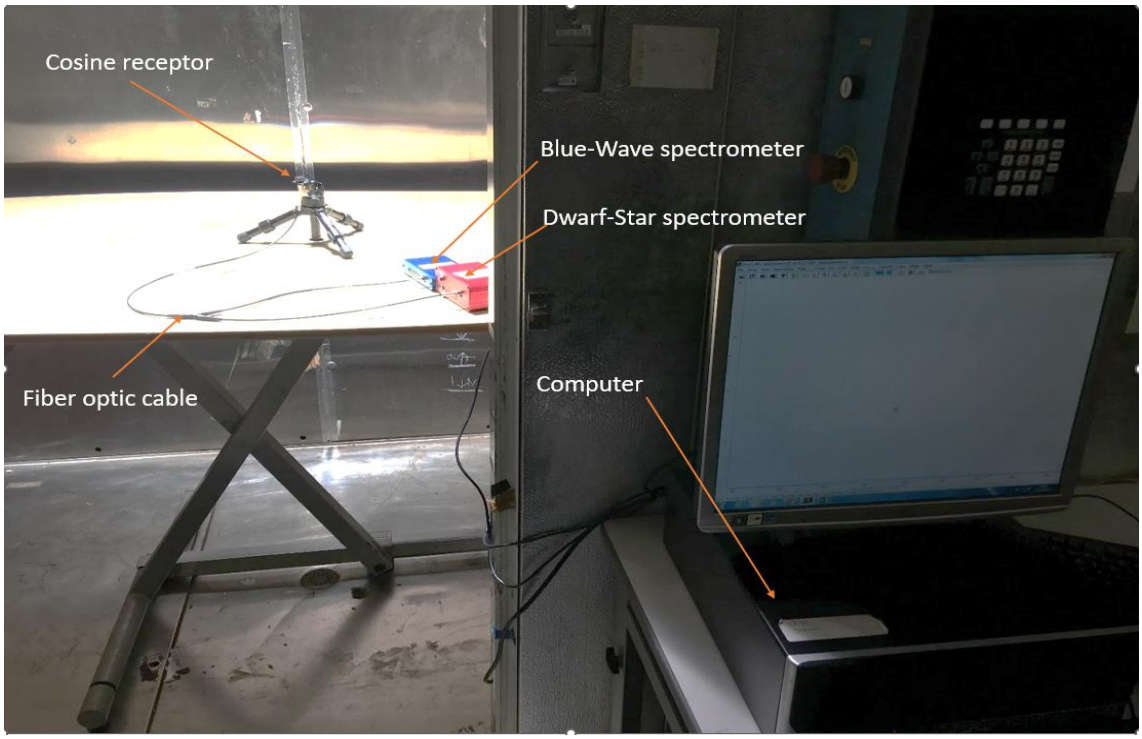

Figure 4.4 The setup of the of light source spectral measurement

To compare the light source spectral to the standard, first the irradiance measured at a resolution of 1nm, then it is normalized for each interval by dividing the sum of irradiance in each interval by the total irradiance of all intervals (400nm-1100nm). Table 4-2 compares the value obtained from the calculation done on the solar simulator light source to the ideal spectral match requirements according to the E927-10 standards and both A and B classes.

Table 4-2 the irradiance as a percentage from the total from 400-1100nm

Wavelength interval (nm)	Irradiance normalised by totalirradiance (%)		Spectral match of Class A (E927-10 standards) (%)		Spectral matchof Class B (E927-10 standards) (%)	
	ARRISUN 60	E927-10 standards ideal match requirements	Upper limit	Lowe rlimit	Uppe rlimit	Lowe rlimit
400-500	24.4	18.4	23.00	13.80	25.76	11.04
500-600	21.3	19.9	24.88	14.93	27.86	11.94
600-700	17.3	18.4	23.00	13.80	25.76	11.04
700-800	10.6	14.9	18.63	11.18	20.86	8.94
800-900	11.7	12.5	15.63	9.38	17.5	7.5
900-1100	14.7	15.9	19.88	11.93	22.26	9.54

The normalized irradiance of the light source exceeded the limits of class A by small amount in both 400-500nm and 700-800nm intervals. But it is within the limits of class B. in all other interval it remains within the limit of class A which leads to the conclusion that the light source of our simulator lays in class B in terms of spectral match according to E927-10 standards.

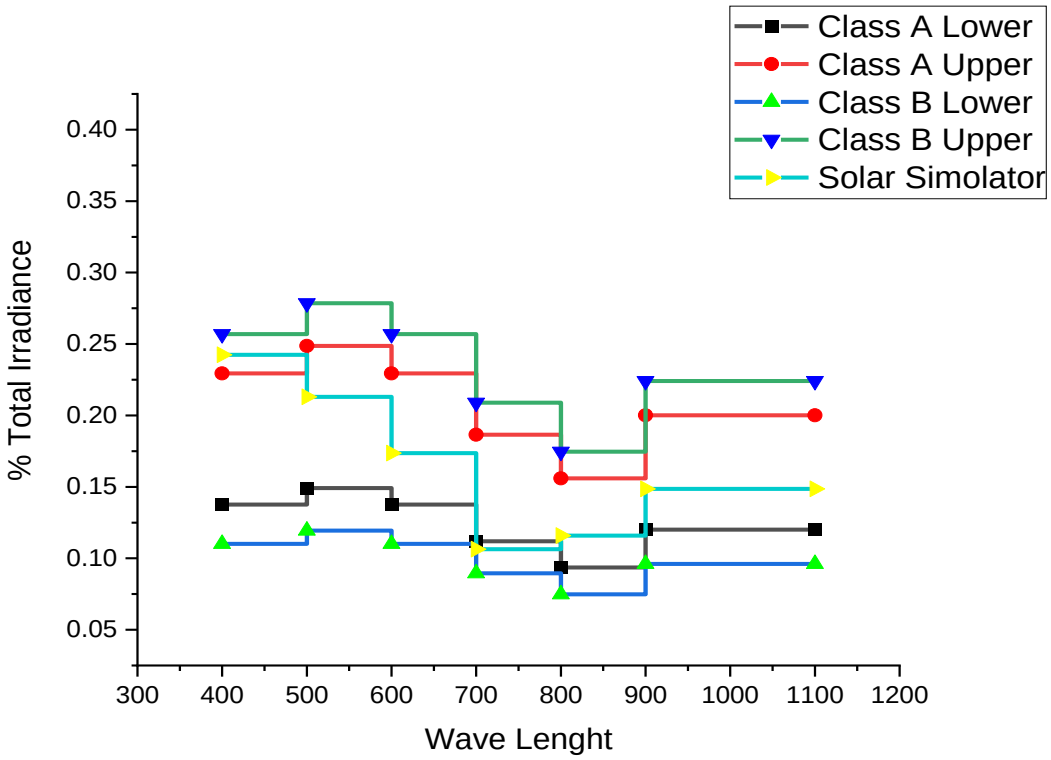

Figure 4.5 Spectral match of the light source compared to the limits of class A and B according to the E927-10 standards

The second analysis is to compare how much the total irradiance of the ARRISUN 60 light source is deviating from the AM 1.5 Global spectrum in each wavelength intervals. The result shown in Table 4-3, it has been found that the ARRISUN 60 light source exhibit the highest deviation between 400-500nm by around 44% from the AM 1.5 G. the other intervals all have lower deviation, and it is ranging from 1.5% to 22%. However, the total deviation over the whole wavelength found to be 9.9%, which means the light source is good in stimulating the sun light.

Table 4-3 Total irradiance for each wavelength interval of ARRISUN-60 light source compared with the Sun AM 1.5G spectrum data of ASTM .

Wavelength Interval (nm)	Irradiance (W/m²)		Absolute Percentage Error(%)
	ARRISUN 60	Sun Spectrum AM 1.5G	
400-500	203.92	140.91	44.7
500-600	177.68	150.98	17.7
600-700	144.65	139.14	4.0
700-800	88.14	113.08	22.1
800-900	97.45	94.37	3.3
900-1100	122.53	120.78	1.5
Total Irradiance	834.37	759.26	9.9

The spectrum of the light source is compared to the sun AM1.5G is shown in Figure 4.6. The spectrum of the light source has a good agreement with the spectrum of the sun AM 1.5G, demonstrating the validity of employing this light source for the intended investigation.

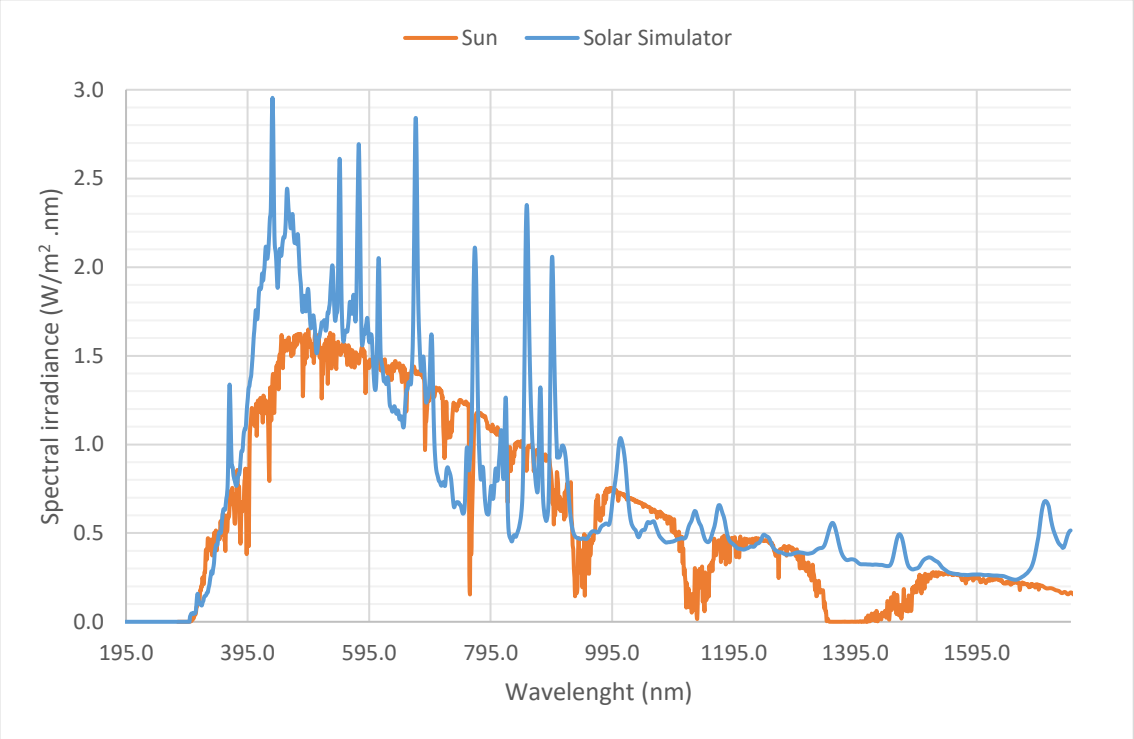

Figure 4.6 comparison between the spectrum of the sun AM 1.5G and the lights source of the solar simulator

4.2.2 The non-uniformity of the irradiance

This is the second test of the E927-10 standard. it is purpose is to give a measure to the degree of the uniformity of the light source over the test area. In order to test the non-uniformity of the simulator, the bench underneath the light source has been divided into a grid of 160 measurement positions has an area of 10*10 cm^2 for each box, the irradiance in each box is measured using a pyranometer. The non-uniformity the calculated using the following formula:

$$\boldsymbol{Non-uniformity}\ (\%) = \left[\frac{\boldsymbol{max\ irradiance - min\ irradiance}}{\boldsymbol{max\ irradiance + min\ irradiance}}\right] \quad 4\text{-}1$$

The pyranometer used is made by Kipp&Zonen and has a model number of CM21, and it measure the irradiance over Spectral range from 300 to 2800 nm. The light first adjusted to be 1000 W/m^2 in the centre of the bench, then the measurement taken in each box and recorded. Figure 4.7 shows the setup used to measure the irradiance to calculate the non- uniformity of the light source.

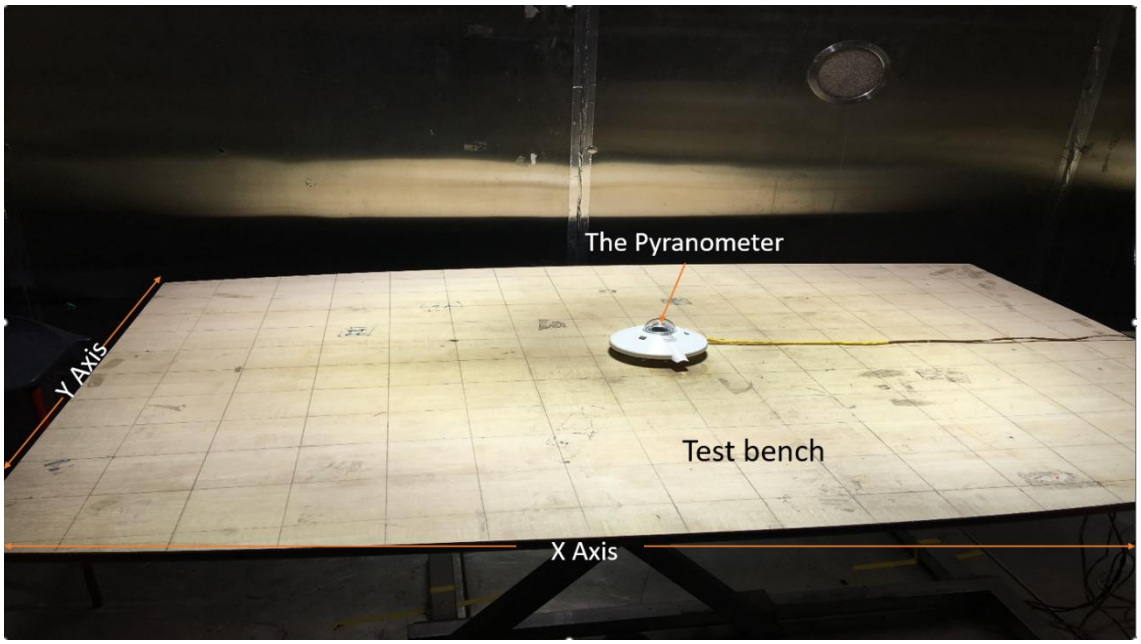

Figure 4.7 the bench underneath the Lightsource and the pyranometer used to identify the non- uniformity

The irradiance measured is mapped on a 3D plot shown in Figure 4.8, which shows that the irradiance is reduced significantly near to the edge of the bench. Using the measured maximum and minimum irradiances and equation 4-1, the spatial non-uniformity over the whole area of the bench was calculated, which is about 82%. This shows that the light source is extremely non-uniform if the entire area of the test bench is considered.

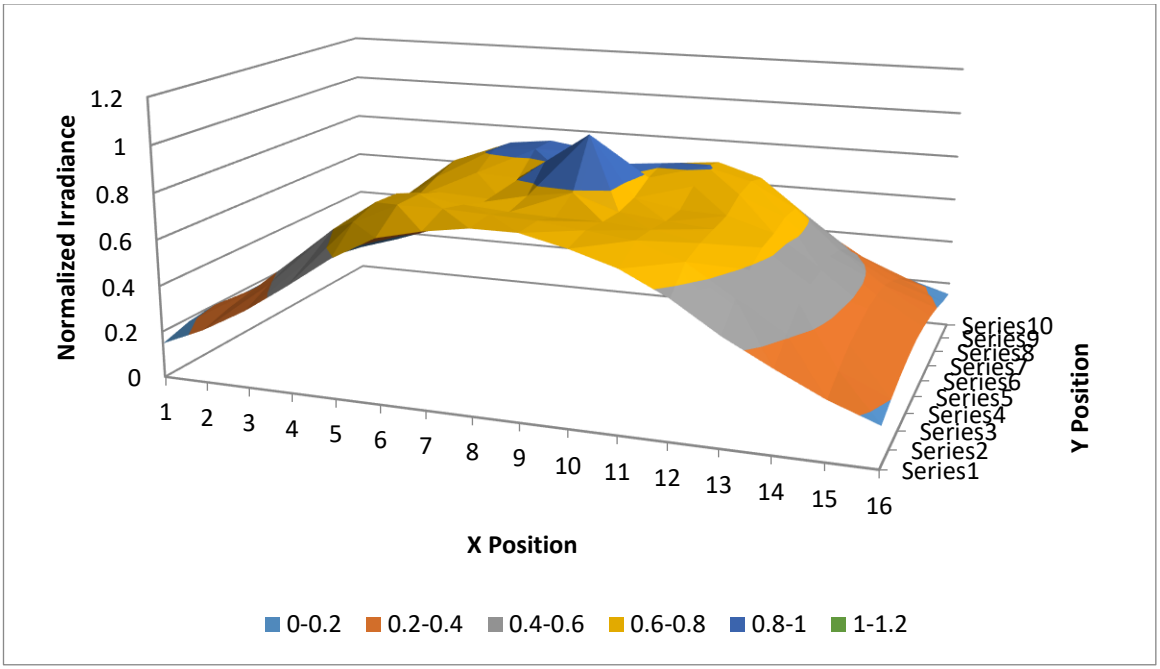

Figure 4.8 Normalized irradiance under the simulator over the whole area of the bench

However, the uniformity improves when considering a limited area around the centre of the bench. The non-uniformity reduces to 21% for an area of 60cm x 80cm in the centre of the bench. Despite this, the non-uniformity for this limited area is still poorer than the value required by the class C of the ASTM standards. Clearly, the smaller the area, the better the uniformity. For example for an area of 40cm x 40cm in the centre, the non-uniformity reduces to 16% and it is only 12% for an area of 20cm x 20cm.

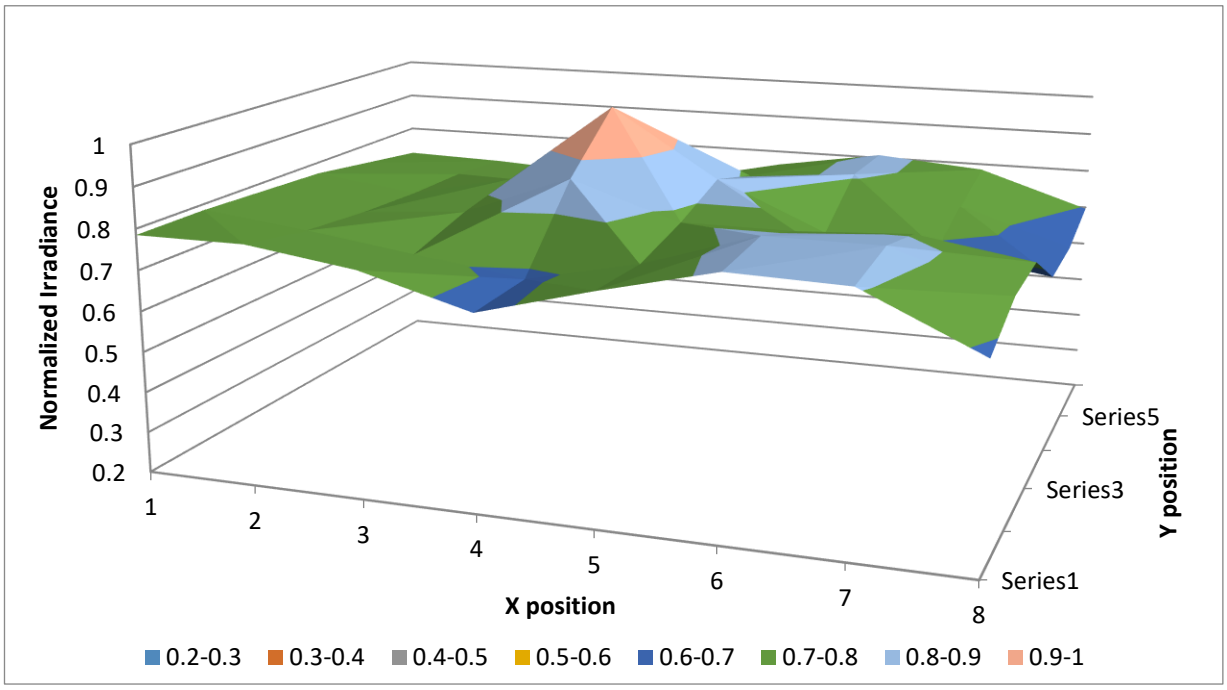

Figure 4.9 Normalized irradiance under the simulator over an area of 60*80cm in the centre of the bench

4.2.3 Irradiance Temporal Instability

This test is designed to evaluate the stability of the light source over a time period, The 927-10 standard suggests taking 20 irradiance measurements over a period of 1 second, however, because of the lack of sophisticated equipment to record data at this rate, we opted to measure the irradiance once every 5 minutes for a period of 4 hours.

the same pyranometer used in the spatial non-uniformity test is used here. it is placed in the middle of the test bench and the irradiance is adjusted to 1000w/m^2.

Figure 4.10 shows that the light source is extremely stable over the period of the test with maximum measured irradiance was 1014.61 W/m^2 and the minimum was 990.25 W/m^2. Using equation 4-1 the temporal instability calculated using the maximum and the minimum irradiance measured during the test period is

only 1.3%, the results indicate that the temporal instability class of the ARRI SUN 60 light source is class A.

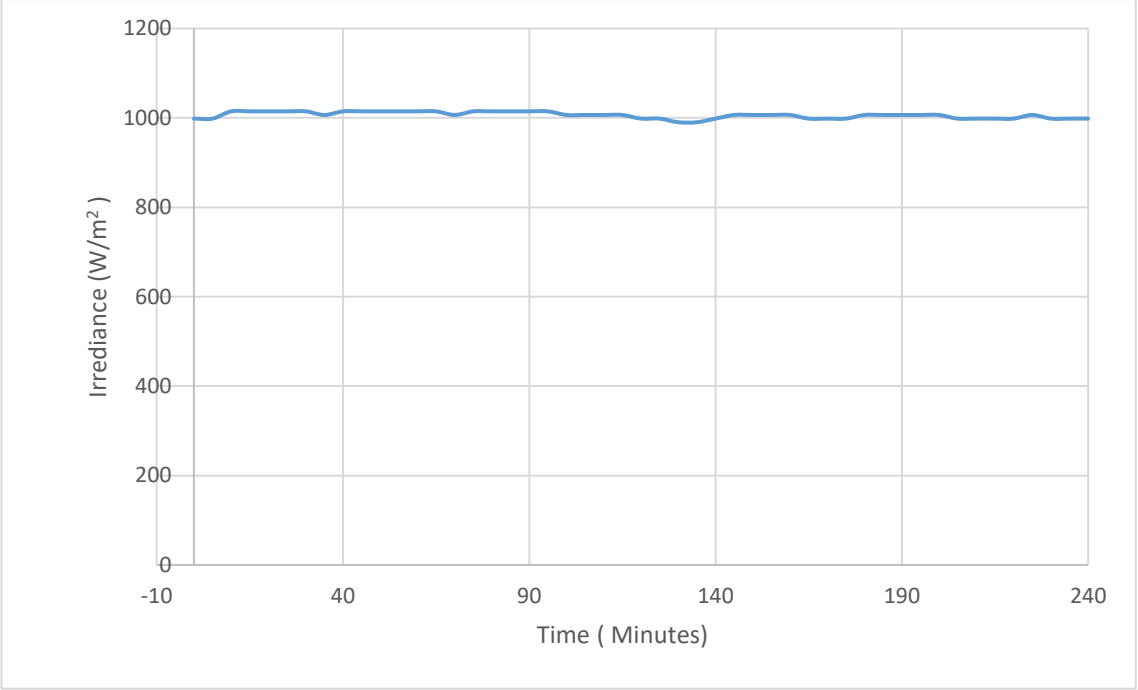

Figure 4.10 The change of irradiance over the period of the Temporal Instability test

4.2.4 Overall Performance Classification of the Solar Simulator

The result obtained from the analysis performed in sections 4.2.1, 4.2.2 and 4.2.3 suggest that the light source has an excellent irradiance temporal instability (class A), good spectral match (class B), but poor uniformity (below class C) against the E927-10 standard. Table 4-4 summaries the performance of the light source employed for this project. Although the non-uniformity is below the class C requirement, experiments were carried out over an area that is smaller than 40cm x 30cm, which has a non-uniformity lower than 16%. In addition, most of experiments were designed and conducted comparatively. The influence of non-uniformity can be minimized.

Table 4-4 Overall Performance Classification of the Solar Simulator

Performance measure	Class
Spectral match	B
Irradiance spatial non-uniformity	C
Irradiance temporal instability	A

4.3 Hybrid PV-T thermoelectric distillation system design

In this section the component of the distillation system and the instruments used are described. The idea is to design an efficient system that takes advantage of the heat collected from the PVT (photovoltaic thermal panel) and the hot side of the thermoelectric module to heat the water, and uses the cold side attached to the condenser to cool the generated vapour to increase the water productivity of the system. The system has been designed with two slops, one has an angle of 30 degrees, to be used to put the solar PVT on. And another with an angle of 65 degrees where the aluminium condenser is mounted to the cold side of the thermoelectric.

In this configuration, the aluminium condensers were used attached to both slopes. The aluminium condenser described earlier was attached to the cold side to the thermoelectric module on the 65-degree slope side, which was extended to the underneath of the 30-degree slope side. The system was designed in such way so as to allow the system to be integrated and compact. The constructed system was then investigated in comparison with a conventional solar still system where the solar irradiation were used directly to heat the water by removing the solar PVT panel from the top of the system with a smaller condenser.

Figure 4.11 and Figure 4.12 show the designed system with dimensions, and an exploded view and projected view of the system.

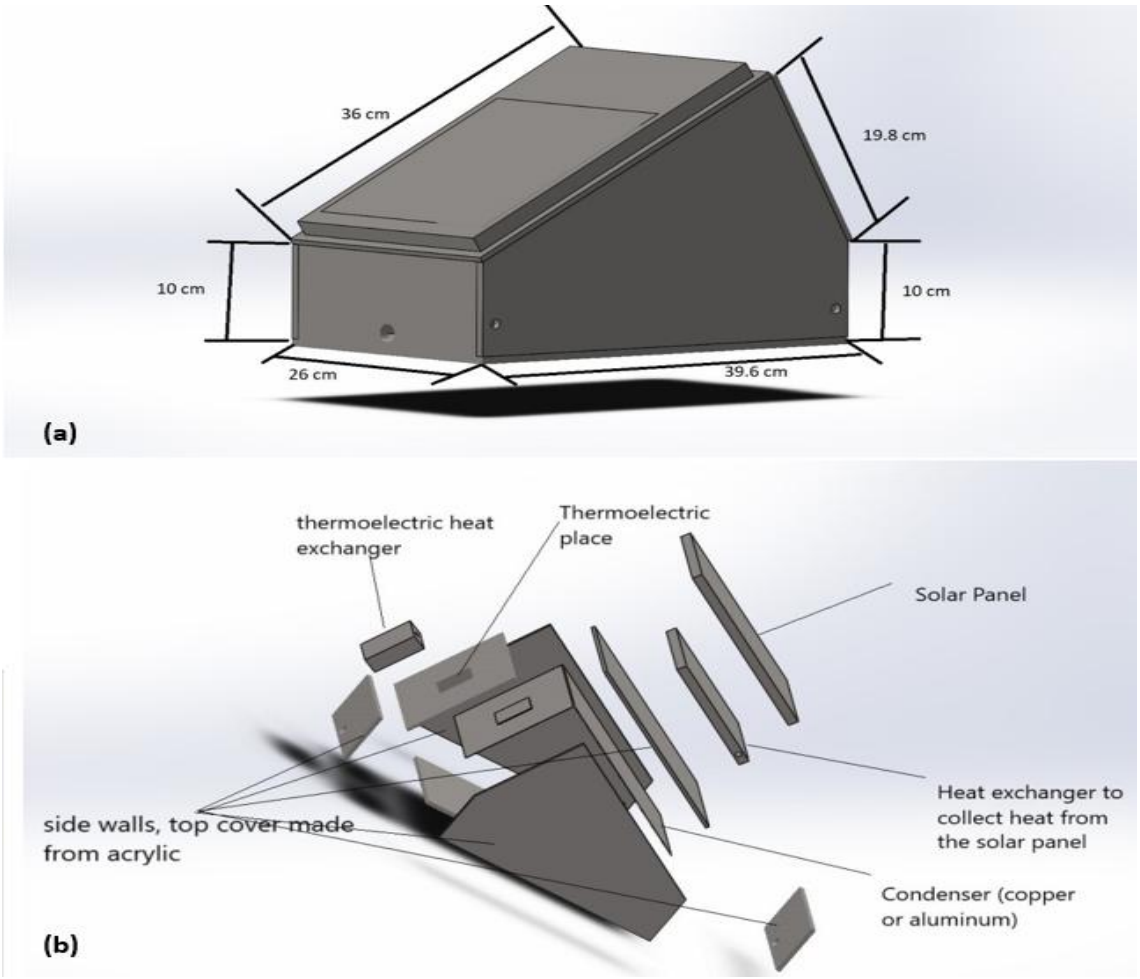

Figure 4.11 (a) the designed system diamention, (b) exploded view of the system and it is component

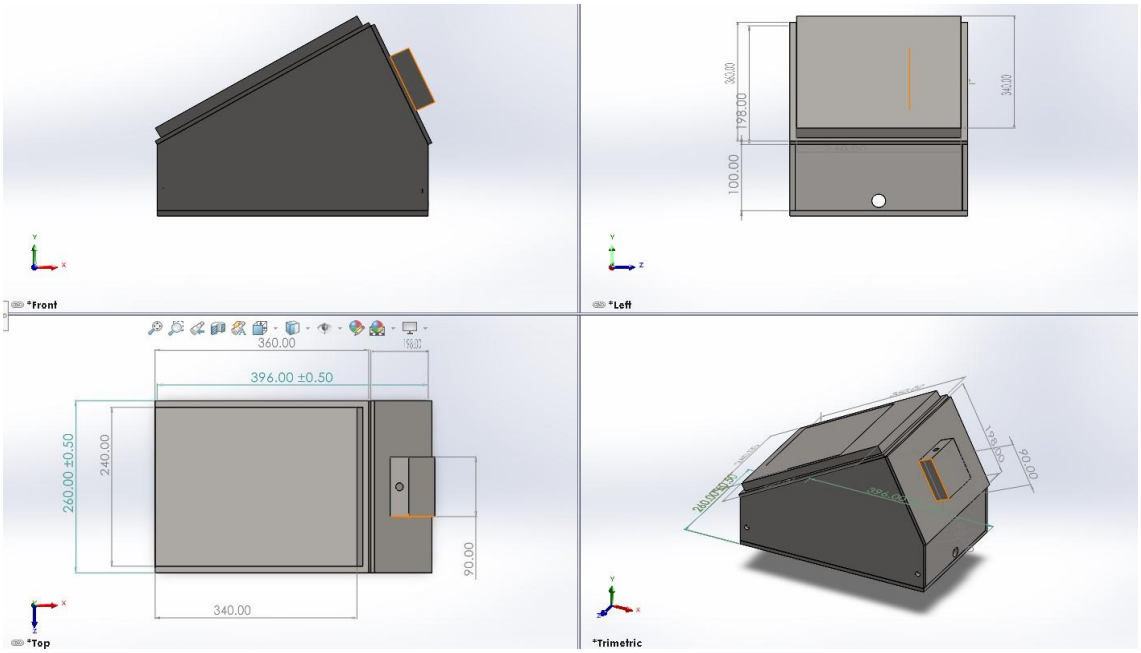

Figure 4.12 projected view of the system

4.3.1 The thermoelectric module

The thermoelectric module has two main roles in the designed system, the first is to heat the water, and the second is to cool the vapor. The thermoelectric module consists of 49 N-type and P-type thermoelements connected in series electrically and in parallel thermally. A thermal conductive and electrical insulating ceramic is used to house the thermoelement. The thermoelectric module used in this study is GM250-49-45-16 (European Thermodynamics Ltd) purchased from RS UK. The dimension of the thermoelectric module is 62 mm x 62 mm x 4 mm as shown in Figure 4.13.

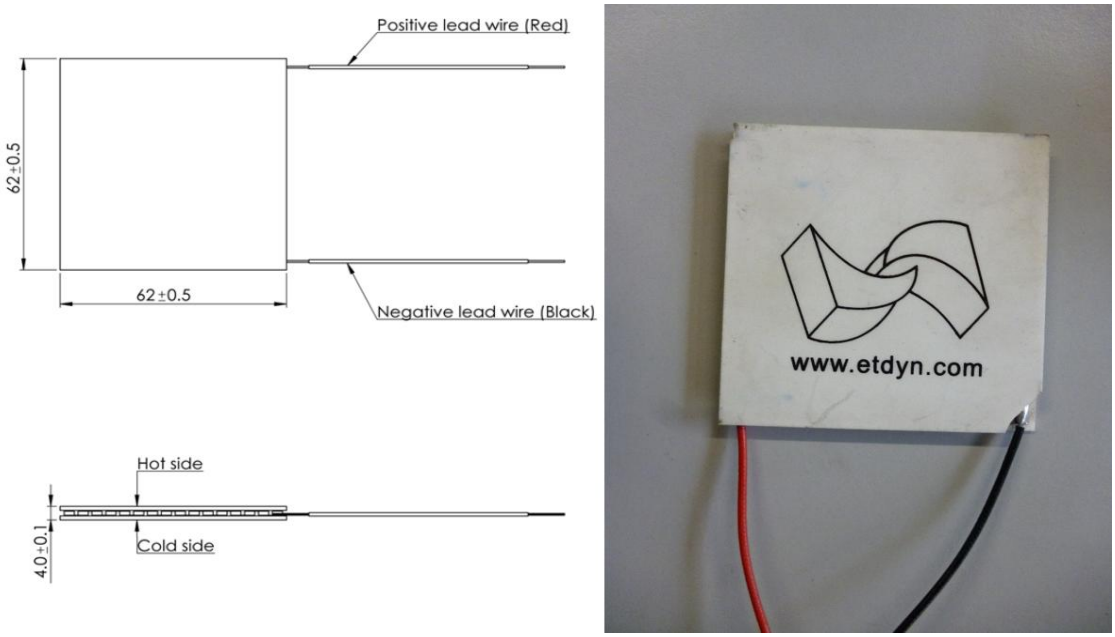

***Figure 4.13** The thermoelectric module used in the design*

The thermoelectric module is sandwiched between two heat exchangers, one mounted on the hot side to transfer the dissipated heat to the water that is circulated from the chamber (heater), and the other on the cold side is used to cool the vapor generated in the chamber (condenser).

Table 4-5 the specification of The thermoelectric module used in the design

Matched load output power	14.07W
Matched load resistance	0.18Ω ± 15%
Open circuit voltage	3.4V
Matched load output	8.8A
Matched load output voltage	1.6V
Heat flow through module	382W
Maximum compress (non-destructive)	1MPa
Maximum operation temperature	Hot side - 250$_0$C. Cold side - 175$_0$C

4.3.2 Evaporation/Condensation chamber

Choosing the right material for the chamber is crucial, it is desirable for the material to have low thermal conductivity, this is in order to reduce the heat transfer from the water and vapor inside the chamber to the surrounding. Heat losses from the chamber to the surrounding will hinder the rate of evaporation and condensation.

The material chosen for the chamber is Polycarbonate Clear Plate with thickness of 8mm, it is chosen as it is thermal conductivity (0.21 W/m.K) is low which will help reduce the heat loss from the water and the vapor to the outside of the chamber. Two collecting channels where mounted underneath the two condensing surfaces, and two holes for the water inlet and outlet is drilled opposite to each to circulate the water from the chamber to the two heat exchangers and back to the chamber.

Figure 4.14 the evaporation/condensation chamber

The dimension of the base is 39.6cm x 26cm, whereas the top of the chamber contains two slope sides; the smaller one where the thermoelectric is mounted has a dimension of 26cm x 19.8cm and the larger one where the glass cover is mounted has a dimension of 26cm x 36cm.

4.3.3 The PV panel.

The PV panel serves two purposes in this design. The first purpose is to power the thermoelectric module, and the second is to collect the waste heat from the panel to heat the water by mounting heat exchanger underneath it. The PV panel used in this experiment is manufactured by HISUNAGE, it is peak power is 10W, the dimension of the PV panel is 34cm x 24cm x 1.7 cm, it weights around 1.16 Kilograms.

The PV panel was tested to check its performance using the solar simulator testing system described above. Figure 4.16 shows the I-V curve obtained at

standard condition (Irradiance of 1000W/m^2, temperature of 25 ^oC). To keep the temperature of the PV panel constant, it is cooled with water using heat exchanger and the water circulation GP-300 mentioned in 3.2.1. The test confirms that the maximum power can be delivered from the PV panel is 10.3W at the maximum power point, the corresponding voltage and current are 0.513 A and 20V.

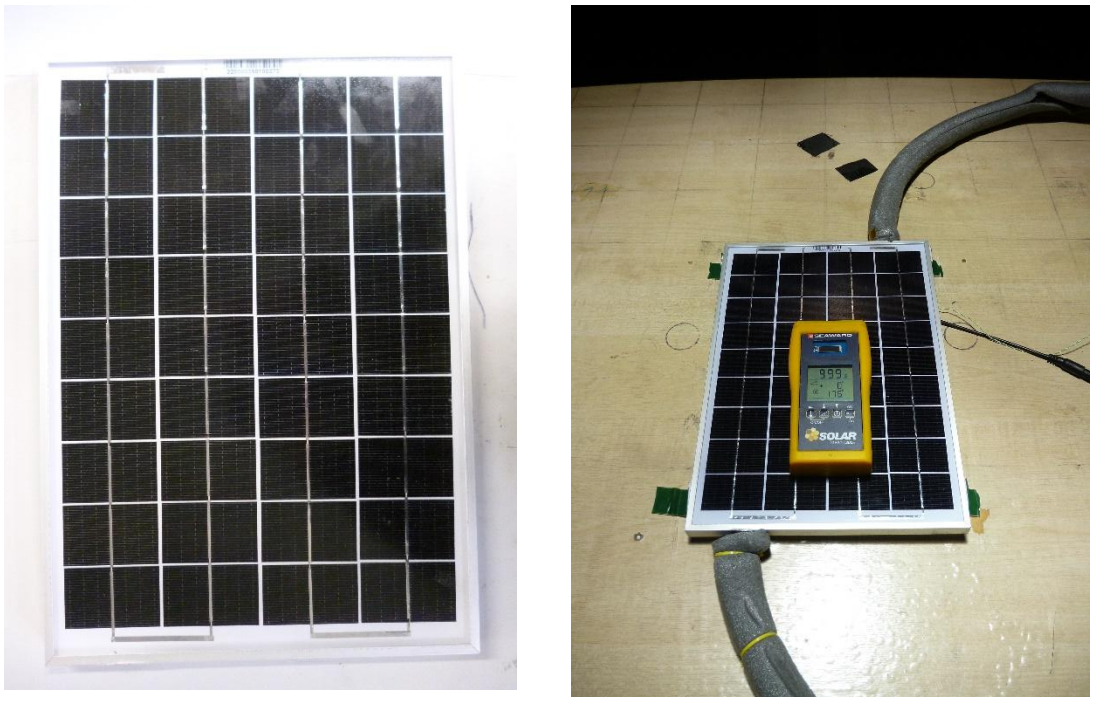

(a) **(b)**

Figure 4.15 (a) the PV panel used for this study, (b) the setup to measure the IV curve and maximum power.

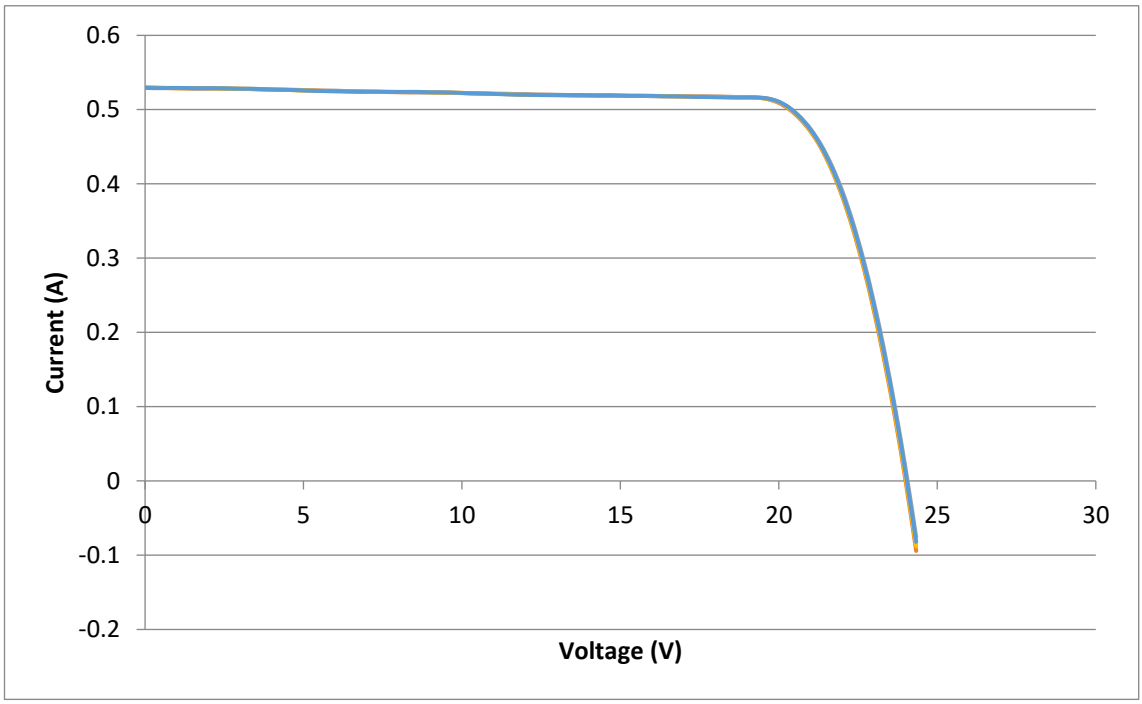

Figure 4.16 IV curve obtained from the PV panel described above.

4.3.4 The Glass Cover

The cover on the top of the 30-degree slope has two purposes. In the first experiment, it was used to mount the PV-T panel. In the second experiment, it was covered by a transparent glass to allow solar irradiation to heat the water directly. In addition, a black coated aluminium sheet submerged in the bottom of the water, which absorbs the sun irradiation and add further heating to the water. A high transmittance is desirable in the second configuration, there was two options of material to choose from, transparent acrylic, and a glass.

An experiment was performed to decide which is the best option for this application. The transmittance of 4mm glass is compared to that of 6mm acrylic, which was measured using the Spectroradiometer system that covers a light wavelength from 200 to1700nm. The setup and the specification were described in section 4.2.1. A measurement was first carried out to determine the spectrum of the light source of the solar simulator as a reference. Then the measurements were repeated with the samples of the glass and the acrylic placed on the top of the light detector as shown in Figure 4.17. The results of spectral measurements

is shown in Figure 4.18 and the calculated transmittances are shown in Figure 4.19.

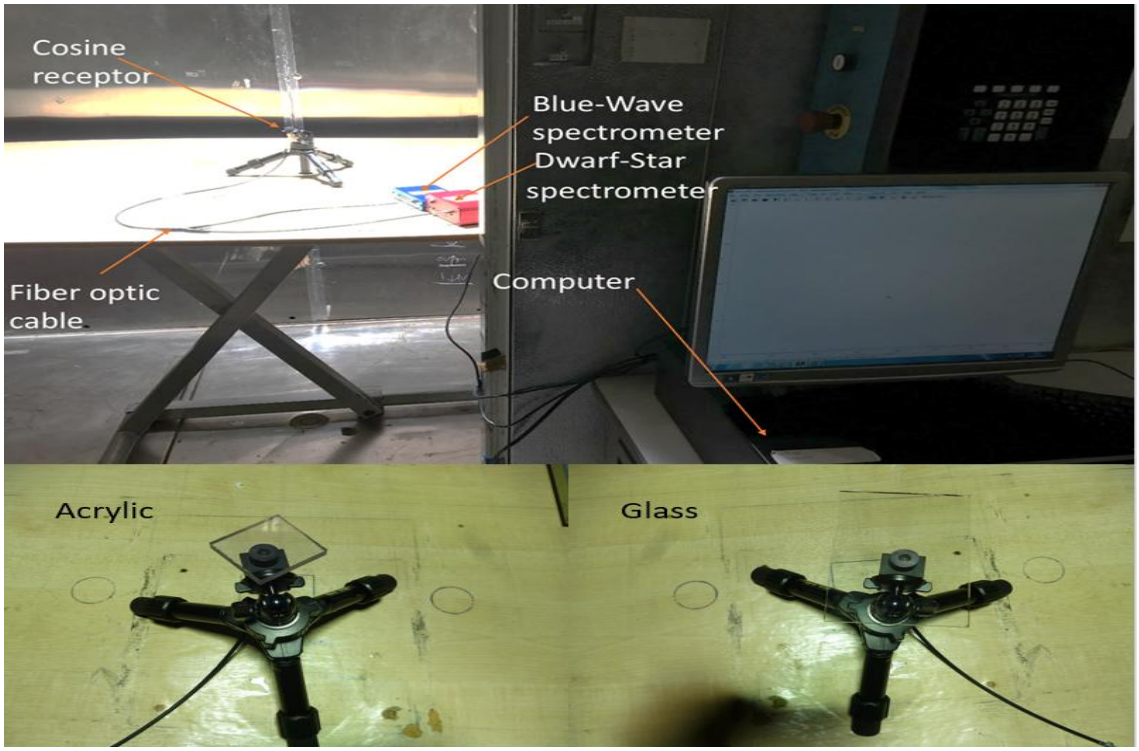

Figure 4.17 the setup used to test and compare the transmittance of the glass to the acrylic

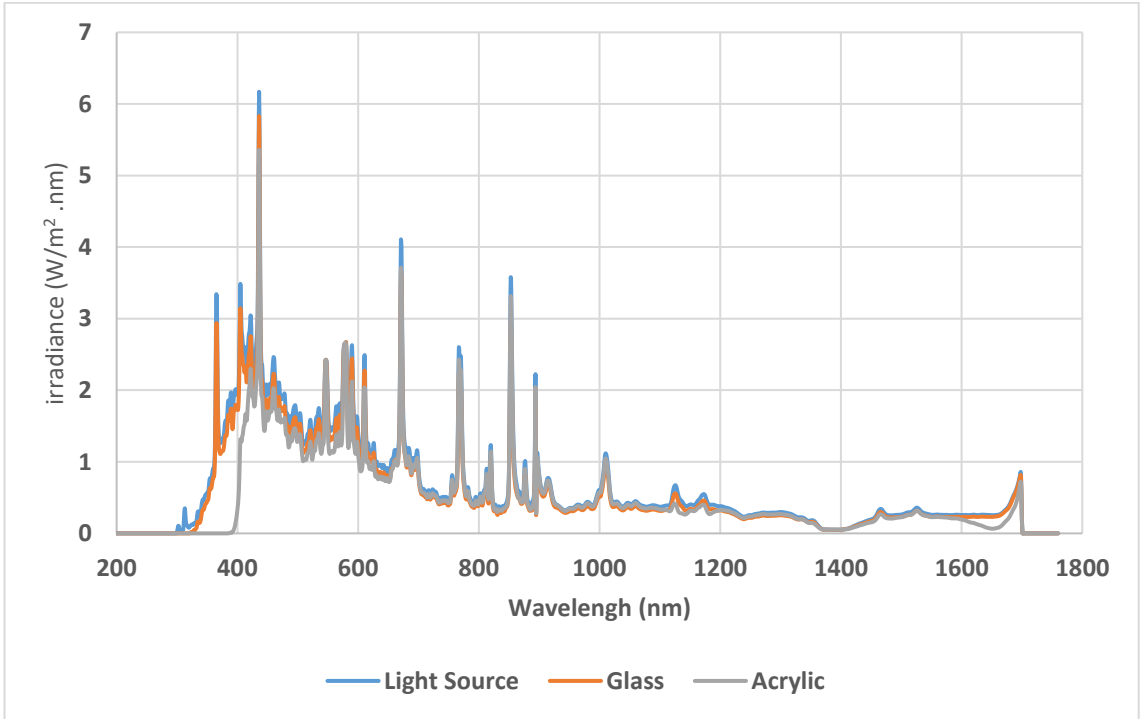

Figure 4.18 Spectrum comparison between the light source ,what is transmitted throw the glass, and throw the Acrylic.

By dividing the spectrum obtained from the glass and the acrylic by the reference spectrum of the light source, the transmittance of both materials are obtained. It can be seen that the glass transmits around 88% of the light while the acrylic transmits around 75% of the light over the measured spectrum. Therefore, the decision was made to use glass in order to maximise the amount of energy that can reach the water.

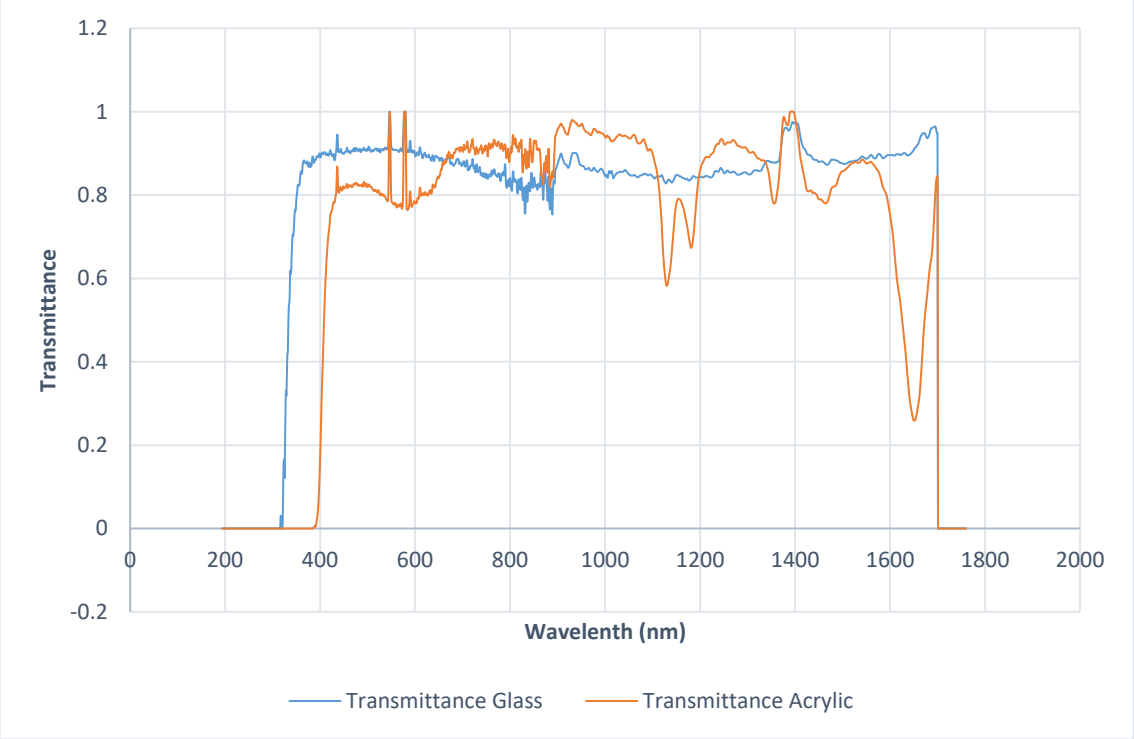

Figure 4.19 Transmittance of the glass and the acrylic

4.3.5 Aluminium condenser

The condenser was made from a 2 mm thick aluminium. The configurations that were set to be tested required fabrication of two different condensers. The one that covers a larger condensing area, and the other that only covers the slope where the thermoelectric is mounted. The big condenser is bent at 19.6 cm from the bottom to follow the shape of the chamber. A smaller aluminium plate was used also in the second conventional like configuration.

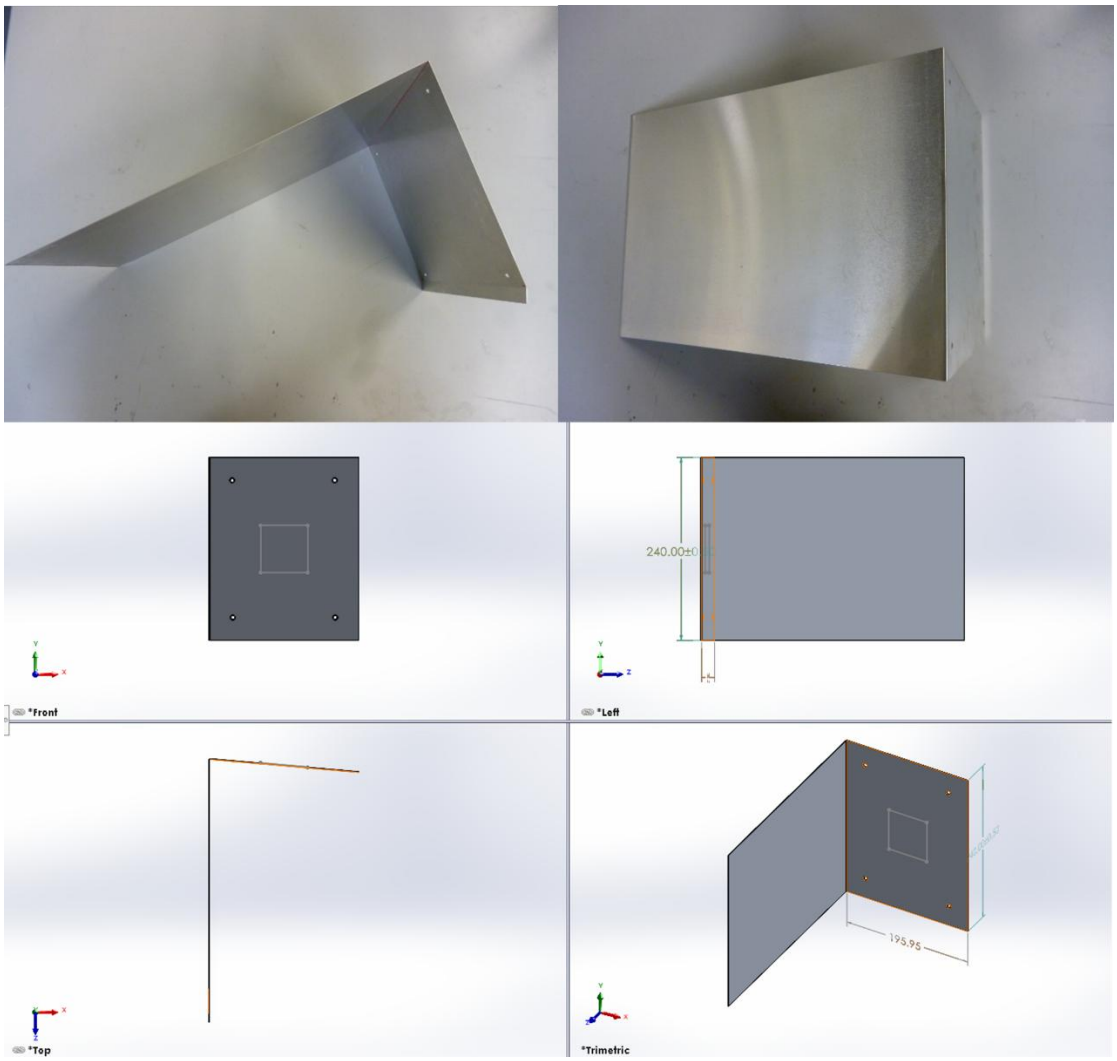

Figure 4.20 the aluminum condenser used in the designed system

4.3.6 Heat Exchanger

Two heat exchangers were employed in this design to heat the sample water, a big one used to collect the heat from the PV panel, the second is smaller and mounted on the hot side of the thermoelectric module.

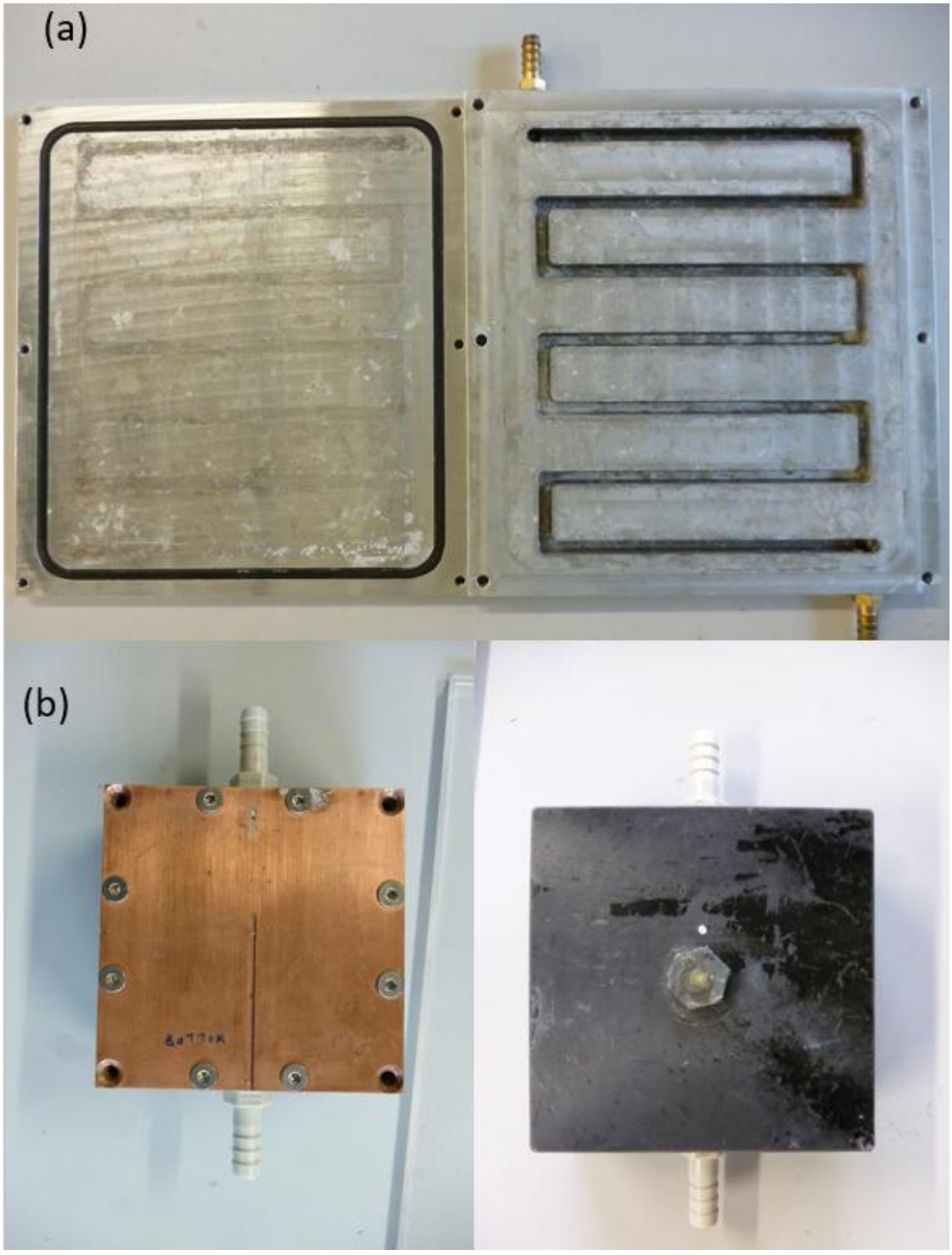

Figure 4.21 (a) the heat exchanger used with the PV panel. (b) the heat exchanger used on the hot side of the thermoelectric.

4.3.7 Instrument and sensors.

To perform the experimental investigation, the hybrid PV-T TE distillation system is connected to a range of sensors and data acquisition instruments. A power supply is used to perform the experiment when using thermoelectric only. To harvest the power generated by the PV-T panel an Epever Tracer-AN MPPT Charge Controller is used. It connected to a small battery. Two Buck converters are connected to the output terminal to supply the power to the TE module and a small pump. The pump is used to circulate the sample water from the evaporation chamber to the two heat exchangers and back to the evaporation chamber.

To monitor the temperature of the system, 8 K-type thermocouples were used to measure the temperatures of the cold and hot side of the thermoelectric module, water, PV-T panel, both condensers, vapor inside the evaporation chamber and ambient, respectively. All thermocouples were connected to TC-08 data logger which allows to record the temperatures to the PC.

The relative humidity was measured and recorded using a EL-USB-2+ data logger. It is a battery-operated device, and the data can be downloaded to the PC after the experiments finished. Two small plastic bottles were used to collect the water from the two condensers through the collecting channels. A small scale was used to measure the amount of water condensed every hour.

4.3.8 Testing and benchmarking the system.

In order to understand the behaviour of the system, a series of experiments were performed to test the system in a way that allows the understanding of the contribution of each component on the system performance. The chamber were filled with 2.7 litres of water each time, and the tests ran for 5 hours with each experiment was repeated for 3 times.

Firstly, the system was tested using the thermoelectric module as the only heat source to heat the water and the big aluminium condenser that covers both condensing slopes were employed. A total power of 10W were supplied to the thermoelectric module and the pump. This power was chosen in order to facilitate the direct comparison with the case when the thermoelectric module is powered by the PV panel, which can deliver a output power of 10W at the maximum power point.

In the second experiment, the electric power generated by the PV panel was used to power the thermoelectric module and the pump. In addition, the heat generated in the PV panel was collected through heat exchanger, together with the heat collected from thermoelectric module, to heat the water. In this configuration, the PV-T panel was mounted on the 30-degree slope and the condenser used was the big one that covers both condensing slopes.

In the third experiment, the PV-T was removed from the top and placed on the side of the system. A smaller aluminium condenser was used and placed on the 65-degree slope surface. This allowed the sunlight to heat the water directly and to be absorbed by the black coated aluminium that was submerged at the bottom of the water. In this configuration, the water was heated by multiple sources including thermoelectric module, PV-T panel, direct sunlight and aluminium absorber.

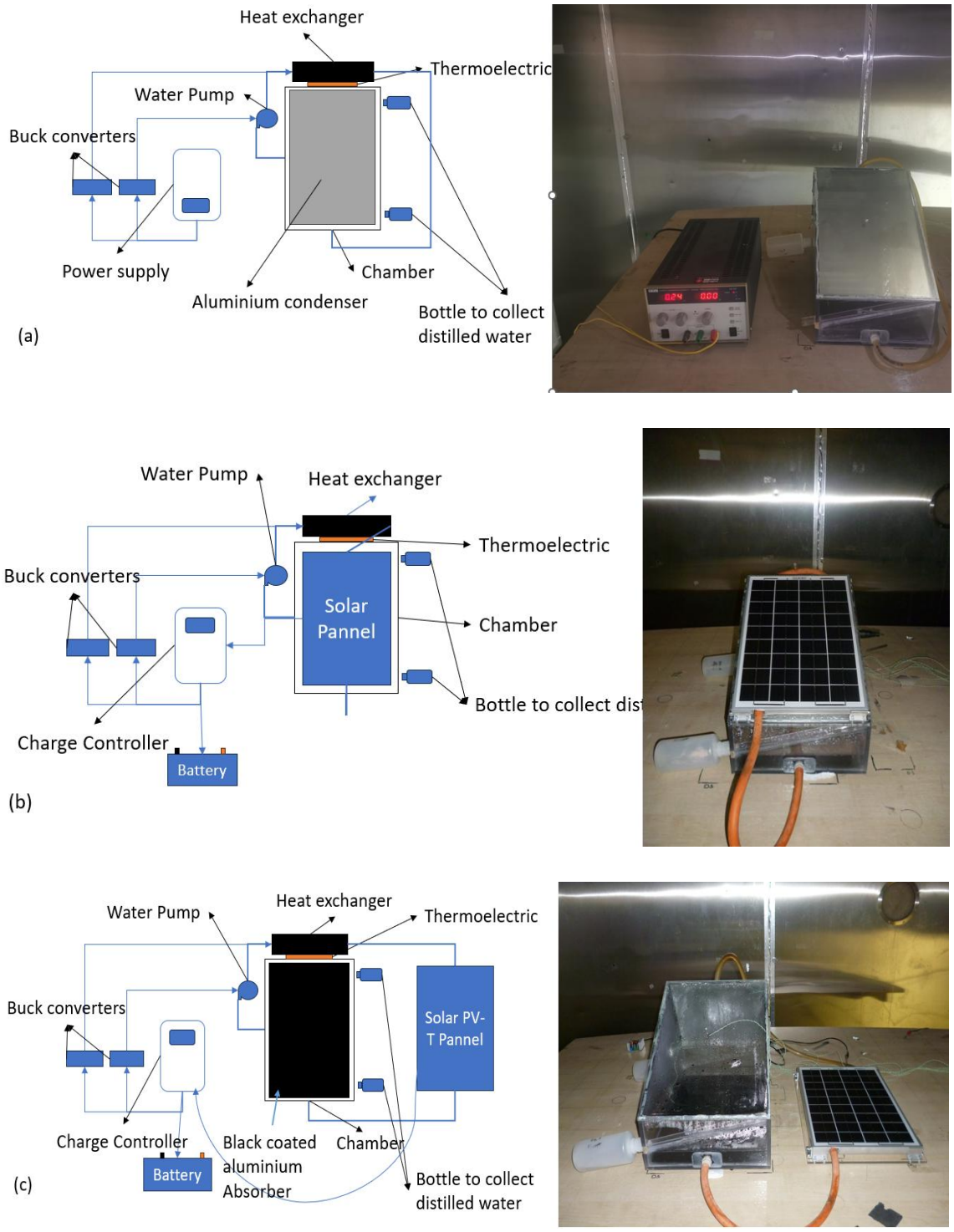

Figure 4.22 the setups and a schematics of the three configuration of the system to be tests.(a) the cofiguration using Thermoelectric only.(b) using PV-T and the TE.(c) using PV-T and TE and black absorber submerged in water.

4.3.9 Results and discussion

4.3.9.1 Thermal behaviour

Figure 4.23 illustrate the temperature profile of the water inside the chamber, the cold and hot side of the thermoelectric, the vapour, the aluminium condenser, the glass cover, the PV-T panel, and the ambient air temperature. the system component reaches almost steady state after the 5 hours time's period of the experiment as it can be seen from the Figure 4.23.

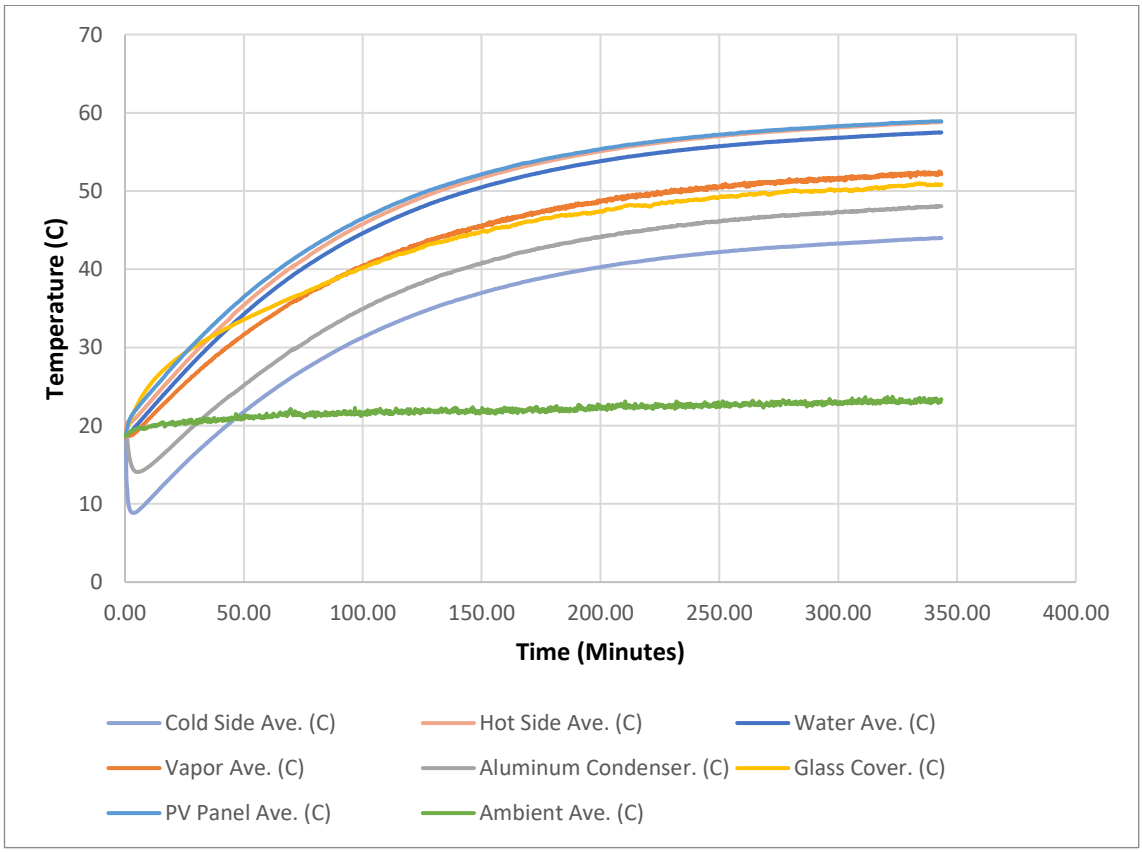

Figure 4.23 The temperature variation of the system components PV-T+TE and black absorber submerged in the water

A comparison of the water temperature change using the three configurations: (Thermoelectric only, PV-T+TE, PV-T+TE and black absorber submerged in the water) is shown in Figure 4.24. It is clear that the configuration where the black absorber submerged in the water gives the highest water temperature increase,

where the water temperature increased from around 18.8C to 56.7C during a period of 5 hours of the experiment. Using only the thermoelectric module as a source of heat proven to be not very effective, as the temperature of the water has risen by only 5.6 °C from 18.3 °C to 23.9 °C. When using both the TE module and the PV-T panel together as the heat source, the temperature of the water increased by 31.5 °C from around 18 °C to 49 °C.

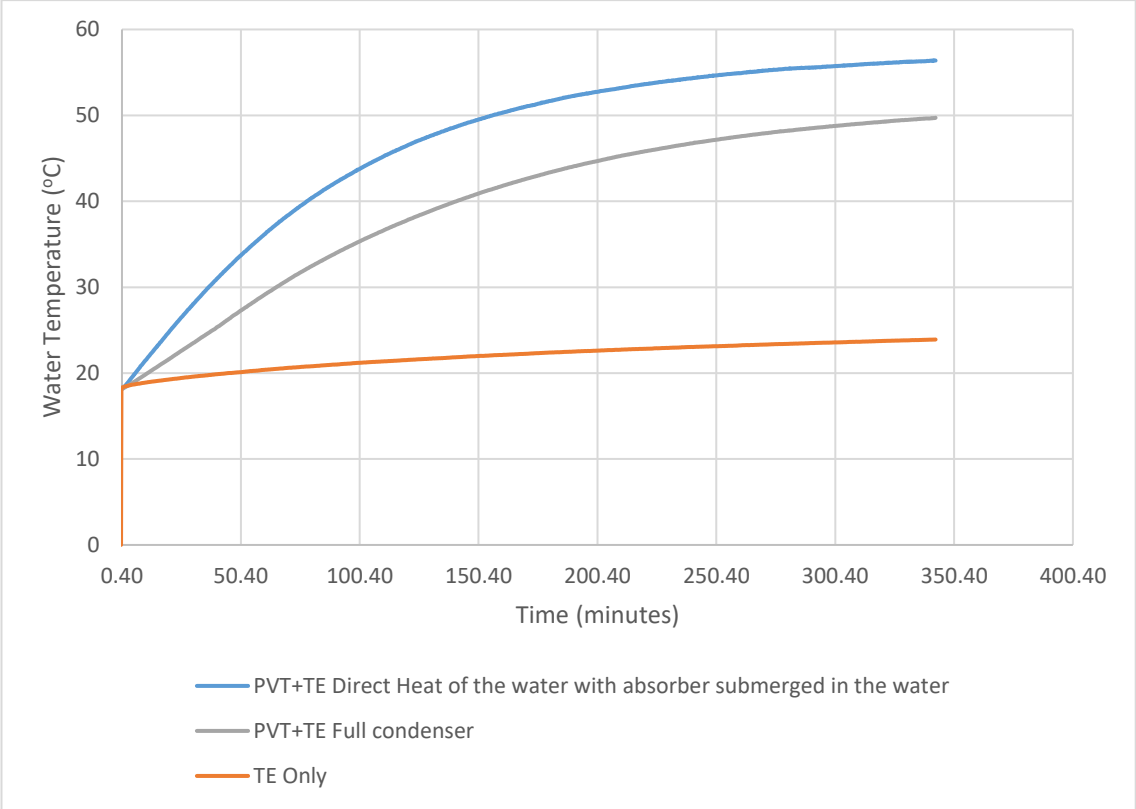

Figure 4.24 Comparing the change of water temperature of different system configurations

The rates of the temperature change for the three experiments are represented in Figure 4.25. The change rate in temperature is very high in the first hour, and it gets lower as time progresses. The highest increase in the first hour was obtained when the water was heated using the sources simultaneously (i.e., PV-T, TE, and the black coated absorber in the water), which is 36% higher than that using the PV-T and TE simultaneously, and 88% higher than that using the TE only. The hourly rate decreases with time as a result of the temperature difference

between the water and the surrounding become larger. As the difference in temperature increases, the heat losses increase to reach a point where the heat added to the water is equal to the heat lost.

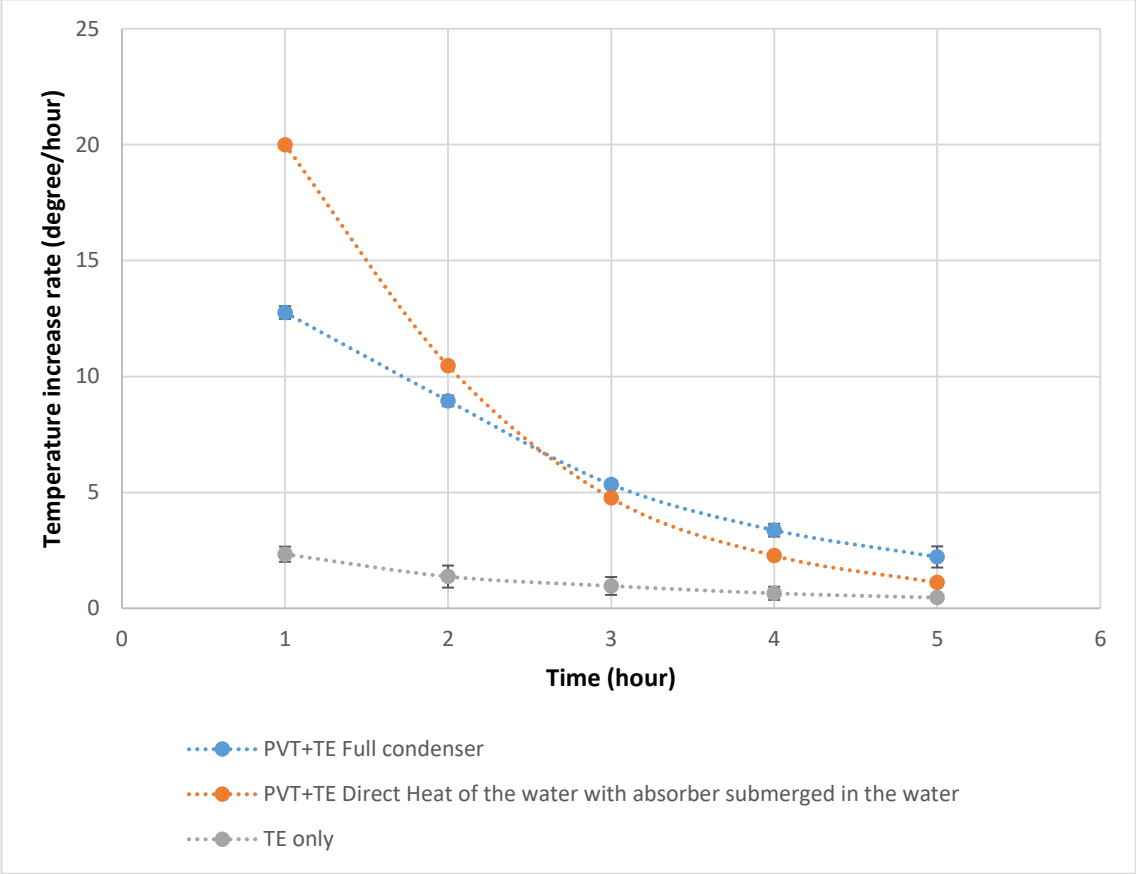

Figure 4.25 the hourly temperature increase rate of the water

The relative humidity inside the chamber was monitored and recorded as shown in Figure 4.26. When using the thermoelectric module only, the relative humidity reaches 98%, which differs significantly from other two configurations where the relative humidity did not exceed 88%. This can be explained from two aspects. For the case of using the thermoelectric module only, the amount of water evaporated is more than the water condensed using this heating process, which led to the air inside the chamber to approach the saturation point. Secondly, the relative humidity is a measure of the maximum capacity on how much water vapor in the air it can hold, which increases with the temperature of air. This

indicates that as the temperature of air increases its ability to hold water vapour increases. In the experiments where the "PV-T+TE" and the "PV-T+TE + black coated absorber" were employed to heat the water, the relative humidity decreases during the first hour, this could give the impression that there is no evaporation happening inside the chamber. However, this is not the case. The decrease in the relative humidity is due to a quick increase in the temperature of the air inside the chamber, even though the evaporation rate was also increased. In another word, despite the decrease in the relative humidity, the amount of water vapor in the air actually increases.

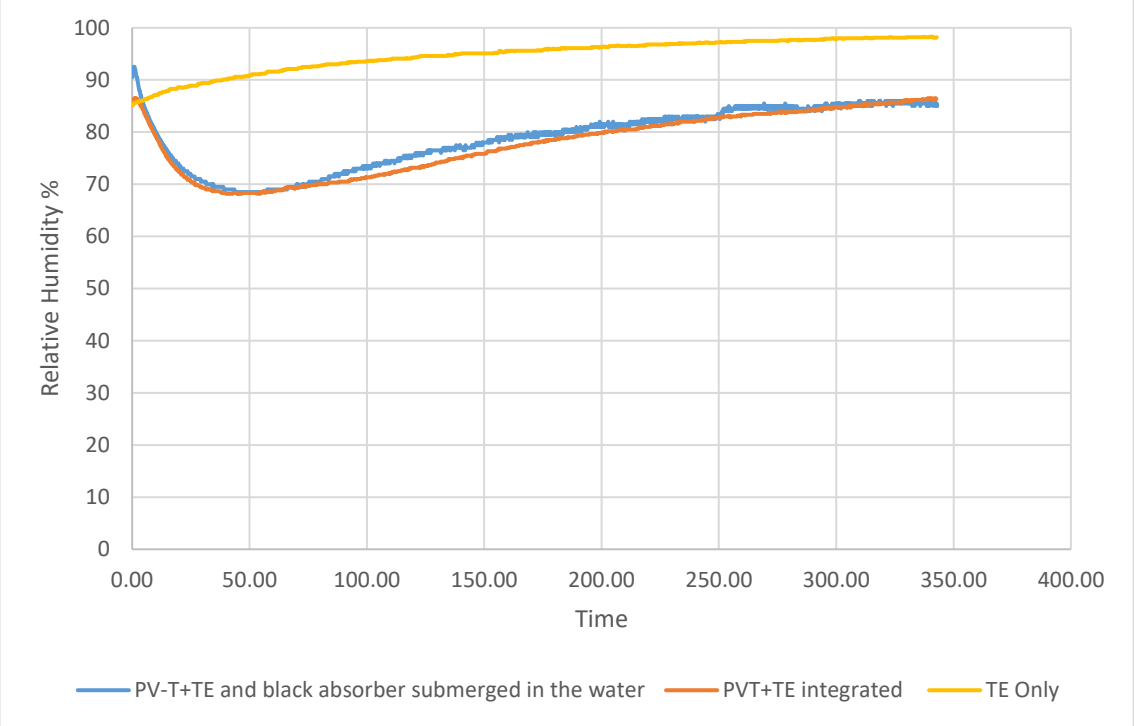

Figure 4.26 The change of humidity insidethe champer

To further understand how the temperature affects the relative humidity and the actual amount of water vapor in the air, the amount of water vapor per volume of air (absolute humidity) was calculated from the measured air temperature and the relative humidity using equation 4-2.

$$\boldsymbol{AH = \frac{RH * Ps}{Rw * T * 100}} \qquad 4\text{-}2$$

where, *RH* is the relative humidity, P_s is the saturation vapor pressure, R_w is the specific gas constant of water vapor which has value of 461.5 J/kg.K [100], and T is the air temperature in the chamber. The calculated results are shown in Figure 4.27. It can be seen that the amount of water vapor per unit volume continues to rise from the beginning to the end of the test.

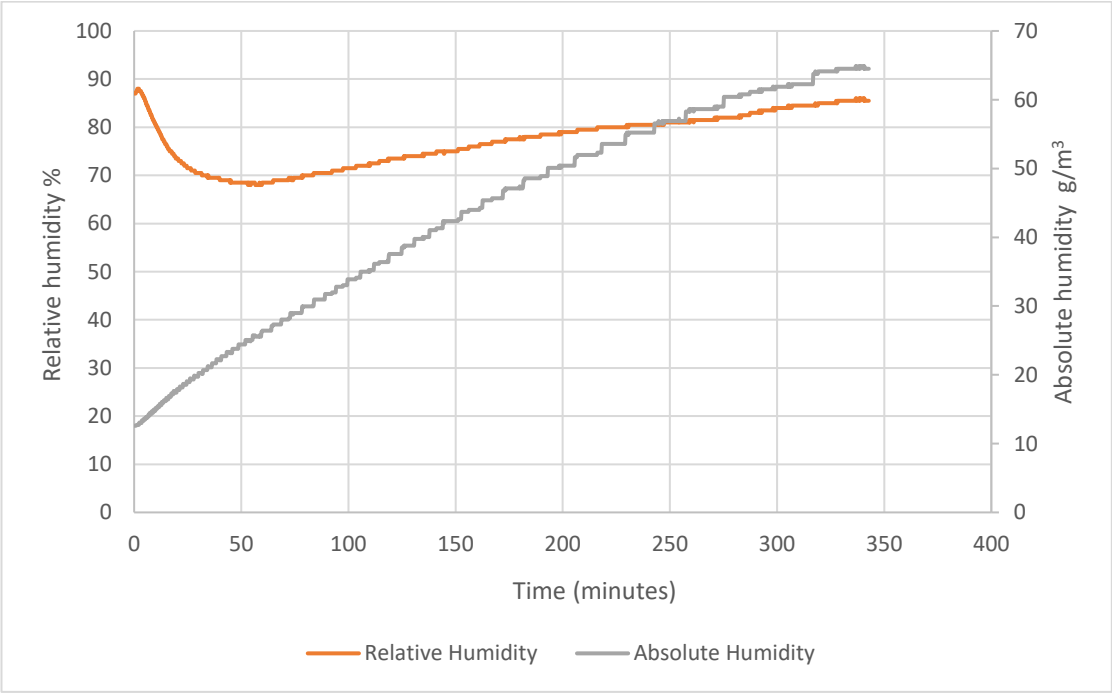

Figure 4.27 comparision between thechange of relative humidity aginst absolute humidity.

One of the most important parameters that affect the performance of the system is the temperature difference between the vapor inside the chamber and the condensing surfaces. as stated earlier that the first two experiments use an aluminium condenser for both slopes which will be cooled by the thermoelectric, in the test where the water will be heated directly by the solar irradiance, the glass cover serve as condensing surface on the 30 degree slope, and small condenser will be mounted on the 65 degree slope and it is cooled by the thermoelectric.

The difference in temperature between the two slope and the vapor in the chamber is shown in Figure 4.28 and Figure 4.29. for the surface mounted on the 65 degree on the cold side of the thermoelectric the temperature stays almost

constant through the test starts at around 7 °C and reaches around 6 °C, except when using the small condenser where it starts similar to the other two but it decreases after around an hour from the beginning of the test to reach around 4.8C° by the end of the 5 hour test. This can be attributed to that the condenser losses some heat because it is being exposed to some irradiance, in contrast with the two other experiments where the first uses only thermoelectric and in the second the PV-T cover the system and blocks the irradiance from reaching the aluminium condenser.

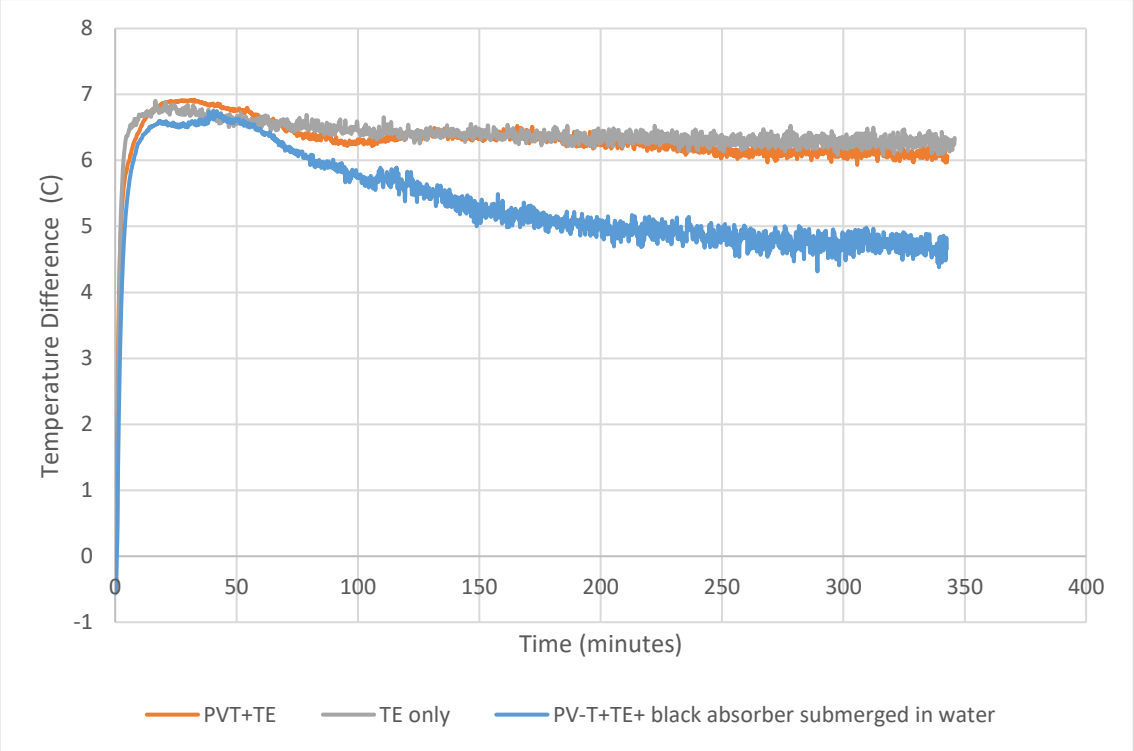

Figure 4.28 the temperature diffrence between the vapor inside the chamber and condinsing surfce on the 65-degree angle

On the other hand, there is a big contrast between the temperature difference on the 30-degree condensing surfaces, a comparison is shown in Figure 4.29. when using the thermoelectric only the temperature difference at the start was around -0.5 C° and it reaches around zero at the end, this indicates the surface temperature stays higher than the vapor temperature. Similarly, when using the integrated PV-T +TE system, the temperature difference stays all the time of the experiment below zero. The only experiment which the surface temperature was

below the vapor temperature was when we use the black absorber submerged in the water, the glass temperature at the beginning of the experiment increased dramatically and the difference in temperature reaches around -4.5 C^o but at around one hour the glass temperature become lower than the vapor temperature and the difference reaches around 1.5 at the end of the experiment. The effect of this will be later seen on the condensation rate of each condensing surface.

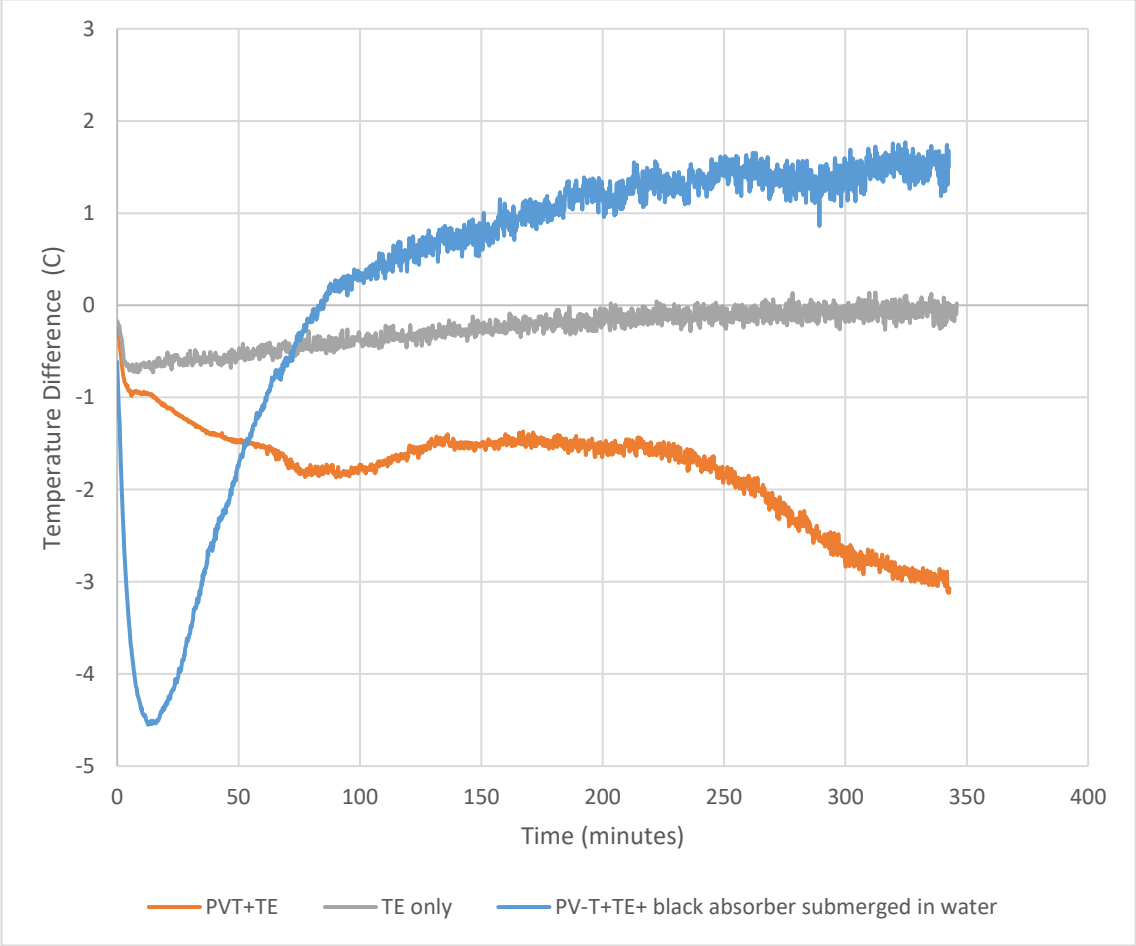

Figure 4.29 the temperature diffrence between the condinsing surfce on the 30-degree angle and the vapor inside the chamber

4.3.9.2 Water Productivity and produced water quality.

The accumulated water production from the three configurations is shown in Figure 4.30. the water weight is measured every hour using a scale. Using the thermoelectric module only, the amount of water produced at the end of 5-hour operation was 14.78 g. An significant increase to 37.57g of water production was obtained when the PV-T was added to the system, representing an improvement by around 154%. A further increase to 84.1g was achieved by adding the direct irradiance heating with the black-coated aluminium absorber, which represents an improvement by further 123%.

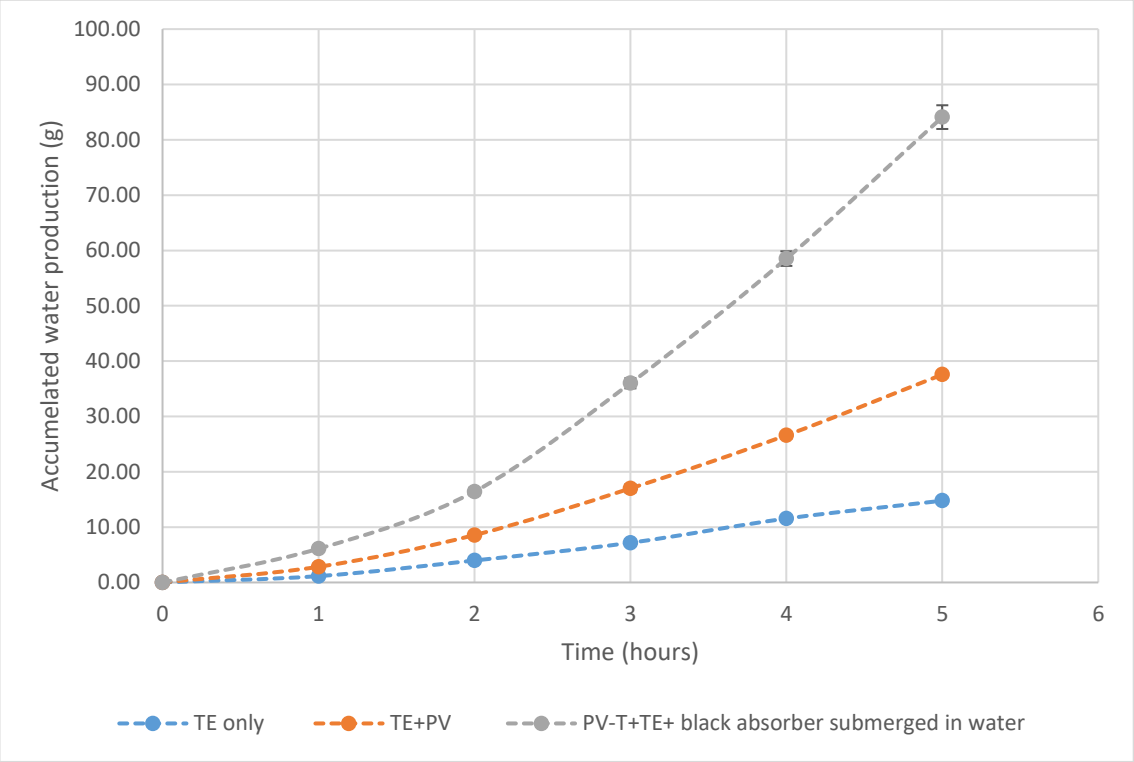

Figure 4.30 Accumelated water production (g)

To investigate the effectiveness of each condenser, the water produced separately by each condenser is shown in Figure 4.31 and Figure 4.32. For the configuration using only the thermoelectric module as the heat source, the amount of water produced by the 30-degree slope condenser did not exceed 22.5% of the total. This percentage is even lower (5%) when the PV-T panel was added to the system. This indicates that most of the water production came from the condenser on the 65-degree slope. The ineffectiveness of the condenser on

the 30-degree slope is likely due to the fact that the TE module was not able to cool this condenser as seen in Figure 4.29 where the surface temperature of the condenser on the 30-degree slope remained above the vapor temperature inside the chamber during whole period of the experiment.

However, the effectiveness of this condenser has increased in the configuration where the water is also heated by the irradiance from the solar simulator and black coated aluminium absorber with the glass cover as the condenser. In this case the glass cover on the 30-degree slope produced around 37% of the total water production.

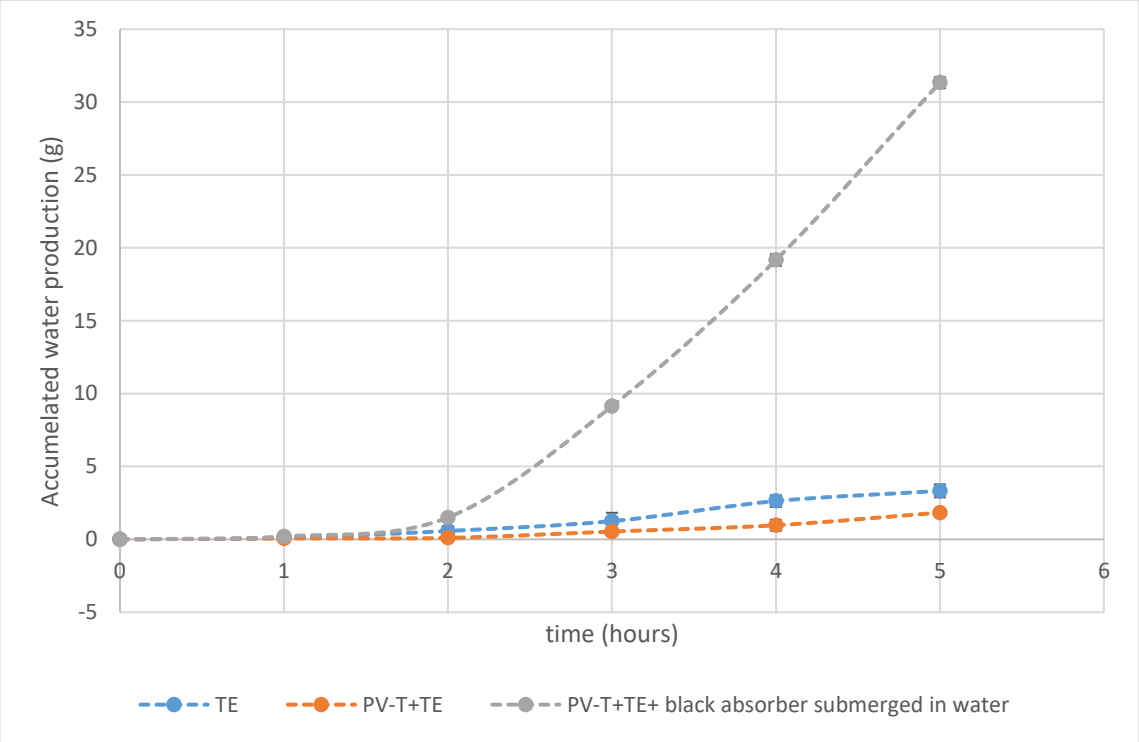

Figure 4.31 Accumelated water production (g) from the 30-degree condesing surface

Despite the improved water production when the glass cover was used as a condenser on the 30-degree slope, the condenser on the 65-degree slope still produce most of the water. To get the production in prospective, the water produced by both condensers was normalized by the area of each condenser. For the configuration using thermoelectric module only, the condenser on the 65-

degree slope can produce 0.19 kg/m^2 while the condenser on the 30-degree slope can only produce 0.04 kg/m^2. For the configuration with PV-T panel added the system, the condenser on the 65-degree slope can produce 0.54 kg/m^2 while the condenser on 30-degree slope can only produce 0.022 kg/m^2. Finally, when the glass cover and submerged black-coated aluminium absorber was further added to system, the condenser on the 65-degree slope produced 0.84 kg/m^2 and the condenser on the 30-degree produced 0.38 kg/m^2.

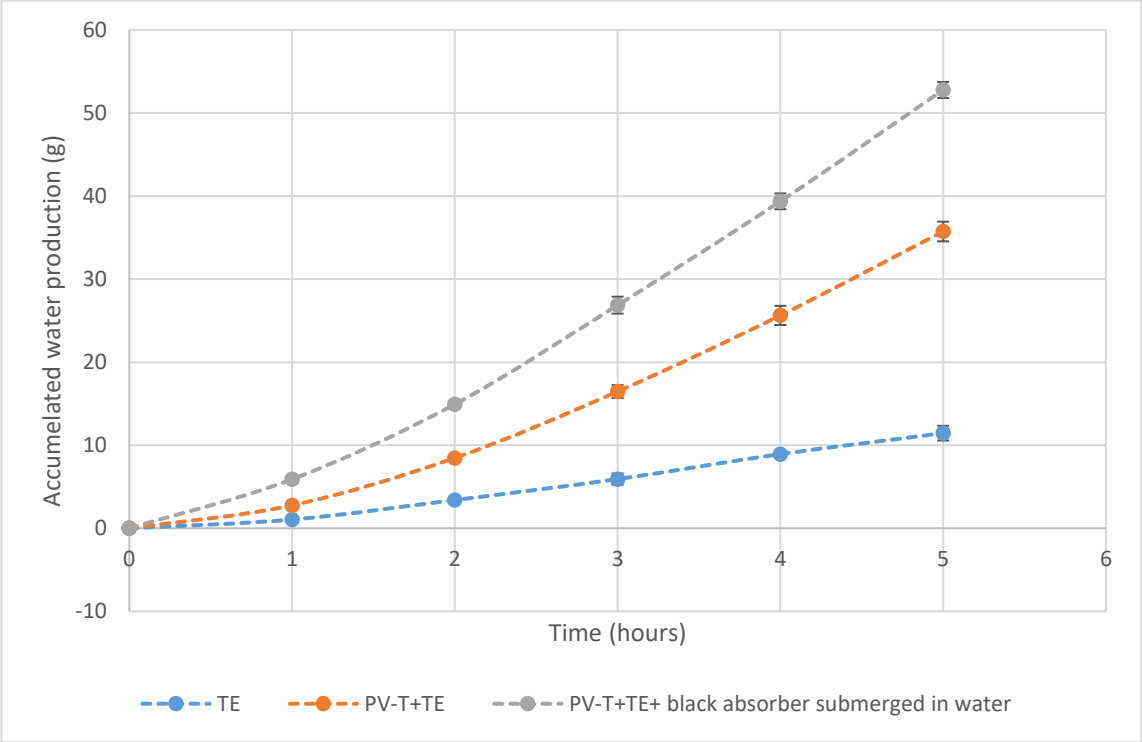

Figure 4.32 Accumelated water production (g) from the 65-degree condesing surface

The quality of the water in terms of total dissolved minerals was measured for the source water before condensing, and for the water produced from each condenser. A small TDS EC Tester Meter is used to measure the total dissolved minerals in the water. It was found that the water collected from the aluminium condenser contained more dissolved minerals than the water collected from the glass cover condenser in the third configuration. The tests show that the source water has a mineral content of around 155 ppm, while the water collected from the aluminium condenser has a mineral content of 16 ppm, and the water

collected from the glass condenser has mineral content of only 2 ppm. This may be attributed the fact that the aluminium is more reactive to water vapor than glass.

Figure 4.33 TDS EC Tester used to mesure the quality of the water.

4.3.9.3 Energy absorbed by the water and the system efficiency.

The heat energy absorbed by the water is equal to the heat input from the heat sources minus the heat losses to the surrounding.

$$\boldsymbol{Q_a = Q_{in} - Q_l} \quad \text{..... 4-3}$$

The heat losses from the water are mainly occur due to convection and radiation, and it proportionate to the temperature difference between the water and the surrounding. At the start of the experiments the heat losses are very small because the temperature difference between the water and the surrounding ΔT is small. Therefore, the heat losses can be neglected and the heat absorbed by the water is approximately equal to the heat input to the system at the initial period. Based on a technique is developed by Ramadan kazuz [13].

$$\boldsymbol{Q_a = Q_{in}} \text{ ..... 4-4}$$

The heat absorbed by the water is equal to the mass of the water multiplied by its specific heat multiplied by the rate of temperature change.

$$\boldsymbol{Q_a = m_w * C_p * \frac{\Delta T}{\Delta t}} \text{ ..... 4-5}$$

The absorbed heat by the water can then be determined from the slope on a T-t plot as shown in Figure 4.34. The results of the energy absorbed by the water compared to the energy available is presented in Figure 4.35. It can be seen that the amount of heat reaches the water when using thermoelectric is higher than the energy supplied to the thermoelectric module due to the thermoelectric module operates like a heat pump. However, when the PV-T panel was added to the system, the amount of energy absorbed by the water is only 68% of the available energy, and it is reduced to around 60% when the glass cover and submerged black coated absorber was further added to the system. This can be attributed to the losses due to the limited absorptivity of the PV-T panel, the black coated absorber, and the transmittance of the glass cover.

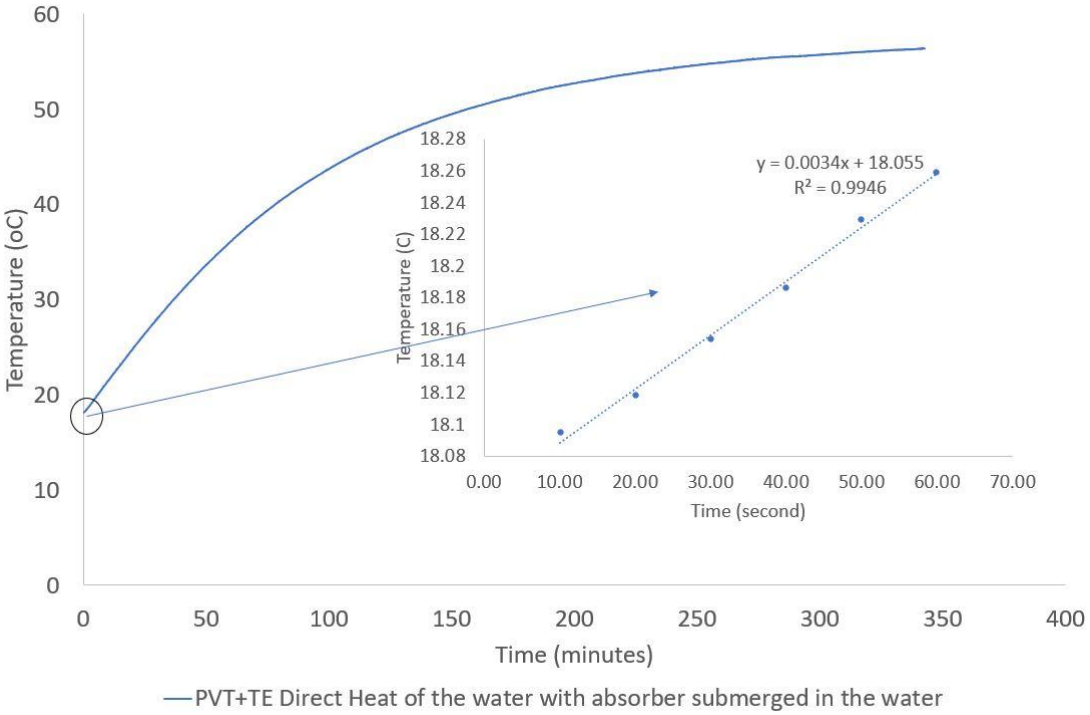

Figure 4.34 Temperature of the water in the evaporation chamber as a function of heating time. The inset shows the temperature profile at the initial period and a linear relationship between the temperature and time is evident.

As can be seen in Figure 4.35, the amount of heat reaches the water when using thermoelectric is higher than the energy supplied to the thermoelectric. but when we add the PV-T the amount of energy absorbed by the water is only 68% of the available energy, and it is reduced to around 60% when we add the absorber in the water. This could be because that of the PV-T and the black absorber does not absorb the whole energy from the irradiance, and the glass cover only transmits around 88% of the whole spectrum.

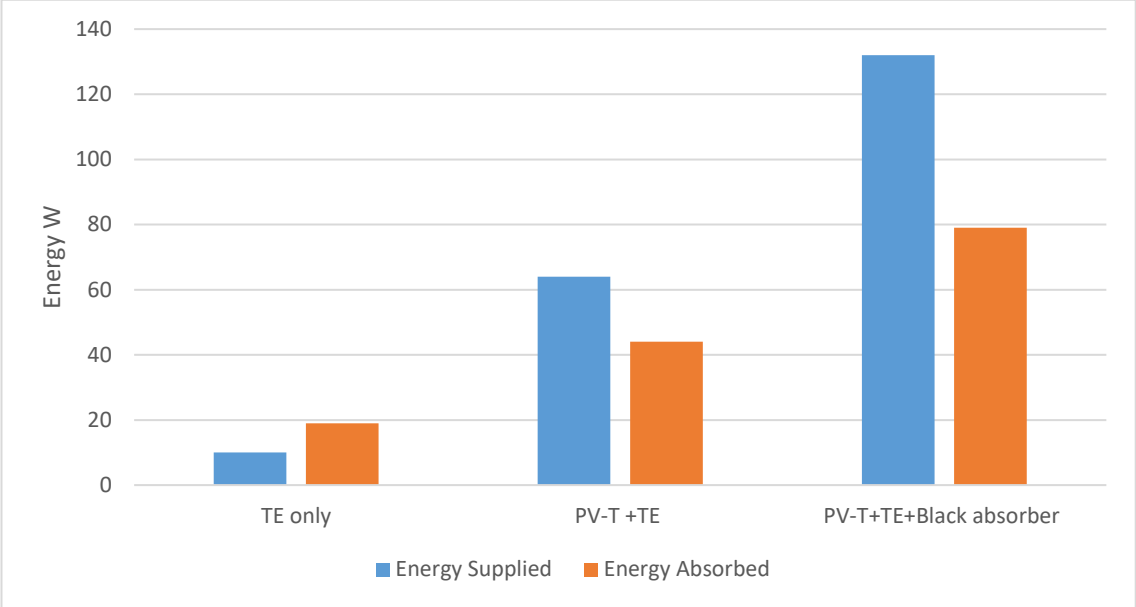

Figure 4.35 comparison between the energy available and absorbed by the water

The efficiency of the distillation system is defined as follow:

Efficiency (η) = [Output Energy (Latent Heat of Condensed Water) / Input Energy] × 100%.

Latent Heat of Condensed Water= m*hfg

Where: m is the amount of water produced in kg

hfg is the heat of vaporization in kj/kg

the input energy is the sum of the energy from the solar radiation and all the electricity input to the pump and the thermoelectric.

The efficiency of the system when using the thermoelectric only is the highest among the three configurations investigated. It is 20% over an operating period of 5 hours. The lowest efficiency of 16.5% was obtained from the configuration that uses the TE, PV-T and submerged absorber. Figure 4.36 shows the efficiency as a function of time for three configurations investigated. It is noted that all available energy is from sunlight, which is free. Therefore, the water productivity per unit area and cost are more important in terms of its economic viability.

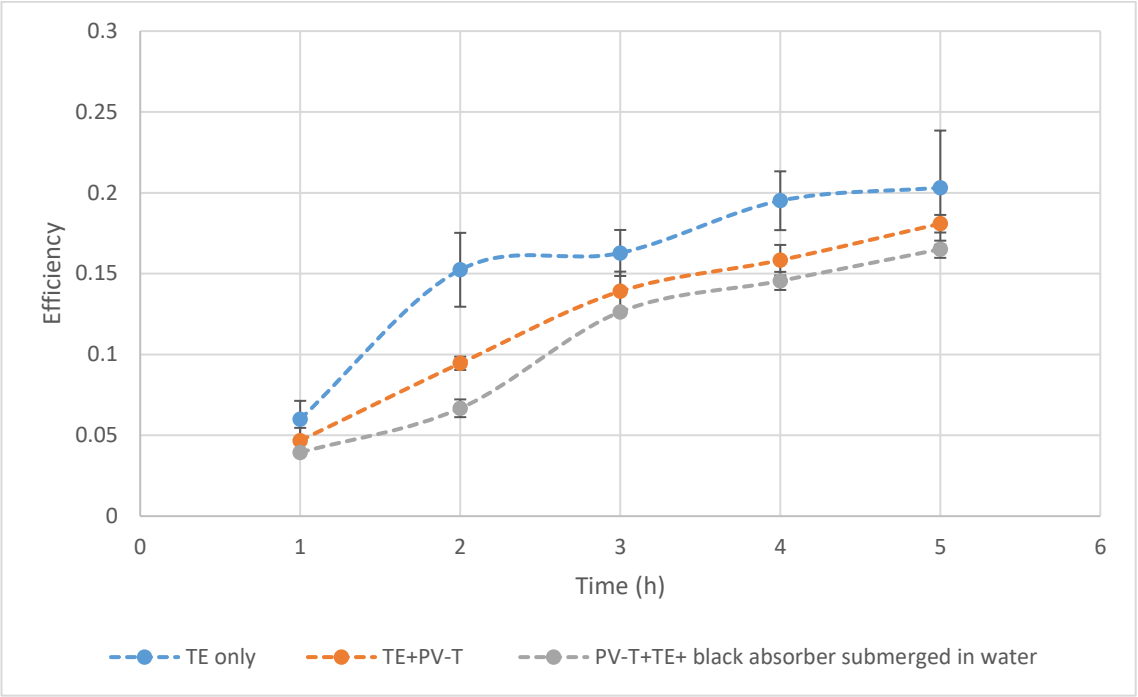

Figure 4.36 Comparing the efficiency of the three configuration of the system

4.4 Conclusion

A test to evaluate the solar simulator was conducted, the solar simulator tested in three categories as specified by E927-10 standards. It has been found that the solar simulator performs very good in terms of spectral match and Temporal Instability. However, the light source performs poorly in nonuniformity test.

The designed Hybrid solar PV-T TE distillation system tested under the solar simulator, it is tested first with the thermoelectric only, then the PV-T is introduced to the system where it is mounted on the top of the 30 degrees angle surface. Last experiment were done using a small condenser covers only the 65 degrees angle surface and a black coated aluminium submerged in the water and heated directly by the light from the simulator. The water temperature increase rate is dramatically increased by adding solar as a source of heat to the system, consequently the productivity increased as well from 14.78 g. using thermoelectric module only, to 37.57g after adding the PV-T, to 84.1g after introducing the submerged black absorber. The best combination to give the

most productivity is the system where the heat from the simulator is collected from the PV-T module using the heat exchanger, and directly by heating a black absorber submerged in the water.

Using thermoelectric cold side to cool the condenser results in almost constant temperature difference between the condenser and the vapour inside the chamber from the beginning of the experiment to the end, in contrast to the glass cover where it is cooled passively, it is temperature stays above the vapor for the first hour.

Chapter 5: Improve the Productivity by Using a Fan to Cool the Glass Cover and Hydrophobic Layer on the aluminium Condenser.

5.1 Introduction

Two ways to improve the water productivity of the Hybrid PV-T TE distillation system will be investigated in this chapter. Firstly, the aluminium condenser mounted on the cold side of the thermoelectric will be treated by chemical etching technique to give it hydrophobic properties. This in theory should help improve the productivity of the system by promoting dropwise condensation, in return this will enhance the heat transfer between the condenser and the vapor. Secondly, the glass cover will be cooled by forced convection using a small fan, which will lead to more condensation and improvement in the water productivity of the system.

5.2 Investigate using hydrophobic layer.

Hydrophobic aluminium condenser has been prepared by using a chemical etching technique. The process aims to give the aluminium condenser a repellent property which will impact the condensation on it is surface. The chosen method is an easy and effective way to interduce the hydrophobic layer on aluminium [3]. It uses potassium hydroxide to achieve the roughening of the surface and lauric acid to lower the surface energy of aluminium surface. The author suggested a way to achieve this by a two-step process where the aluminium surface first roughed with the potassium hydroxide (KOH) solution and then its surface energy lowered by the lauric acid solution. This method is the one adopted in this study. and a one-step where the KOH solution mixed with Lauric acid solution, and the aluminium submerged in it, the roughness and lowering the surface energy of aluminium were done in a single step.

5.2.1 Preparing the hydrophobic layer.

The aluminium condenser initially cleaned with distilled water and acetone; this is to ensure that the surface is free from any contamination that may affect the result. then it is submerged in a solution of 10mg/litre of potassium hydroxide in distilled water for 60 minutes. The condenser the then rinsed with ethanol and distilled water. Finally, it is immersed in 20gm/litre of ethanol solution of lauric acid for 30 minutes. The aluminium condenser then left to dry in air for 20 hours.

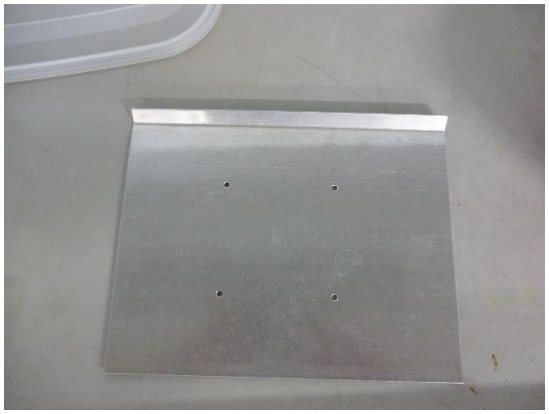

a)

b)

c)

Figure 5.1 a) The aluminium condenser before the hydrophobic layer. b) the aluminium condenser submerged in potassium hydroxide solution. c) The aluminium condenser after the hydrophobic layer

The modified aluminium condenser has a better contact angle as it is increased from around 70° to 113° as shown in Figure 5.2. This means that the aluminium condenser is now more repellent to water and the condensed water will bead up and form droplets instead of spreading out as a continuous film. This should encourage the droplets to roll off the condenser quickly. In addition, it should also increase the heat transfer between the vapor and the condenser because no water film between the vapor and condenser.

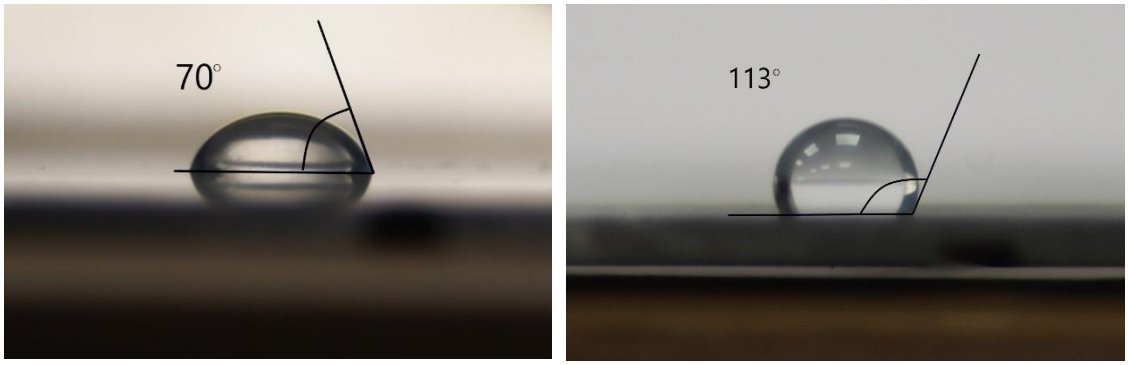

Figure 5.2 a) Shape of the water droplet without the hydrophobic layer .b) Shape of the water droplet with the hydrophobic layer

The treated condenser then installed on the cold side of the thermoelectric and the experiment repeated with the configuration that gave the best productivity in chapter 4.

5.2.2 Result

The effect of the hydrophobic layer on the system performance were investigated using untreated and treated aluminium absorbers, respectively, operated under the identical conditions. The hourly change of temperature of the water before and after introducing the hydrophobic layer is shown in Figure 5.3. The change is almost identical, and the maximum water temperature reaches almost the same value of 56.7 C for both cases.

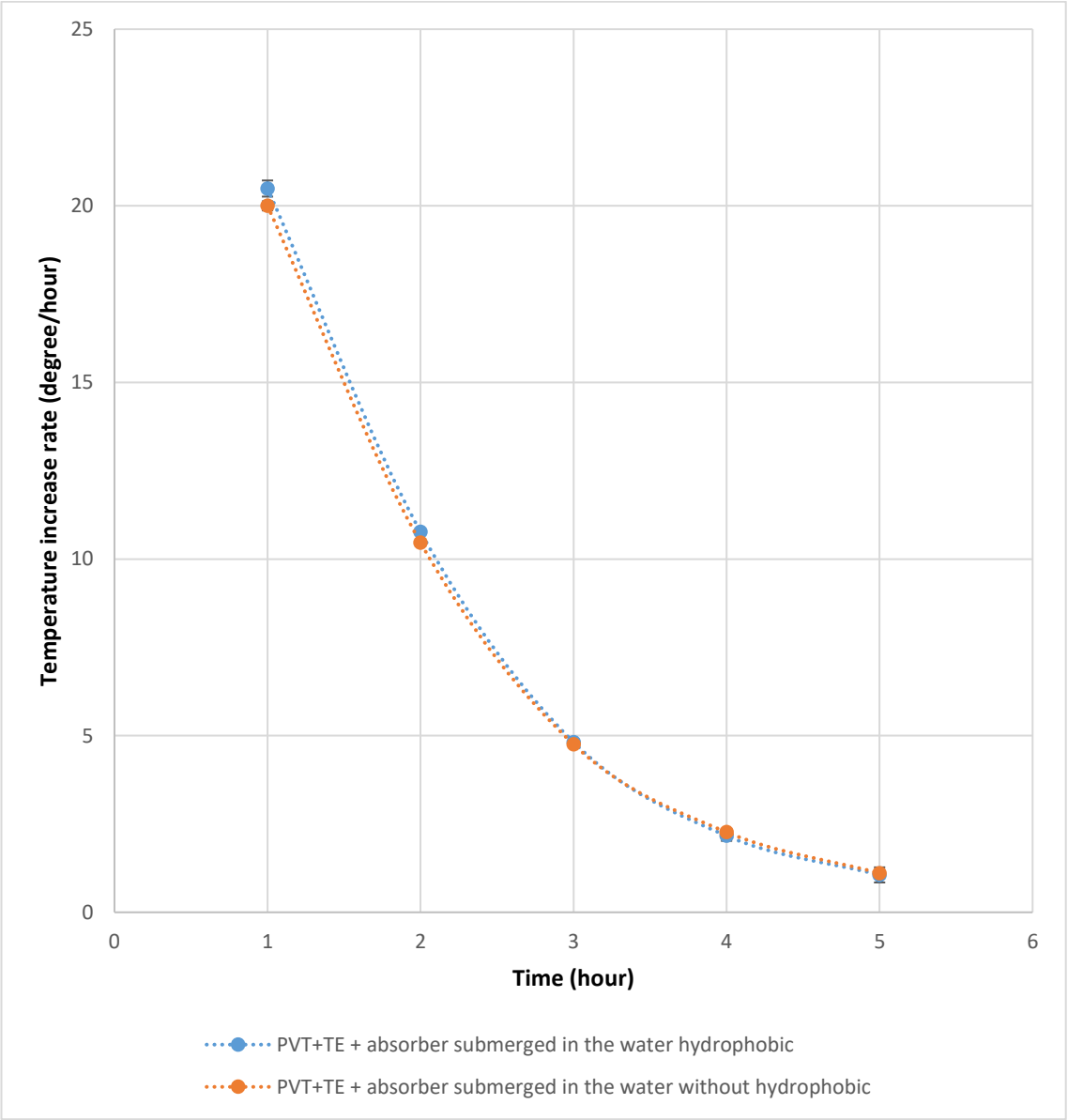

Figure 5.3 Comparing the hourly change of temperature of the water before and after introducing the hydrophobic layer

Figure 5.4 shows comparison between the amount of water produced before and after applying the hydrophobic layer. The total amount of water produced from the system are approximately the same before and after the introduction of the hydrophobic layer. After 5 hours of operation, the system produced 83.07 grams of water using the aluminium condenser with hydrophobic layer, compared to 84.1 grams using the aluminium condenser without hydrophobic layer. This represents around 1% reduction in total water production, which is within the

limit of the experimental errors. It is clear that, despite the improvement in the water droplet contact angle with the hydrophobic layer, it has no impact on the system performance and water productivity.

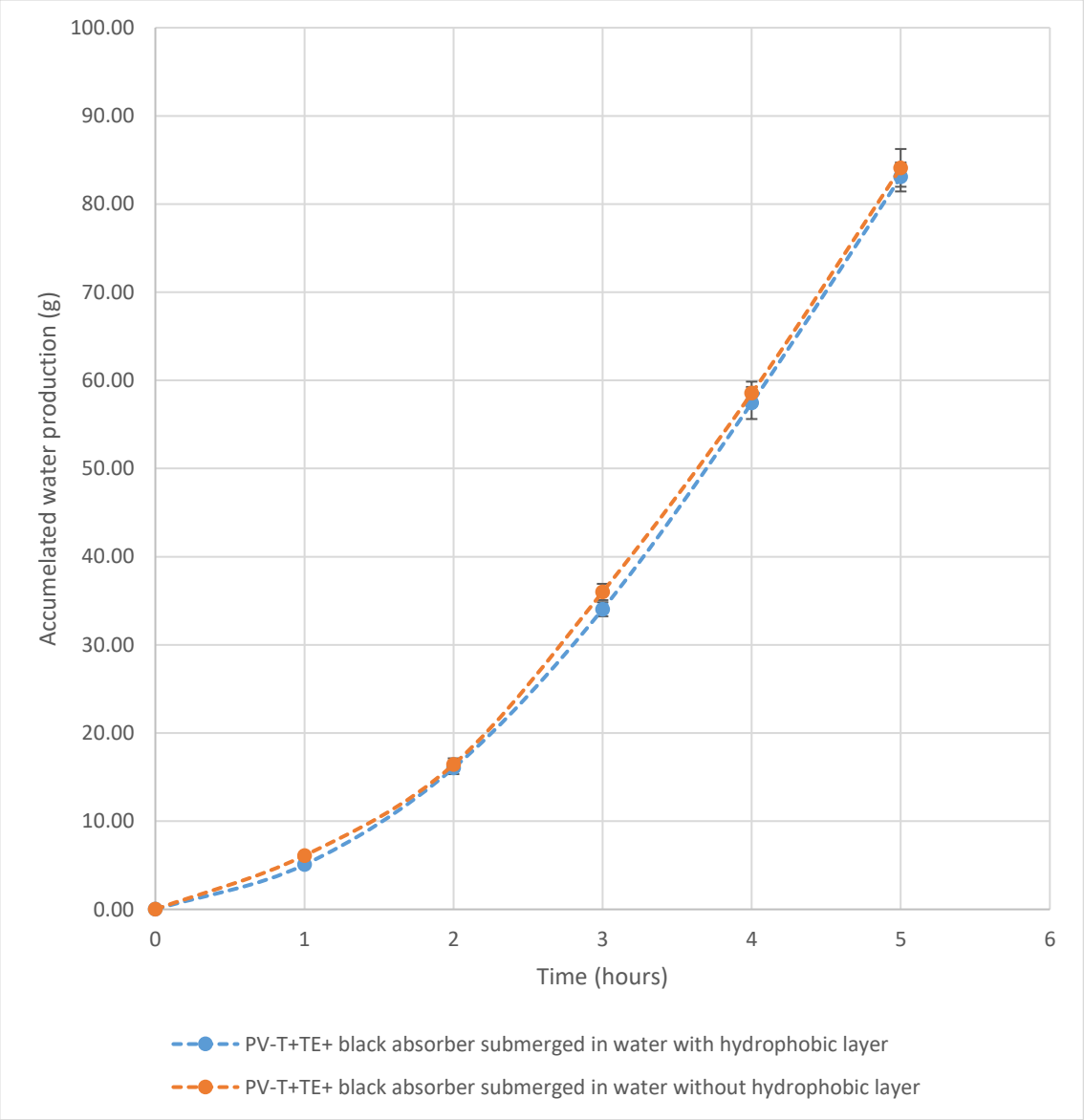

Figure 5.4 total water production from the system before and after the hydrophobic layer applied to the aluminum condenser.

To confirm the above observation, further investigations were carried out on the water production from the aluminium condenser and the glass cover and the results are shown in Figure 5.5 and Figure 5.6, respectively. It can be seen that both condensing surfaces produced almost the same amount of water as the previous experiment when hydrophobic is not introduced. It can be concluded

that the hydrophobic layer has no impact on the performance of the systems investigated in this study.

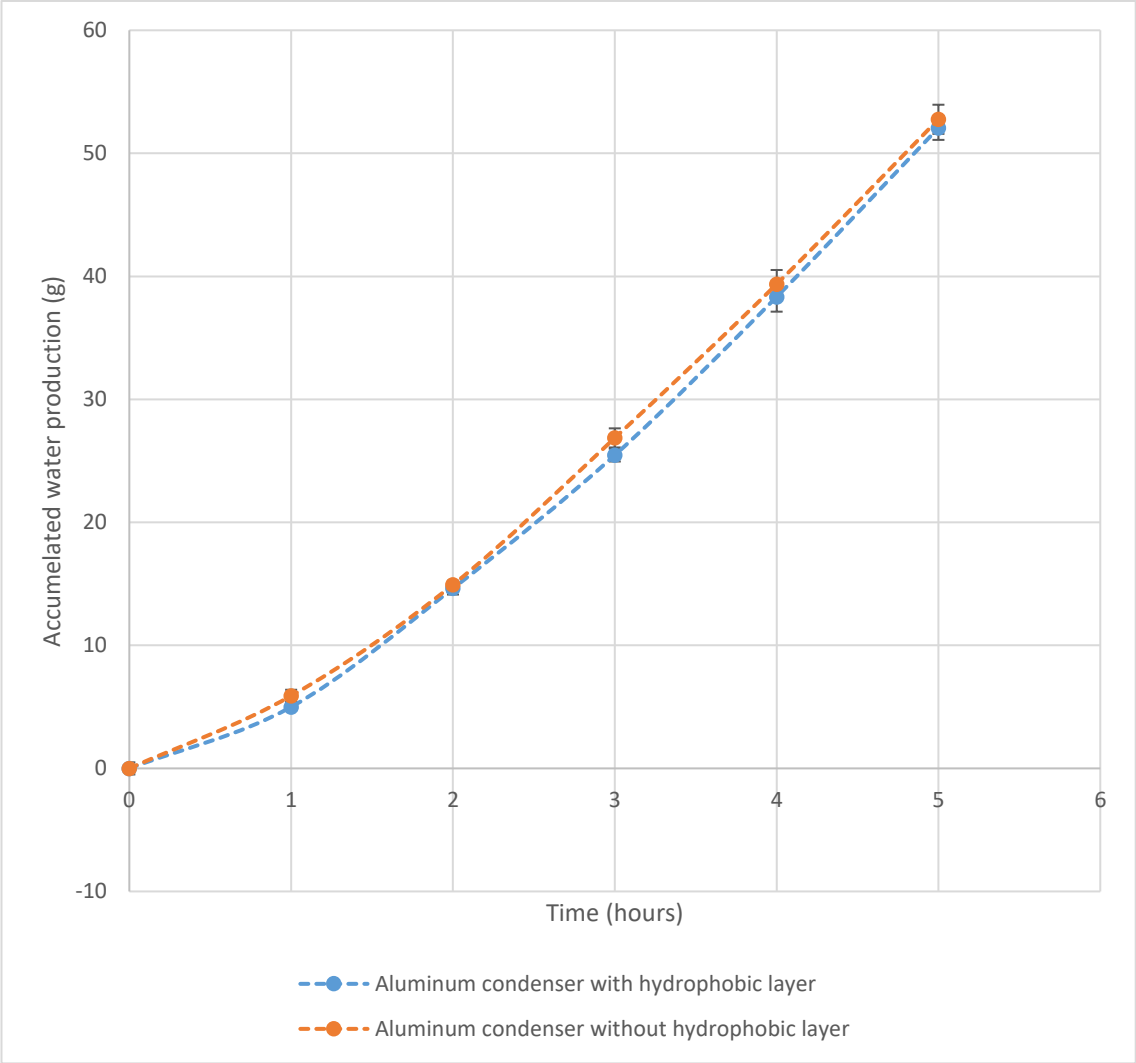

Figure 5.5 Comparing the water production of the aluminum condenser with and without the hydrophobic layey

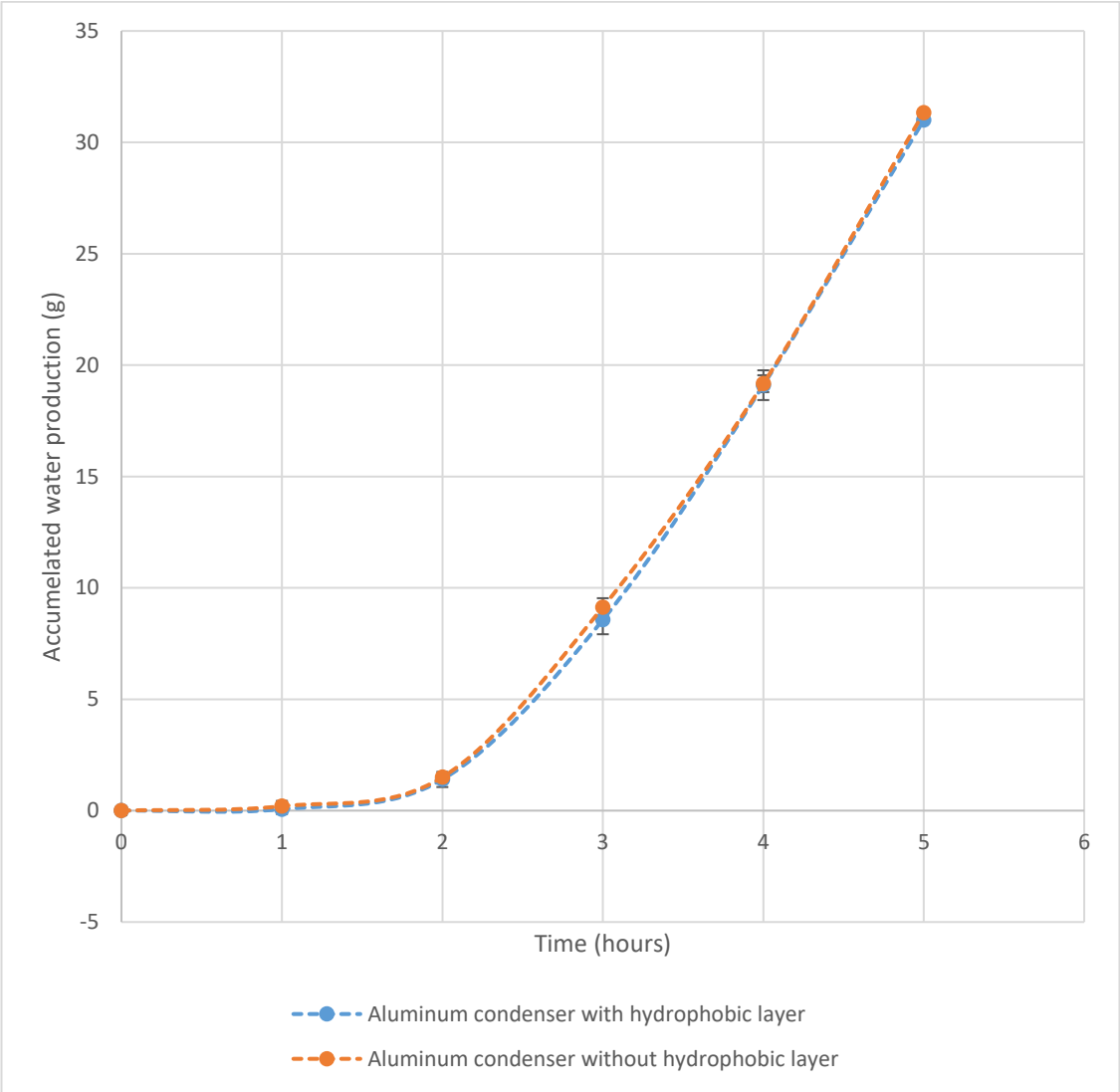

Figure 5.6 Comparing the water production of the glass cover befor and after the hydrophobic layey aapplied to the aluminum.

To further investigate if the hydrophobic layer has any influence on the water condensation on the surface of the aluminium condenser, the images of the condensation patterns before and after the application of the hydrophobic layer are shown in Figure 5.7. It is clearly that the water droplets have larger contact angle and look more round on the aluminium condenser with hydrophobic layer. Unfortunately, this feature does not lead to any improvement in this study. This is probably because the aluminium condenser without the hydrophobic layer in the current design (with a slope of 65 degree) is already sufficient in transporting the water droplets to the water outlets. It is anticipated that the advantage and effectiveness of the aluminium condenser with the hydrophobic layer will

become apparent if the slope of the aluminium condenser is smaller. Further investigation is needed.

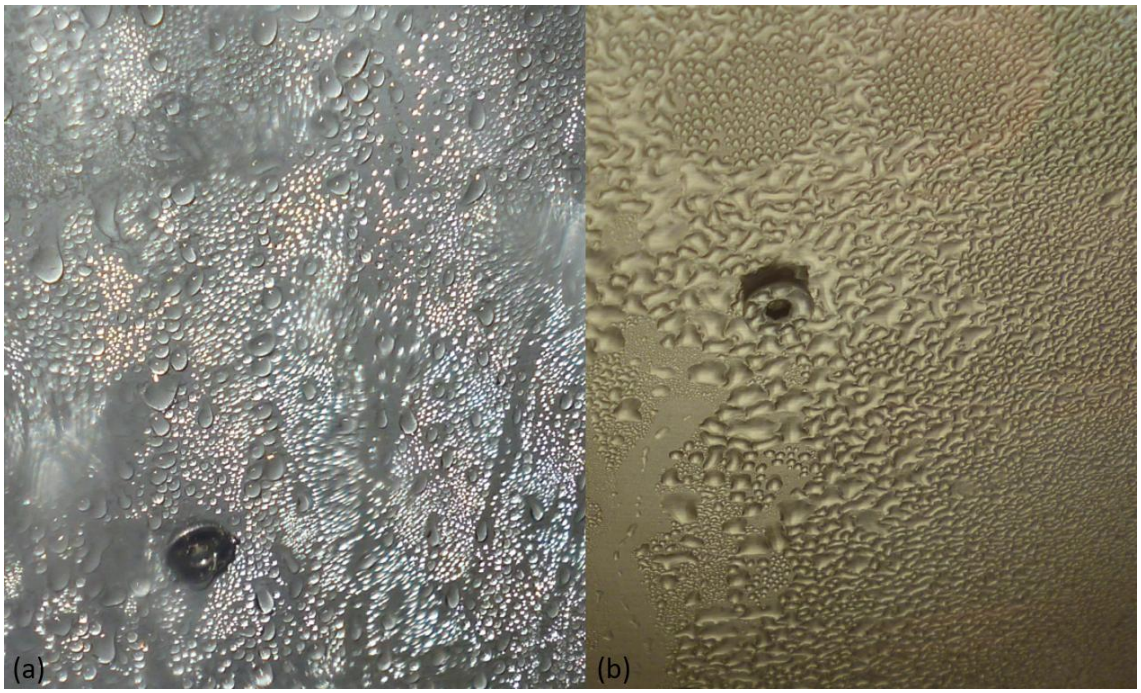

Figure 5.7 Condensation on the aluminum, a) with the hydrophopic layer, b) without the hydrophopic layer

5.3 Using a Fan to Cool the Glass Cover

Previously noted in chapter 4 that the glass cover temperature stays high during the experiment, it took the glass cover more than an hour to start producing water as a result of the temperature being higher the vapor temperature which means that no condensation is taking place. The objective of this work is to investigate the possibility of improving the water production of the glass cover by reducing its operation temperature.

5.3.1 Experimental Setup

The setup used in this experiment is the same configuration used in chapter 4, plus a small fan mounted to the front of the system as shown in Figure 5.8. The fan is used to increase the heat transfer by forced convection between the glass and the ambient, and consequently reduce the glass temperature. It is powered by an external power supply. The wind speed above the glass cover is measured with anemometer and it is found to be around 1.7m/s. To ensure fair comparison, the experiments were carried out under the same conditions as the previous one.

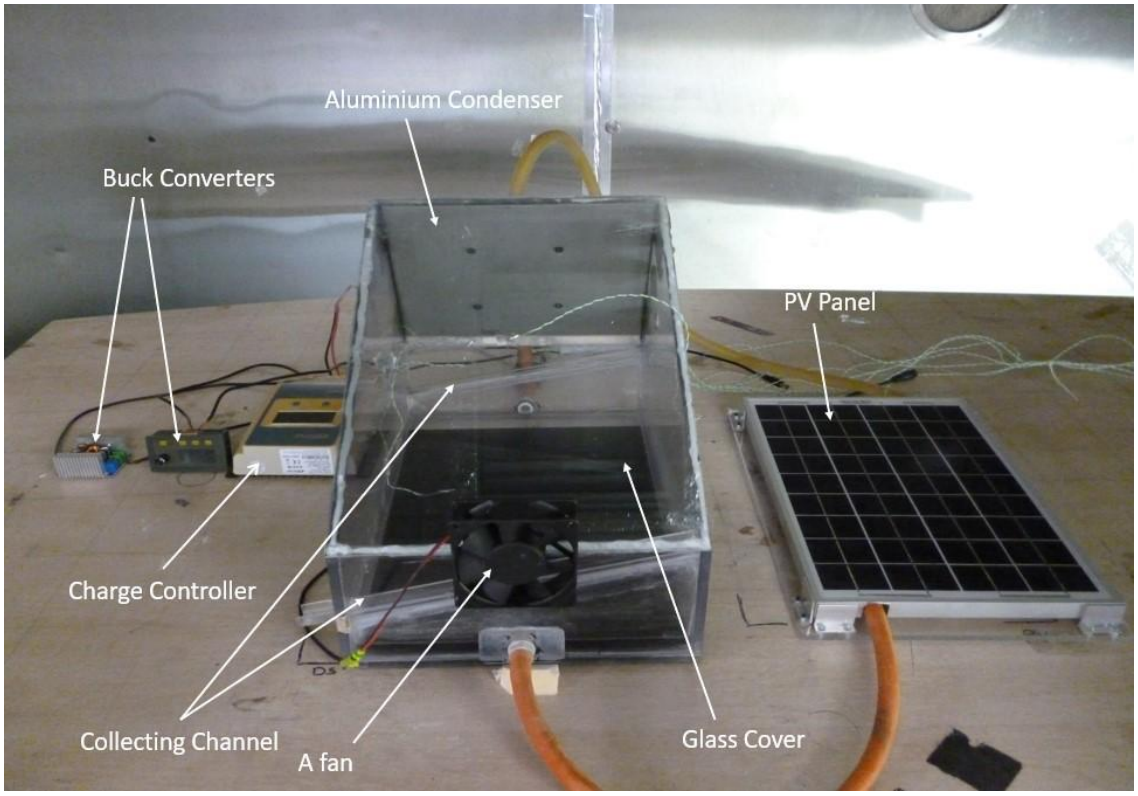

Figure 5.8 the experiment setup

5.3.2 Results

Figure 5.9 shows the change of water temperature as an hourly rate before and after using the fan used to cool the glass cover. It seems that the fan has a slight impact on the water temperature change and it became less than the system

without the fan. In fact, the maximum temperature of the water has decreased by around 4.2 °C, from 57.2 °C before the fan used to 52.9 °C after, this represents around 7% decreases. This can be explained by the increase of heat transfer between the glass cover and the water because of the greater temperature difference.

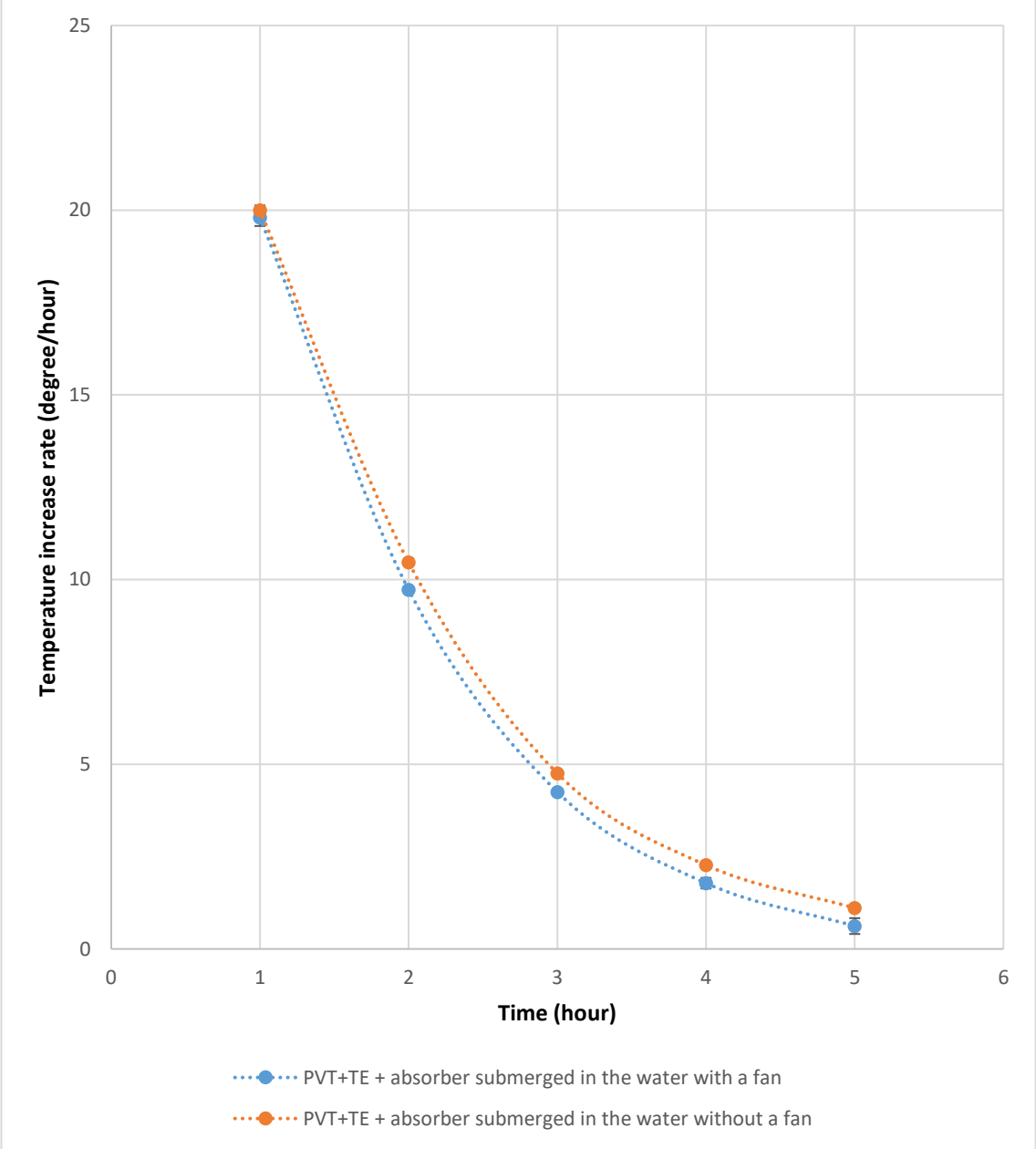

Figure 5.9 Comparing the hourly change of temperature of the water before and after using the fan to cool the glass cover

Figure 5.10 shows the change of the temperature of the glass cover before and after the fan is used. When the fan is used, the maximum temperature of the glass cover is reduced by 10 °C (the temperature starts at around 18 °C and it reaches 50 °C without using the fan and 39 °C when using the fan).

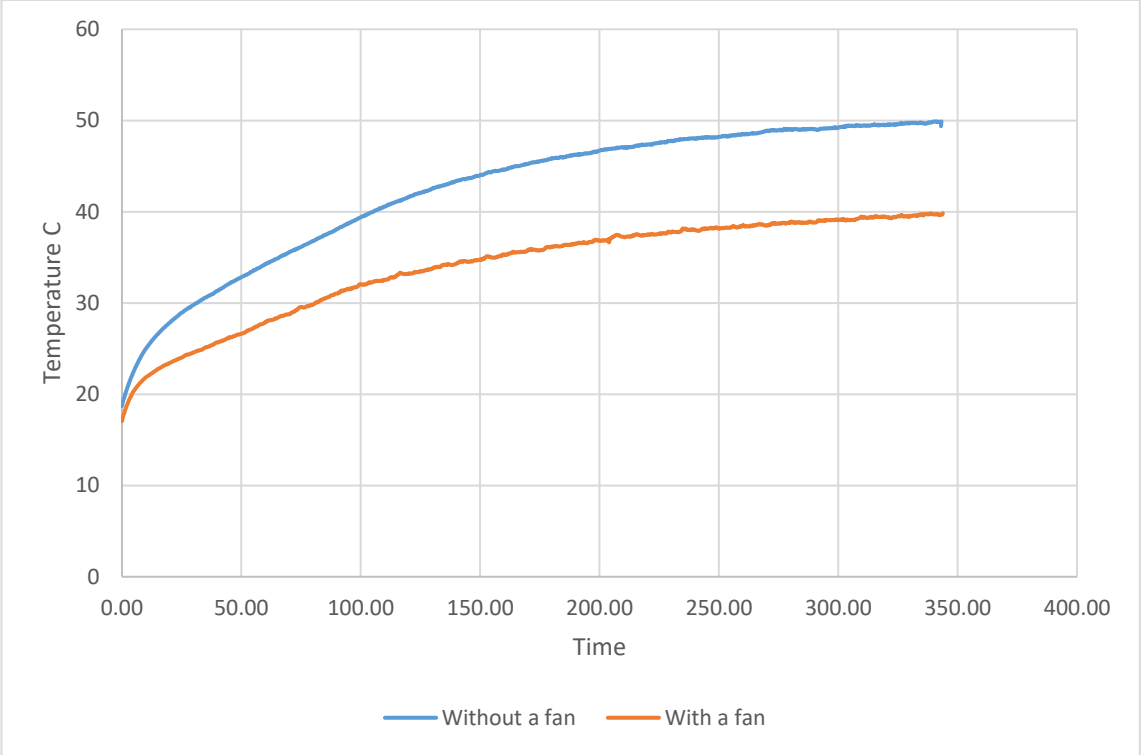

Figure 5.10 Glass cover temperature change over the time period of the experiment

The benefit of using the fan can be seen in Figure 5.11. The difference in temperature between the vapor inside the chamber and the glass cover before and after using the fan is significant. The time it took for the glass cover to reach a temperature less than the vapor is reduced. Furthermore, the maximum temperature difference is increased by 6 °C. Without using the fan, the glass cover temperature was only around 1.5 °C below the vapor temperature by the end of the experiment. In addition, it took the glass cover more than an hour to get to a temperature below the vapor temperature. This has been improved dramatically when the fan is used. The maximum temperature difference between the vapor

and the glass cover reached around 7 °C by the end of the experiment and the time it took for the glass cover to reach a temperature below the vapor is also reduced by more than 50% to around half an hour from the beginning of the experiment.

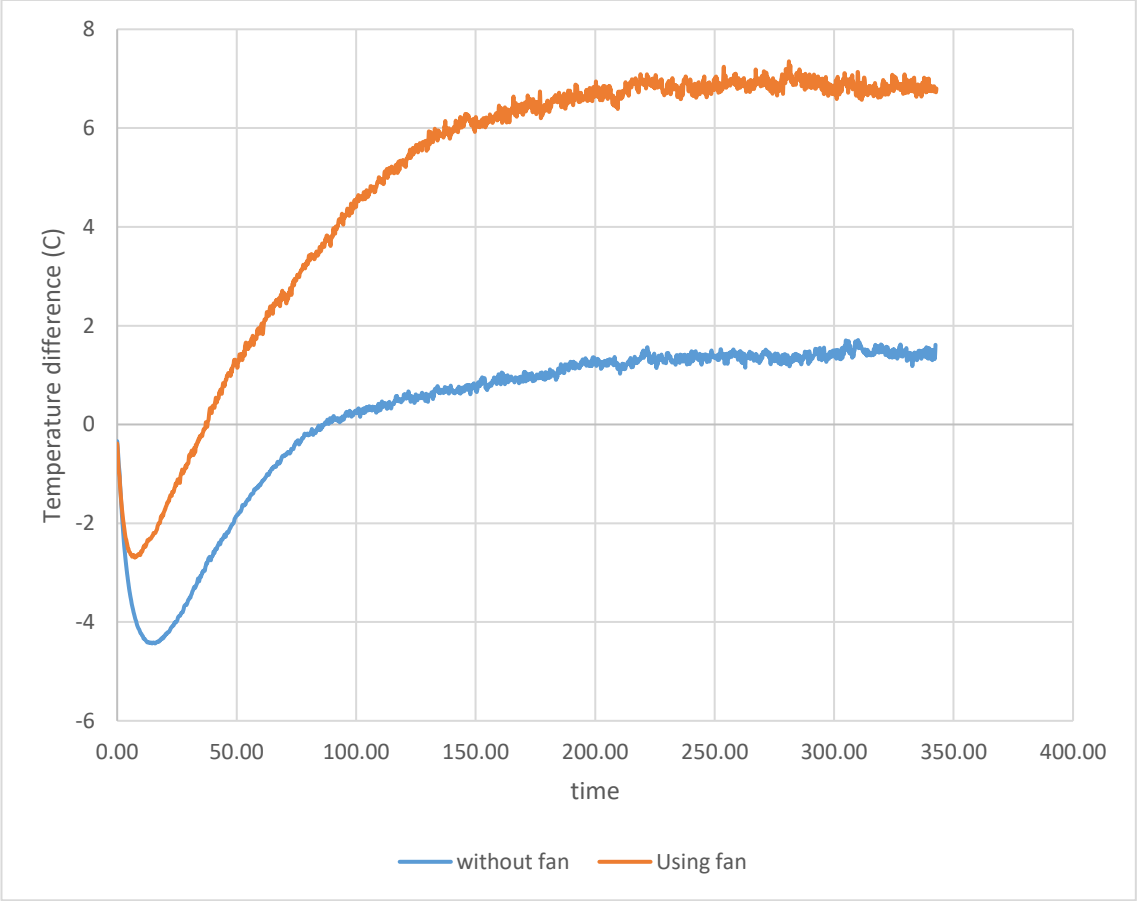

Figure 5.11 The temperature difference between the vapor inside the chamber and the glass cover.

An increase in the temperature difference between the vapor inside the chamber and the glass cover has significant effect on the water productivity of the system. Figure 5.12 shows a compression of the water productivity of the system before and after using the fan. The total water produced by the system jumped from 84.1 g to 112.4g by the end of the 5 hours experiment period. This change represents around an increase by 33.7%. To further understand the change in the

productivity, the water produced from each condensing surface is compared individually.

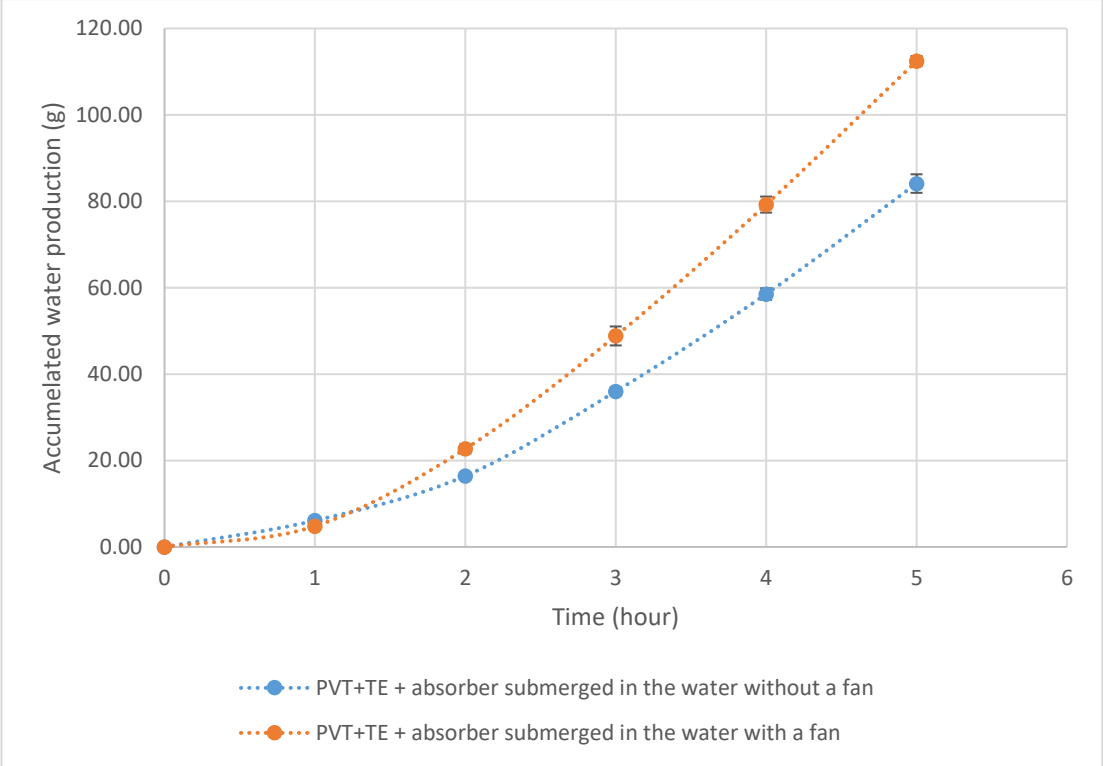

Figure 5.12 The accumulated productivity of the system before and after the fan

Starting with the aluminium condenser, the amount of water produced after using the fan is actually lower than that without using the fan as shown in Figure 5.13. The water produced without using the fan is 52.7 g at the end of the experiment, while the water produced with using the fan is 36.7 g. This represents a reduction by 30% after the fan is used. However, the water produced by the glass cover after using the fan was increased by 141%, from 31.3 g to 75.6 g over a 5-hour operating period as shown in Figure 5.14. Since the gain from the glass cover after using a fan is much higher than the loss from the aluminium condenser, the overall water productivity is significantly increased after using the fan, demonstrating the important and benefit of cooling the glass cover.

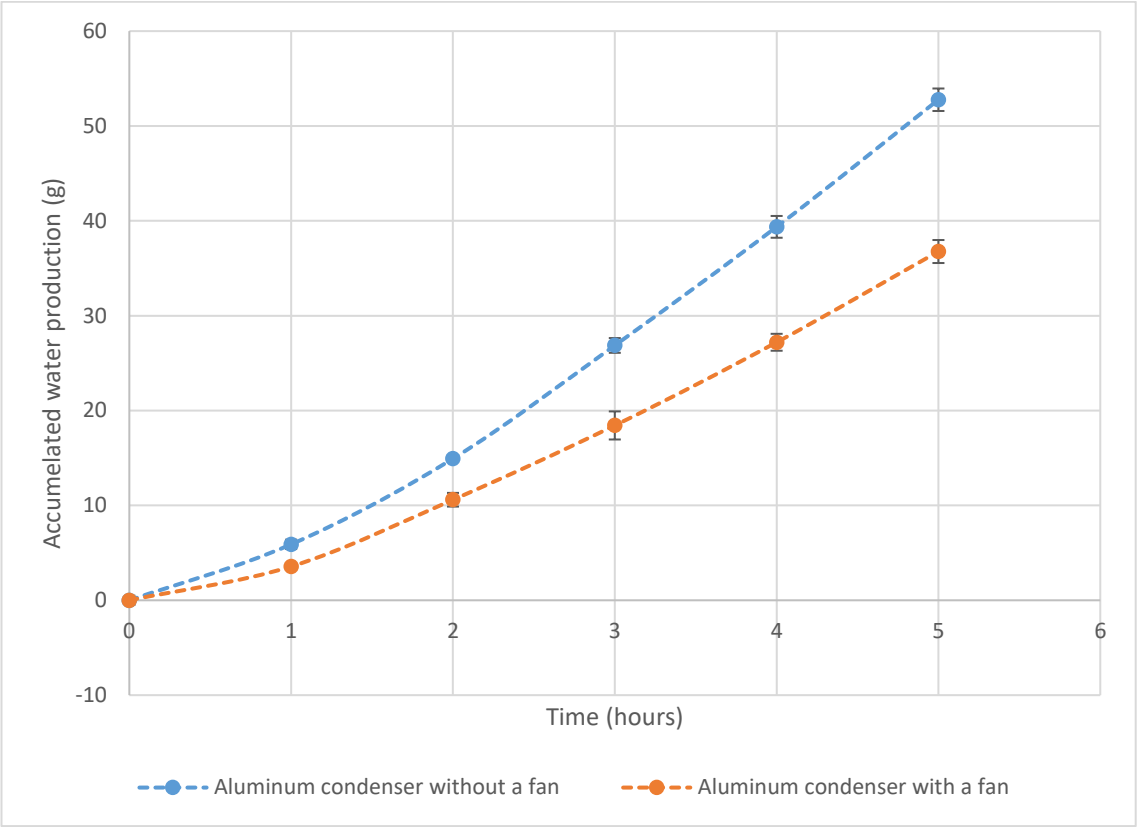

Figure 5.13 The accumulated productivity from the aluminum condenser before and after the fan

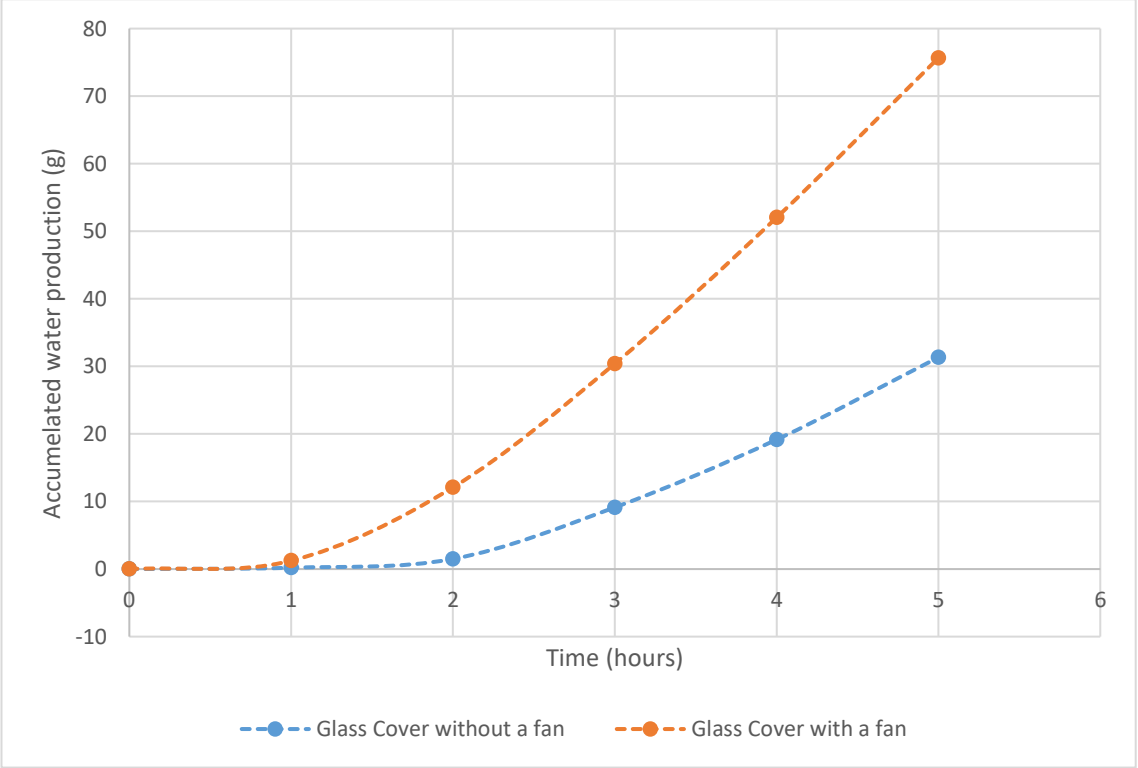

Figure 5.14 The accumulated productivity from the glass cover before and after the fan

The decrease in water production of the aluminium condenser after using the fan can be attributed to the fact that the heat transfer from the vapor to the condenser is reduced due to lower vapour temperature. The temperature difference between the vapor and the aluminium condenser before and after using the fan shown in Figure 5.15. It can be seen that the fan has impacted the temperature of the vapor and, in turn, the temperature difference between the condenser and the vapor. This reduction in the temperature difference (hence the heat transfer from the vapor to condenser) is responsible for the reduction of the water production by the aluminium condenser. The temperature difference between the vapor and the aluminium condenser settled at around 4.8 ^{o}C at the end of the 5 hours experiment period before using the fan and around 3.8 ^{o}C after using the fan.

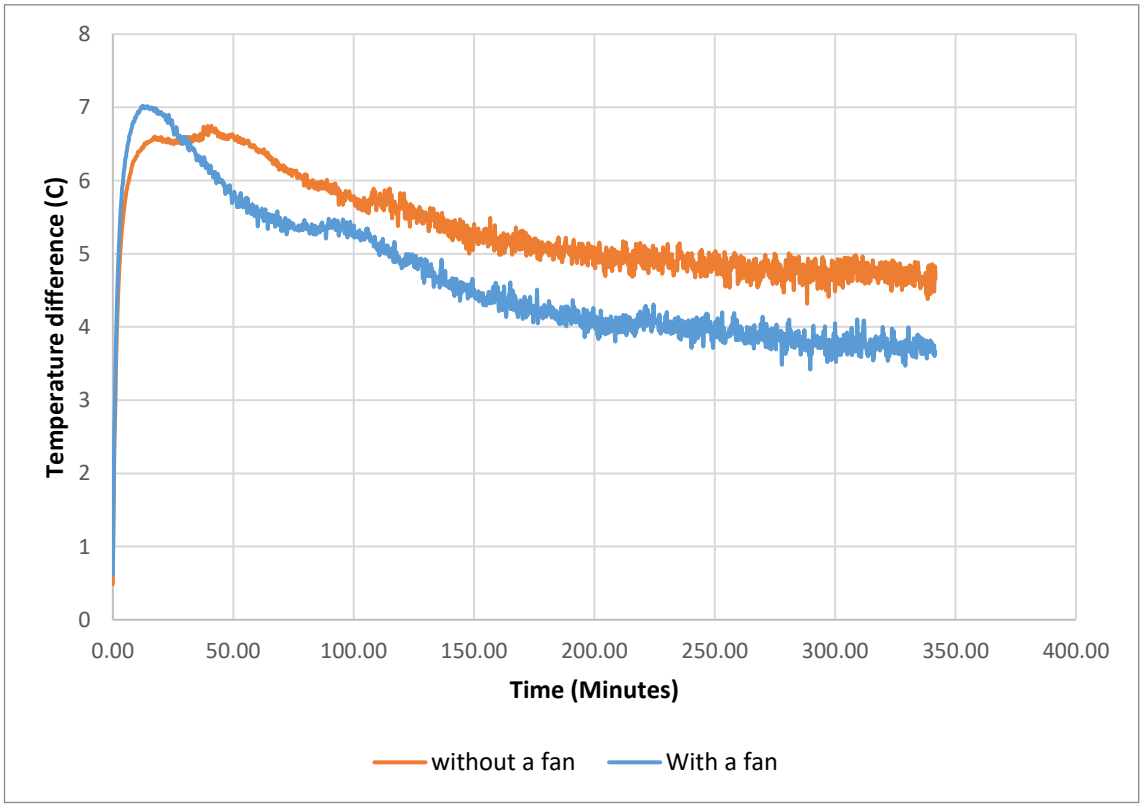

Figure 5.15 The temperature difference between the vapor inside the chamber and the the aluminum condenser.

Finally, the efficiency of the system before and after using the fan was calculated from the experimental data. The results are shown in Figure 5.16. The system efficiency after using the fan is increased due to an increase in the water productivity. In the final hour of the experiment, the system efficiency is found to be 21.2% after using the fan while it is 16.5% before using the fan. This represents an increase by around 28% of the system efficiency.

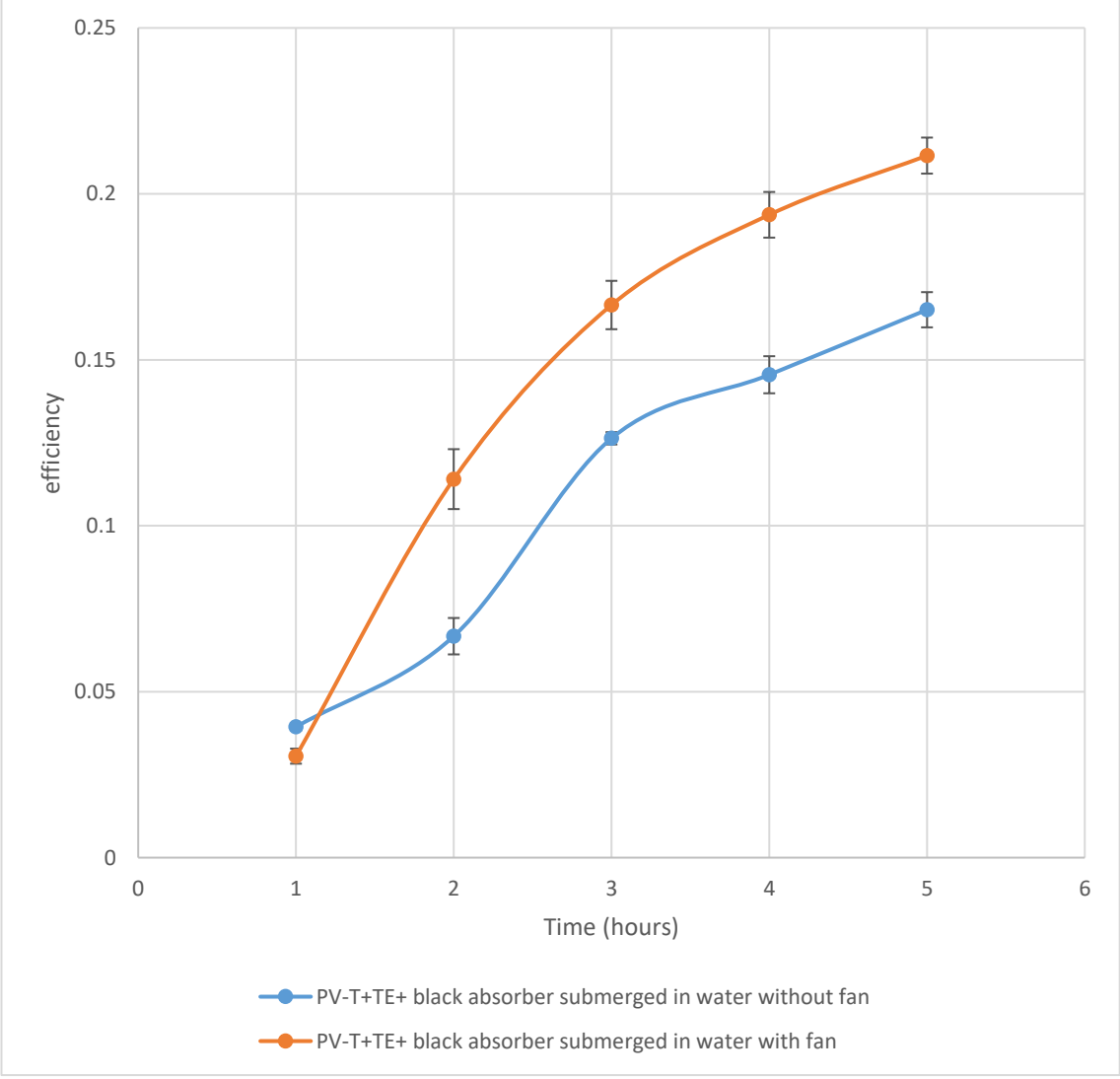

Figure 5.16 the efficiency of the system before and after the fan introduced.

5.4 Conclusion

An experiment was carried out to study the effect of a hydrophobic layer on the water productivity of the system. The results show that an effective hydrophobic layer was fabricated, which resulted in an increase in the water droplet contact angle from around 70^{o} in an untreated aluminium condenser to around 113^{o} in a treated aluminium condenser, demonstrating the formation of a desirable hydrophobic layer. However, the results of water production experiment show that there is no noticeable improvement in the water productivity of the system incorporated with the hydrophobic layer. This is due to the fact the system used in this study has been designed with a steep slope of the condenser, enabling effective water collection using untreated aluminium condenser. It is anticipated that the benefit of the fabricated hydrophobic layer will be demonstrated when a condenser plate with less steep slope is used.

The effect of cooling the glass cover was investigated. The experimental results from this work show that the introduction of forced convection to the glass cover by using a fan has dramatically increased the water productivity of the system by around 33.65%, compared to the same system without fan. It is interesting to note that although the cooling of the glass cover has a positive effect on the water production by the glass cover, it led to a reduction in water production by the aluminium condenser due to a decrease in the temperature difference between the vapor and the condenser. Nevertheless, the gain from the glass cover (~141%) is significantly higher than the loss (~30%). Consequently, an overall improvement is obtained by cooling the glass cover with a fan.

Chapter 6: Conclusion

6.1 Conclusions

Water is the most important substance to mankind, although earth surface is almost 70% water, many regions in the world is facing challenges to meet the demand of fresh water for both domestic and industrial sectors. Water desalination is one of the most common ways to supply this demand by removing the salts and minerals from seawater and brackish water. These technologies mainly used in large scale plants and often require high energy and very expensive. This limit the ability of current desalination technologies to be implemented in developing countries market. In this thesis a concept of self-power small scale hybrid solar PV-T TE distillation system is presented.

To understand how evaporation and condensation affected by the temperature of the water and the condenser, two initial experiments were conducted. The evaporation rate found to be increasing in exponential form with the temperature increase. The condensation rate was found to be more sensitive to the change of the water temperature compared to the condenser temperature. In both cases the evaporation rate and the condensation rate obtained from the mathematical solution is overestimated compared to the experimental results.

The system designed, constructed and tested under solar simulator for 5 hours, the experiment designed to unsure the understanding of the effect of each energy input used (TE, PV-T, and the black absorber in the water) on the water production of the system. When using thermoelectric only to heat the water and cool the vapour, the system accumulated water production after 5 hours was 14.78g. this has increased to 37.5g when the PV-T panel is used to heat the water, and to 84.1g when the system uses the black absorber in the water beside the thermoelectric and the PV-T panel.

It has been found that the highest efficiency is obtained when the thermoelectric module only is used, as we add more heat input the efficiency of the system drops, the efficiency of the system for the three configuration TE only, TE +PV-T,

and TE+PV-T+Black absorber submerged in the water are 20%, 18%, 16.5% respectively. The water quality was measured in terms of the total dissolved minerals, it has been found that the water condensed on the glass cover has a lower PPM in terms of the total dissolved minerals (TDS) than the one condensed on the aluminium condenser.

A hydrophobic layer is used to investigate any benefits that might have on the condensation rate from the aluminium condenser, the results shows that there was no change in the amount of water condensed, this is due to the high angle of 65^{o}. The use of active cooling to cool the glass cover also investigated, a fan is used blow ambient air on the glass cover, the glass cover temperature is reduced from 50 C to 39C by end of the experiment and the accumulated water production increased by 33.65%.

The proposed system is compared to some of the system in literature in terms of specific power consumption, it has been found that the hybrid PV-T TE distillation system has specific power consumption of 0.0062 kWh/mL. this has decreased to 0.004835 kWh/mL when the fan is used to cool the glass cover. Table 6-1 compare the specific power consumption of the proposed system to some found in the literature.

Table 6-1 the specific power consumption of the proposed system and some from literature.

Reference	specific power consumption kWh/mL
PV/TE distillation system [101]	0.00542
solar still system [102]	0.00517
PV/TE distillation system [103]	0.00515
solar TE distillation system [104]	0.00426
solar still system [105]	0.025
TE Distillation system [106]	0.05945
PV-T+TE+ black absorber submerged in water	0.006201
PV-T+TE+ black absorber submerged in water with fan	0.004835

6.2 Future Work

For future work, it is suggested to test the system under real-life conditions with exposure to direct sunlight. This will allow for a comparison with other solar distillation systems and provide a practical assessment of its performance. Additionally, it is recommended to explore the use of insulation materials to insulate the evaporation chamber and the heat exchanger on the hot side of the thermoelectric module. This will help reduce heat losses to the surroundings and enable the system to achieve higher water temperatures.

Another area of investigation could focus on increasing the temperature difference between the aluminium condenser and the vapor inside the chamber. This can be achieved by replacing the heat exchanger used to heat the water from the thermoelectric module with a fin, which would lower the condenser temperature, potentially improving the condensation rate despite sacrificing some heat absorption by the water.

Further research could also explore the use of aluminium condensers with higher thermal conductivity values. This would help absorb more heat from the vapor and efficiently transfer it to the thermoelectric module. Finally, enhancing heat transfer between the water and the heat exchangers by using nanofluids is another potential area for future work, which may increase system efficiency

References

[1] W. W. A. P. (United Nations), *The United Nations World Water Development Report*, no. 3. UNESCO Pub., 2009.

[2] Martin Armstrong, “Where Water Stress Will Be Highest by 2040,” Statista.

[3] “2050 High-Level Experts Forum: Expert papers.” Accessed: Mar. 10, 2023. [Online]. Available: https://www.fao.org/wsfs/forum2050/wsfs-background-documents/wsfs-expert-papers/en/

[4] World Bank Group, “High and Dry: Climate Change, Water, and the Economy,” Washington, DC, 2016. Accessed: Mar. 07, 2023. [Online]. Available: http://hdl.handle.net/10986/23665

[5] S. Schlosser, “Distillation – from Bronze Age till today,” *38th International Conference of Slovak Society of Chemical Engineering Hotel*, no. May 2011, pp. 1–12, 2016.

[6] M. D. Saltzman, “the Art of Distillation and the Dawn of the Hydrocarbon Society,” *Bull. Hist. Chem*, vol. 24, pp. 53–60, 1999.

[7] M. Lagi and R. S. Chase, “Distillation: integration of a historical perspective,” *Australian Journal of*, pp. 5–10, 2009, [Online]. Available: http://www.raci.org.au/sitebuilder/divisions/knowledge/asset/files/38/ausjecissue702009.pdf#page=5

[8] B. Sri, H. Priya, V. Sridevi, R. Santhoshi, and K. M. Tukaram Bai, “Review on Water Desalination using Renewable Solar Energy,” *IJIRST-International Journal for Innovative Research in Science & Technology|*, vol. 2, 2015, [Online]. Available: www.ijirst.org

[9] H. Sharon and K. S. Reddy, “A review of solar energy driven desalination technologies,” Jan. 01, 2015, *Elsevier Ltd*. doi: 10.1016/j.rser.2014.09.002.

[10] “StandardSpecification for Solar Simulation for Photovoltaic Testing 1”, doi: 10.1520/E0927-10.

[11] D. Michael. Rowe, *Thermoelectrics handbook : macro to nano*. CRC/Taylor & Francis, 2006. [Online]. Available: https://books.google.co.uk/books/about/Thermoelectrics_Handbook.html?id=0iwERQe5IKQC

[12] A. V. Da Rosa, *Fundamentals of renewable energy processes*. Academic Press, 2012.

[13] R. Mawi and Y. Kazuz, “Hybrid Solar Thermo-Electric Systems for Combined Heat and Power,” 2014.

[14] A. Date, A. Date, C. Dixon, and A. Akbarzadeh, “Progress of thermoelectric power generation systems: Prospect for small to medium scale power generation,” *Renewable and Sustainable Energy Reviews*, vol. 33, pp. 371–381, 2014, doi: 10.1016/j.rser.2014.01.081.

[15] D. M. Rowe and Gao Min, “Evaluation of Thermoelectric Modules for Power Generation,” *J Power Sources*, vol. 73, no. 2, pp. 193–198, 1998.

[16] J. Xiao, T. Yang, P. Li, P. Zhai, and Q. Zhang, “Thermal design and management for performance optimization of solar thermoelectric generator,” *Appl Energy*, vol. 93, pp. 33–38, 2012, doi: 10.1016/j.apenergy.2011.06.006.

[17] S. B. Riffat and X. Ma, “Thermoelectrics: a review of present and potential applications,” *Appl Therm Eng*, vol. 23, no. 8, pp. 913–935, 2003.

[18] S. Kim, S. Park, S. Kim, and S. H. Rhi, “A thermoelectric generator using engine coolant for light-duty internal combustion Engine-Powered Vehicles,” *J Electron Mater*, vol. 40, no. 5, pp. 812–816, 2011, doi: 10.1007/s11664-011-1580-6.

[19] N. Baatar and S. Kim, “A Thermoelectric Generator Replacing Radiator for Internal Combustion Engine Vehicles,” *TELKOMNIKA (Telecommunication Computing Electronics and Control)*, vol. 9, no. 3, p. 523, 2015, doi: 10.12928/telkomnika.v9i3.744.

[20] M. E. Demir and I. Dincer, “Performance assessment of a thermoelectric generator applied to exhaust waste heat recovery,” *Appl Therm Eng*, vol. 120, pp. 694–707, 2017, doi: 10.1016/j.applthermaleng.2017.03.052.

[21] S. K. Kim, B. C. Won, S. H. Rhi, S. H. Kim, J. H. Yoo, and J. C. Jang, “Thermoelectric power generation system for future hybrid vehicles using hot exhaust gas,” *J Electron Mater*, vol. 40, no. 5, pp. 778–783, 2011, doi: 10.1007/s11664-011-1569-1.

[22] J. Martins, L. M. Goncalves, J. Antunes, and F. P. Brito, “Thermoelectric Exhaust Energy Recovery with Temperature Control through Heat Pipes,” *SAE Technical Paper Series*, vol. 1, pp. 1–19, 2011, doi: 10.4271/2011-01-0315.

[23] F. P. Brito, J. Martins, E. Hançer, N. Antunes, and L. M. Gonçalves, “Thermoelectric Exhaust Heat Recovery with Heat Pipe-Based Thermal Control,” *J Electron Mater*, vol. 44, no. 6, pp. 1984–1997, 2015, doi: 10.1007/s11664-015-3638-3.

[24] F. P. Brito, L. M. Goncalves, J. Martins, N. Antunes, and D. Sousa, “Influence of Heat Pipe Operating Temperature on Exhaust Heat Thermoelectric Generation,” *SAE International Journal of Passenger Cars - Mechanical Systems*, vol. 6, no. 2, pp. 652–664, 2013, doi: 10.4271/2013-01-0559.

[25] B. Matonak and H. Peabody, “An Introductory Guide to Variable Conductance Heat Pipe Simulation.”

[26] C. Lertsatitthanakorn, “Electrical performance analysis and economic evaluation of combined biomass cook stove thermoelectric (BITE)

generator," *Bioresour Technol*, vol. 98, no. 8, pp. 1670–1674, 2007, doi: 10.1016/j.biortech.2006.05.048.

[27] D. Mastbergen, D. Bryan Willson, and B. Willson@colostate, *Generating Light from Stoves using a Thermoelectric Generator*. 2005.

[28] P. Li, L. Cai, P. Zhai, X. Tang, Q. Zhang, and M. Niino, "Design of a concentration solar thermoelectric generator," *J Electron Mater*, vol. 39, no. 9, pp. 1522–1530, 2010.

[29] K. Yazawa and A. Shakouri, "System optimiztion of hot water concentrated solar thermoelectric generation," *Thermal Issues in Emerging Technologies Theory and Applications (ThETA), 2010 3rd International Conference on*, pp. 283–290, 2010.

[30] N. Miljkovic and E. N. Wang, "Modeling and optimization of hybrid solar thermoelectric systems with thermosyphons," *Solar Energy*, vol. 85, no. 11, pp. 2843–2855, 2011.

[31] Z. Zhang, W. Li, and J. Kan, "Behavior of a thermoelectric power generation device based on solar irradiation and the earth's surface-air temperature difference," *Energy Convers Manag*, vol. 97, pp. 178–187, Jun. 2015, doi: 10.1016/j.enconman.2015.03.060.

[32] D. Kraemer *et al.*, "High-performance flat-panel solar thermoelectric generators with high thermal concentration," *Nat Mater*, vol. 10, no. 7, pp. 532–538, 2011.

[33] W. He, Y. Su, Y. Q. Wang, S. B. Riffat, and J. Ji, "A study on incorporation of thermoelectric modules with evacuated-tube heat-pipe solar collectors," *Renew Energy*, vol. 37, no. 1, pp. 142–149, 2012.

[34] R. Singh, S. Tundee, and A. Akbarzadeh, "Electric power generation from solar pond using combined thermosyphon and thermoelectric modules," *Solar Energy*, vol. 85, no. 2, pp. 371–378, 2011.

[35] J. Xiao, T. Yang, P. Li, P. Zhai, and Q. Zhang, “Thermal design and management for performance optimization of solar thermoelectric generator,” *Appl Energy*, vol. 93, pp. 33–38, 2012.

[36] V. Verma, A. Kane, and B. Singh, “Complementary performance enhancement of PV energy system through thermoelectric generation,” *Renewable and Sustainable Energy Reviews*, vol. 58, pp. 1017–1026, 2016.

[37] W. Pridasawas and P. Lundqvist, “An exergy analysis of a solar-driven ejector refrigeration system,” *Solar Energy*, vol. 76, no. 4, pp. 369–379, 2004, doi: 10.1016/j.solener.2003.11.004.

[38] Y. Dai, R. Wang, and L. Ni, “Experimental investigation and analysis on a solar thermoelectric refrigerator,” *Taiyangneng Xuebao/Acta Energiae Solaris Sinica*, vol. 23, no. 6, pp. 377–391, 2002.

[39] G. Min and D. M. Rowe, “Experimental evaluation of prototype thermoelectric domestic-refrigerators,” *Appl Energy*, vol. 83, no. 2, pp. 133–152, 2006, doi: 10.1016/j.apenergy.2005.01.002.

[40] S. A. Abdul-Wahab *et al.*, “Design and experimental investigation of portable solar thermoelectric refrigerator,” *Renew Energy*, vol. 34, no. 1, pp. 30–34, 2009, doi: 10.1016/j.renene.2008.04.026.

[41] N. Putra, “Design, manufacturing and testing of a portable vaccine carrier box employing thermoelectric module and heat pipe,” *J Med Eng Technol*, vol. 33, no. 3, pp. 232–237, 2009, doi: 10.1080/03091900802454517.

[42] A. A. Adeyanju, E. Ekwue, and W. Compton, “Experimental and theoretical analysis of a beverage chiller,” *Res J Appl Sci*, vol. 5, no. 3, pp. 195–203, 2010.

[43] C. Lertsatitthanakorn, L. Wiset, and S. Atthajariyakul, “Evaluation of the thermal comfort of a thermoelectric ceiling cooling panel (TE-CCP) system,” *J Electron Mater*, vol. 38, no. 7, pp. 1472–1477, 2009, doi: 10.1007/s11664-008-0637-7.

[44] M. Gillott, L. Jiang, and S. Riffat, “An investigation of thermoelectric cooling devices for small-scale space conditioning applications in buildings,” *Int J Energy Res*, vol. 34, no. 9, pp. 776–786, 2010.

[45] P. K. Bansal and A. Martin, “Comparative study of vapour compression, thermoelectric and absorption refrigerators,” *Int J Energy Res*, vol. 24, no. 2, pp. 93–107, 2000, doi: 10.1002/(SICI)1099-114X(200002)24:2<93::AID-ER563>3.0.CO;2-6.

[46] K. V. Wong and C. Pecora, “Recommendations for Energy–Water–Food Nexus Problems,” *J Energy Resour Technol*, vol. 137, no. 3, p. 032002, 2015, doi: 10.1115/1.4028139.

[47] B. Jimenez-Cisneros, “Responding to the challenges of water security: The Eighth Phase of the International Hydrological Programme, 2014-2021,” *IAHS-AISH Proceedings and Reports*, vol. 366, no. June 2014, pp. 10–19, 2015, doi: 10.5194/piahs-366-10-2015.

[48] H. T. El-Dessouky and H. M. Ettouney, *Fundamentals of Salt Water Desalination."* *Department of Chemical Engineering, College of Engineering and Petroleum, Kuwait University: Elsevier, Amsterdam.* 2002.

[49] I. C. Watson, O. J. Morin, and L. Henthorne, “Desalting Handbook for Planners,” *Journal of pain palliative care pharmacotherapy*, vol. 72, no. 4, pp. 1–310, 2003, doi: 10.3109/15360288.2011.620691.

[50] A. Al-Karaghouli and L. L. Kazmerski, “Energy consumption and water production cost of conventional and renewable-energy-powered desalination processes,” *Renewable and Sustainable Energy Reviews*, vol. 24, pp. 343–356, 2013, doi: 10.1016/j.rser.2012.12.064.

[51] A. Alkaisi, R. Mossad, and A. Sharifian-Barforoush, “A Review of the Water Desalination Systems Integrated with Renewable Energy,” *Energy Procedia*, vol. 110, no. December 2016, pp. 268–274, 2017, doi: 10.1016/j.egypro.2017.03.138.

[52] U. R. S. Australia, “Introduction to desalination technologies in Australia,” *Report for Agriculture, Fisheries and Forestry–Australia*, no. September 2002, 2002.

[53] Semiat R, “Energy issues in desalination processes,” *Environ Sci Technol*, vol. 42, no. 22, pp. 8193–8201, 2008.

[54] S. A. Avlonitis, K. Kouroumbas, and N. Vlachakis, “Energy consumption and membrane replacement cost for seawater RO desalination plants,” *Desalination*, vol. 157, no. 1–3, pp. 151–158, 2003, doi: 10.1016/S0011-9164(03)00395-3.

[55] M. Sadrzadeh and T. Mohammadi, “Sea water desalination using electrodialysis,” *Desalination*, vol. 221, no. 1–3, pp. 440–447, 2008, doi: 10.1016/j.desal.2007.01.103.

[56] S. B. Sadineni, R. Hurt, C. K. Halford, and R. F. Boehm, “Theory and experimental investigation of a weir-type inclined solar still,” *Energy*, vol. 33, no. 1, pp. 71–80, 2008, doi: 10.1016/j.energy.2007.08.003.

[57] S. Kumar and A. Tiwari, “An experimental study of hybrid photovoltaic thermal (PV/T)-active solar still,” *Int J Energy Res*, vol. 32, no. 9, pp. 847–858, 2008, doi: 10.1002/er.1388.

[58] R. Tripathi and G. N. Tiwari, “Effect of water depth on intemal heat and mass transfer for active solar distillation,” *Desalination*, vol. 173, pp. 187–200, 2005, doi: 10.1016/j.desal.2004.08.03.

[59] N. Gakkhar, M. S. Soni, and S. Jakhar, “Second law thermodynamic study of solar assisted distillation system: A review,” Apr. 01, 2016, *Elsevier Ltd*. doi: 10.1016/j.rser.2015.11.076.

[60] S. Aggarwal and G. N. Tiwari, “Convective mass transfer in a double-condensing chamber and a conventional solar still,” 1998.

[61] Z. Hongfei, Z. Xiaoyan, Z. Jing, and W. Yuyuan, “A group of improved heat and mass transfer correlations in solar stills.” [Online]. Available: www.elsevier.com/locate/enconman

[62] J. A. Esfahani, N. Rahbar, and M. Lavvaf, “Utilization of thermoelectric cooling in a portable active solar still - An experimental study on winter days,” *Desalination*, vol. 269, no. 1–3, pp. 198–205, 2011, doi: 10.1016/j.desal.2010.10.062.

[63] V. P. S. P. Joshi, V. P. S. P. Joshi, H. A. Kothari, M. D. Mahajan, M. B. Chaudhari, and K. D. Sant, “Experimental Investigations on a Portable Fresh Water Generator Using a Thermoelectric Cooler,” *Energy Procedia*, vol. 109, no. November 2016, pp. 161–166, 2017, doi: 10.1016/j.egypro.2017.03.085.

[64] S. Nazari, H. Safarzadeh, and M. Bahiraei, “Performance improvement of a single slope solar still by employing thermoelectric cooling channel and copper oxide nanofluid: An experimental study,” *J Clean Prod*, vol. 208, pp. 1041–1052, 2019, doi: 10.1016/j.jclepro.2018.10.194.

[65] S. İ. Yıldırım C, Soylu SK, Atmaca İ, “Experimental investigation of a portable desalination unit configured by a thermoelectric cooler,” *Energy Convers Manag*, vol. 85, pp. 140–145, 2014, doi: 10.1016/j.enconman.2014.05.071.

[66] H. Al-Madhhachi and G. Min, “Effective use of thermal energy at both hot and cold side of thermoelectric module for developing efficient thermoelectric water distillation system,” *Energy Convers Manag*, vol. 133, pp. 14–19, 2017, doi: 10.1016/j.enconman.2016.11.055.

[67] H. Al-Madhhachi and G. Min, “Key factors affecting the water production in a thermoelectric distillation system,” *Energy Convers Manag*, vol. 165, no. March, pp. 459–464, 2018, doi: 10.1016/j.enconman.2018.03.080.

[68] J. A. Esfahani, N. Rahbar, and M. Lavvaf, “Utilization of thermoelectric cooling in a portable active solar still - An experimental study on winter days,” *Desalination*, vol. 269, no. 1–3, pp. 198–205, 2011, doi: 10.1016/j.desal.2010.10.062.

[69] A. Al-Karaghouli and L. L. Kazmerski, “Energy consumption and water production cost of conventional and renewable-energy-powered desalination processes,” 2013, *Elsevier Ltd*. doi: 10.1016/j.rser.2012.12.064.

[70] S. Gabarrón, W. Gernjak, F. Valero, A. Barceló, M. Petrovic, and I. Rodríguez-Roda, “Evaluation of emerging contaminants in a drinking water treatment plant using electrodialysis reversal technology,” *J Hazard Mater*, vol. 309, pp. 192–201, May 2016, doi: 10.1016/j.jhazmat.2016.02.015.

[71] S. A. Avlonitis, K. Kouroumbas, and N. Vlachakis, “Energy consumption and membrane replacement cost for seawater RO desalination plants Presented at the EzlropeaJl Conjerence on Desalination and the Environment: Fresh Water for All,” European Desalination SocieO~, lnlernatio~tal Water Association, 2003. [Online]. Available: www.elsevier.com/locate/desal

[72] V. G. Gude, N. Nirmalakhandan, and S. Deng, “Renewable and sustainable approaches for desalination,” 2010, *Elsevier Ltd*. doi: 10.1016/j.rser.2010.06.008.

[73] M. A. Eltawil, Z. Zhengming, and L. Yuan, “A review of renewable energy technologies integrated with desalination systems,” Dec. 2009. doi: 10.1016/j.rser.2009.06.011.

[74] A. Al-Karaghouli, D. Renne, and L. L. Kazmerski, “Technical and economic assessment of photovoltaic-driven desalination systems,” Feb. 2010. doi: 10.1016/j.renene.2009.05.018.

[75] N. G. Tran and D. M. Chun, “Green manufacturing of extreme wettability contrast surfaces with superhydrophilic and superhydrophobic patterns on aluminum,” *J Mater Process Technol*, vol. 297, Nov. 2021, doi: 10.1016/j.jmatprotec.2021.117245.

[76] C. Neinhuis and W. Barthlott, “Characterization and Distribution of Water-repellent, Self-cleaning Plant Surfaces,” 1997.

[77] Y. Yuan and T. R. Lee, “Contact angle and wetting properties,” *Springer Series in Surface Sciences*, vol. 51, no. 1, pp. 3–34, 2013, doi: 10.1007/978-3-642-34243-1_1.

[78] W. Qian, Y. Hua, R. Chen, P. Xu, and J. Yang, “Fabrication of superhydrophobic nickel-aluminum bronzes using picosecond laser for enhancing anti-corrosion property,” *Mater Lett*, vol. 268, Jun. 2020, doi: 10.1016/j.matlet.2020.127570.

[79] Y. Wang, Z. Zhang, J. Xu, and H. Yu, “One-step method using laser for large-scale preparation of bionic superhydrophobic & drag-reducing fish-scale surface,” *Surf Coat Technol*, vol. 409, Mar. 2021, doi: 10.1016/j.surfcoat.2020.126801.

[80] B. Subeshan, A. Usta, and R. Asmatulu, “Deicing and self-cleaning of plasma-treated superhydrophobic coatings on the surface of aluminum alloy sheets,” *Surfaces and Interfaces*, vol. 18, Mar. 2020, doi: 10.1016/j.surfin.2020.100429.

[81] N. Sharifi, M. Pugh, C. Moreau, and A. Dolatabadi, “Developing hydrophobic and superhydrophobic TiO2 coatings by plasma spraying,” *Surf Coat Technol*, vol. 289, pp. 29–36, Mar. 2016, doi: 10.1016/j.surfcoat.2016.01.029.

[82] T. A. Saleh and N. Baig, “Efficient chemical etching procedure for the generation of superhydrophobic surfaces for separation of oil from

water," *Prog Org Coat*, vol. 133, pp. 27–32, Aug. 2019, doi: 10.1016/j.porgcoat.2019.03.049.

[83] J. H. Kim, A. Mirzaei, H. W. Kim, and S. S. Kim, "Facile fabrication of superhydrophobic surfaces from austenitic stainless steel (AISI 304) by chemical etching," *Appl Surf Sci*, vol. 439, pp. 598–604, May 2018, doi: 10.1016/j.apsusc.2017.12.211.

[84] A. Caldarelli, M. Raimondo, F. Veronesi, G. Boveri, and G. Guarini, "Sol-gel route for the building up of superhydrophobic nanostructured hybrid-coatings on copper surfaces," *Surf Coat Technol*, vol. 276, pp. 408–415, Aug. 2015, doi: 10.1016/j.surfcoat.2015.06.037.

[85] B. Xia, H. Liu, Y. Fan, W. Zhu, and C. Geng, "Preparation of Robust CuO/TiO2 Superamphiphobic Steel Surface through Chemical Deposition and Sol–Gel Methods," *Adv Eng Mater*, vol. 19, no. 2, Feb. 2017, doi: 10.1002/adem.201600572.

[86] H. Yang, F. Ji, Z. Li, and S. Tao, "Preparation of hydrophobic surface on PLA and ABS by fused deposition modeling," *Polymers (Basel)*, vol. 12, no. 7, Jul. 2020, doi: 10.3390/polym12071539.

[87] Y. Zhang, Z. Zhang, J. Yang, Y. Yue, and H. Zhang, "Fabrication of superhydrophobic surface on stainless steel by two-step chemical etching," *Chem Phys Lett*, vol. 797, Jun. 2022, doi: 10.1016/j.cplett.2022.139567.

[88] "Thermocouples RS PRO Type K Thermocouple 1m Length, 0.3mm Diameter-100°C → +250°c." [Online]. Available: https://uk.rs-online.com/

[89] N. Musolino and B. L. Trout, "Insight into the molecular mechanism of water evaporation via the finite temperature string method," *Journal of Chemical Physics*, vol. 138, no. 13, pp. 1–17, 2013, doi: 10.1063/1.4798458.

[90] P. E. Mason, “Molecular dynamics study on the microscopic details of the evaporation of water,” *Journal of Physical Chemistry A*, vol. 115, no. 23, pp. 6054–6058, 2011, doi: 10.1021/jp1104517.

[91] P. Varilly and D. Chandler, “Water evaporation: A transition path sampling study,” *Journal of Physical Chemistry B*, vol. 117, no. 5, pp. 1419–1428, 2013, doi: 10.1021/jp310070y.

[92] Y. Nagata, K. Usui, and M. Bonn, “Molecular Mechanism of Water Evaporation,” *Phys Rev Lett*, vol. 115, no. 23, pp. 1–5, 2015, doi: 10.1103/PhysRevLett.115.236102.

[93] C. C. Smith, R. W. Jones, and G. O. G. Löf, “Energy requirements and potential savings for heated indoor swimming pools.,” 1994.

[94] J. P. Holman, “Heat Transfer (McGraw-Hill Series in Mechanical Engineering),” 2010, *The McGraw-Hill Companies, Inc*.

[95] T. L. Bergman, F. P. Incropera, D. P. DeWitt, and A. S. Lavine, *Fundamentals of heat and mass transfer*. John Wiley & Sons, 2011.

[96] T. L. Bergman, F. P. Incropera, D. P. DeWitt, and A. S. Lavine, *Fundamentals of heat and mass transfer*. John Wiley & Sons, 2011.

[97] T. Fujii, “Condensation of Pure Vapors,” *Theory of Laminar Film Condensation*, pp. 71–95, 1991, doi: 10.1007/978-1-4612-3152-3_5.

[98] V. P. Carey, “Liquid-Vapor Phase-Change Phenomena : An Introduction to the Thermophysics of Vaporization and Condensation Processes in Heat Transfer Equipment, Third Edition,” *Liquid-Vapor Phase-Change Phenomena*, Sep. 2020, doi: 10.1201/9780429082221.

[99] D. W. Hughes, “Two-phase flow and heat transfer. Edited By D. Butterworth and G. F. Hewitt. Oxford University Press (Harwell Series), 1977. No. of Pages: 514. Price: £14.00,” *Int J Energy Res*, vol. 2, no. 4, pp. 407–408, Sep. 1978, doi: 10.1002/ER.4440020408.

[100] "Absolute Humidity Calculator." [Online]. Available: https://www.omnicalculator.com/physics/absolute-humidity

[101] M. Jradi, N. Ghaddar, and K. Ghali, "Experimental and theoretical study of an integrated thermoelectric-photovoltaic system for air dehumidification and fresh water production," *Int J Energy Res*, vol. 36, no. 9, pp. 963–974, Jul. 2012, doi: 10.1002/er.1848.

[102] N. M. Wade, "Distillation plant development and cost update," 2001. [Online]. Available: www.elsevier.com/locate/desal

[103] R. Sathyamurthy, S. A. El-Agouz, and V. Dharmaraj, "Experimental analysis of a portable solar still with evaporation and condensation chambers," *Desalination*, vol. 367, pp. 180–185, Jul. 2015, doi: 10.1016/j.desal.2015.04.012.

[104] J. A. Esfahani, N. Rahbar, and M. Lavvaf, "Utilization of thermoelectric cooling in a portable active solar still - An experimental study on winter days," *Desalination*, vol. 269, no. 1–3, pp. 198–205, Mar. 2011, doi: 10.1016/j.desal.2010.10.062.

[105] H. E. S. Fatha, M. El-Samanoudyb, K. Fahmy', and A. H. Ssaboud, "Thermal-economic analysis and comparison between pyramid-shaped and single-slope solar still configurations." [Online]. Available: www.elsevier.com/locate/desal

[106] R. Semiat, "Energy issues in desalination processes," Nov. 15, 2008. doi: 10.1021/es801330u.